Nanochannel regulations of graphene oxide membranes for nanofiltration

周, 思雨

(Degree)
博士（学術）

(Date of Degree)
2024-03-25

(Date of Publication)
2025-03-01

(Resource Type)
doctoral thesis

(Report Number)
甲第8936号

(URL)
https://hdl.handle.net/20.500.14094/0100490161

Doctoral Dissertation

Nanochannel regulations of graphene oxide membranes for nanofiltration

(ナノろ過用酸化グラフェン膜のナノチャネルの制御)

January 2024

Graduate School of Engineering
Kobe University

ZHOU SIYU
周 思雨

Acknowledgment

In order to welcome the arrival of today, I have traveled a long journey. On this road, I have experienced happiness and success as well as disappointment and failure. Through this doctoral experience, my research abilities, compression ability, and capacity in life have all been significantly enhanced. I am deeply grateful for everything that this experience has brought me, whether it was good or bad. I believe that every step I take will provide guidance and help for my future life. Of course, I also have regrets and remorse in my past life. However, as an old Chinese saying goes, "悟已往之不谏，知来者之可追。实迷途其未远，觉今是而昨非", I will continue to work hard and make progress in the future.

First of all, please allow me to show my highest respect to Prof. Matsuyama. The successful completion of this dissertation is inseparable from the earnest guidance of Prof. Matsuyama. Prof. Matsuyama's rigorous academic attitude and profound knowledge are worth a lifetime of learning for me. In addition, I want to express special gratitude to Takagi sensei for his meticulous guidance in my research. Takagi sensei is gentle and knowledgeable, and he gives me lots of valuable suggestions and solutions regarding my research and dissertation. Here, I hope to convey my sincerest gratitude to them and wish them all the best in their future work and life.

Secondly, I would like to express my sincere thanks to Ogino sensei and Mori sensei for their extensive efforts dedicated to this doctoral dissertation. In addition, I sincerely thank Dr. Guan for his substantial contributions to the completion of this doctoral dissertation. Furthermore, I would like to express my gratitude to Kumagai sensei, Ms. Miyake, Ms. Kamio, and Ms. Ono in Membrane Engineering Group; the smooth development of scientific research is closely related to their kind support and help. I sincerely wish them all the best and all their wishes come true. Meanwhile, I also hope everyone of my friends can smooth their research and realize their dreams in the future.

Finally, I would like to express my gratitude to my family and friends in China. Their care and support have been of immense help and comfort to me. In the future, I will continue to work hard.

ZHOU SIYU

Graduate School of Engineering

Kobe University, Japan

January 15, 2024

Table of contents

Chapter 1

General introduction

1.1 Research background

Water, the precious resource on which life on earth depends, is becoming extremely scarce and seriously polluted [1]. Water shortage induced by population growth, climate change, and freshwater pollution has become one of the major global challenges that people need to face in the 21st century [2]. The imbalance between supply and demand due to insufficient water quantity and poor water quality increasingly hinders the sustainable development of industrial and social activities (**Fig. 1.1**) [3]. By 2035, up to 40% of the world's population will live in areas with severe water stress, and the ability of ecosystems to provide freshwater supplies will be increasingly compromised [4]. In addition to overall water shortages, inferior water quality caused by water pollution has attracted widespread attention around the world [5]. According to the World Health Organization, approximately 1.2 billion people lack access to safe water and 2.6 billion lack adequate sanitation. In addition, up to 2.2 million people die every year from diarrhea and other diseases closely related to water-borne infections. Therefore, the growing global demand for drinking water and wastewater treatment has promoted extensive research, development, and application of water treatment technology [6].

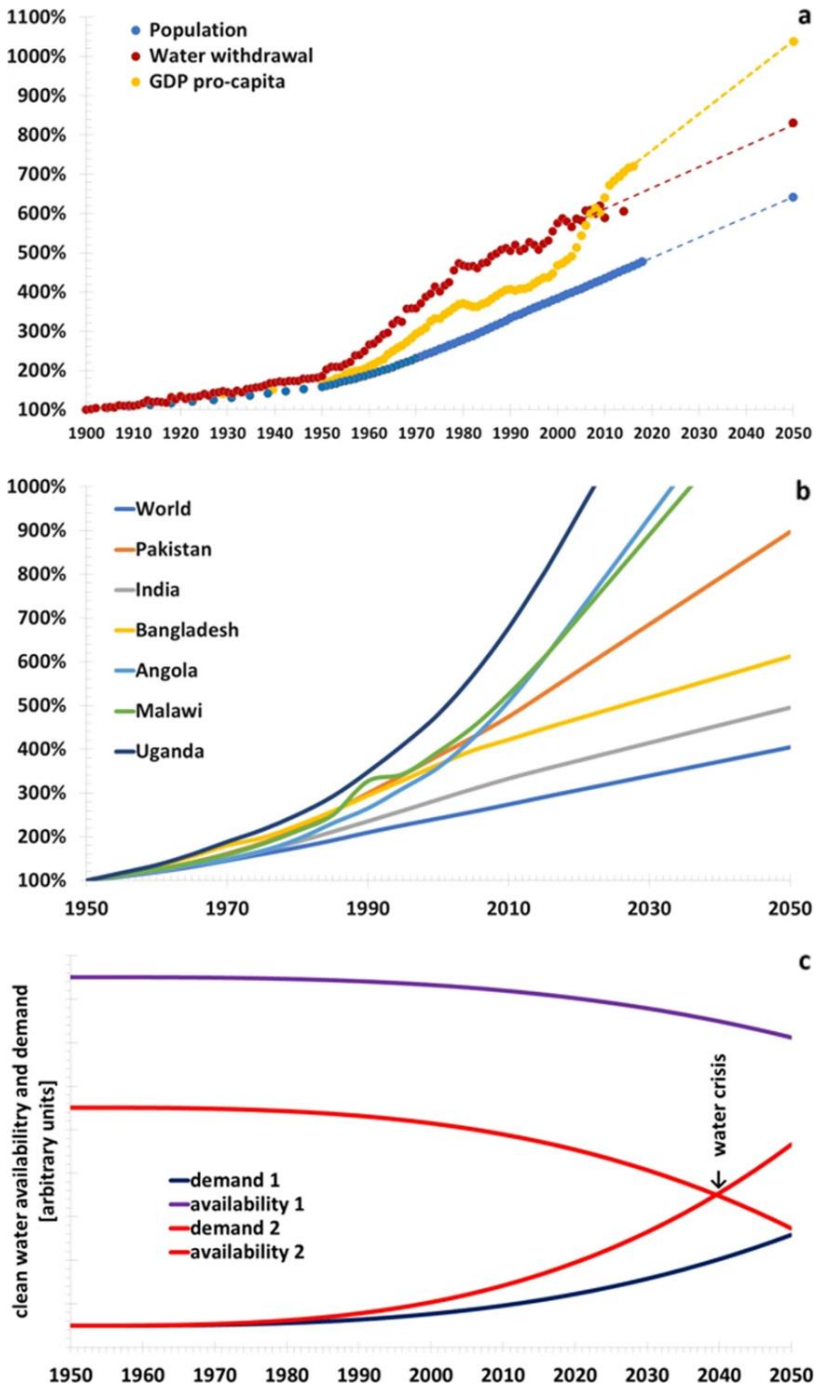

Fig. 1.1 (a) Water withdrawal, GDP pro-capita, and world population, (b) the population of the world and selected countries of Asia and Africa, (c) graphical concept of water scarcity, resulting from a more than linear growing demand and a similarly more than a linear reduction of clean water availability [7].

In order to solve the shortage of freshwater and promote the sustainable development of water resources, there are two main measures, including the

development of emerging freshwater sources through the desalination of seawater, and the utilization of water resources improved by the recycling and reprocessing of water bodies such as domestic wastewater and industrial sewage [8]. To date, various conventional treatment processes have been applied to treat water pollution, mainly including screening, coagulation/flocculation, filtration, and chlorination/fluoridation [9]. Compared with energy-intensive traditional separation processes, membrane separation technology, as an emerging green separation technology, has been widely used in the fields of seawater desalination, advanced sewage treatment, and resource utilization [10].

1.2 Membrane and membrane technology

The separation process is the foundation of the biopharmaceutical, food, agricultural, chemical, and petrochemical industries. Membrane separation, as an advanced separation technology, originated in the early 20th century and experienced rapid development in the 1960s. In recent years, membrane separation technology has been widely applied and played a positive role in separation processes in various fields, including chemical engineering, environmental protection, metallurgy, pharmaceuticals, food, energy, and more. Generally, membrane separation technology involves chemical synthesis, materials, membrane fabrication and modification, module design, and process engineering, among other aspects. Therefore, advancements in membrane technology not only improve practical industrial processes but also stimulate the development of related scientific and manufacturing industries, which is indeed an important and sustainable foundational separation technology. In addition, membrane separation is a technique driven by differences of transmembrane concentration and/or pressure that enables selective separation by allowing the transport of smaller molecules while rejecting solutes with larger sizes [11]. As an emerging wastewater treatment technology, membrane separation has developed rapidly in recent years due to its advantages of no phase change, lower energy consumption, more facile operations, and better selectivity (**Fig. 1.2**). According to the pore size of the membrane, membrane

separation technology could be divided into microfiltration (MF) [12], ultrafiltration (UF) [13], nanofiltration (NF) [14] and reverse osmosis (RO) [15] membranes (**Fig. 1.3**).

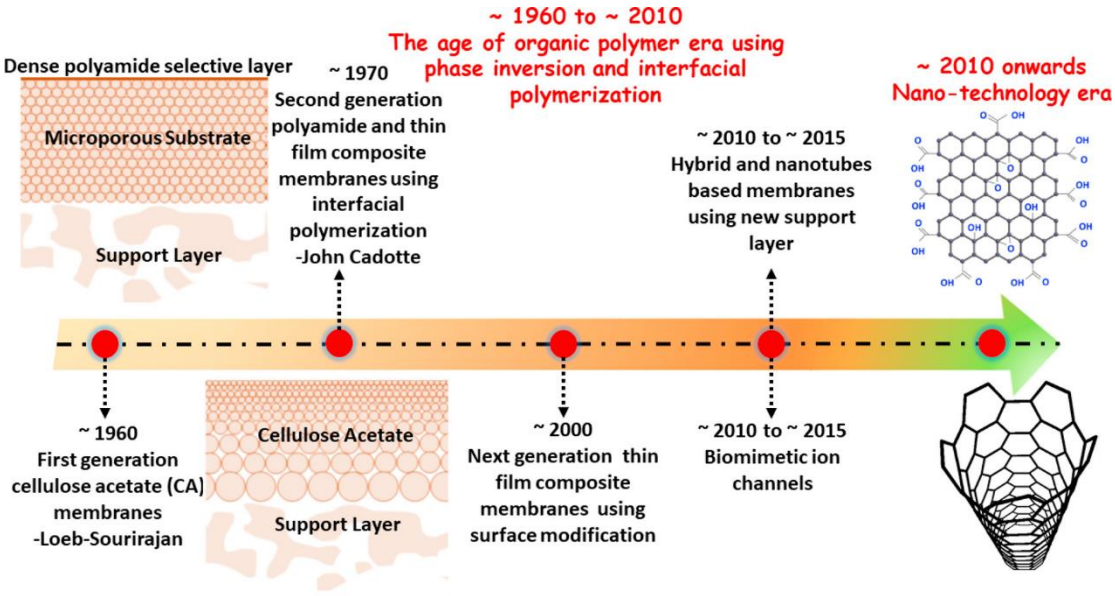

Fig. 1.2 Trends and developments in membrane materials from 1960 to the present [16].

1.2.1 Microfiltration membrane

Microfiltration (MF) membranes find applications in a wide range of industries, from water treatment to the pharmaceutical and food industries, due to their versatile and cost-effective separation capabilities. MF [17], also known as microporous filtration, refers to a separation technology with a pore size typically ranging from 0.1 to 10 μm, and it is the primary method for treating suspensions. The particle retention mechanisms of MF primarily include screening, adsorption, and bridging. Screening refers to mechanical retention applied to intercept particles larger than the membrane pore size or equivalent to the membrane pore size. Adsorption refers to particles being retained on the membrane surface through physical and/or chemical interactions. Bridging appears when most contaminants cannot enter the membrane pores or get stuck within the pores due to the accumulation and compression of particles, leading to effective retention. The advantages of MF technology: (1) Comprehensive retention of particles larger than the membrane pore size; (2) High filtration precision and strong

reliability; (3) High flux; (4) Thin membrane thickness; (5) No media shedding, which prevents secondary pollution. However, MF technology with some shortcomings, such as small particle capacity, easy clogging, and almost no interception effect on small molecules and inorganic salts.

1.2.2 Ultrafiltration membrane

Ultrafiltration (UF) is used in environmental applications, such as groundwater remediation and the removal of contaminants from industrial wastewater. In addition, UF is also one of the pressure-driven membrane separation technologies with a pore size range of 2-100 nm. This pore size between microfiltration (MF) and nanofiltration (NF) is mainly applied to reject macromolecules, colloids, proteins, particles, etc. with a molecular weight cutoff greater than 500 Da [18]. Recently, the UF process has been widely used in production and life with the advantages of no phase change, high separation coefficient, low operating pressure, superb water flux, and no secondary pollution [19]. However, there are some disadvantages of UF membranes that will limit their performance. The inherent hydrophobicity and low hydrophilicity of UF cause the membrane surface extremely susceptible to contamination during long-term operation. Meanwhile, increased frequency of membrane surface cleaning, shortened service life of the membrane and increased operating costs are induced due to the adsorption and accumulation of pollutants on the outer surface of the membrane and within the channels [20].

1.2.3 Reverse osmosis membrane

Reverse osmosis (RO) is a membrane treatment technology that employs the pressure difference on the feed and permeate sides of the membrane as a driving force to overcome the osmotic pressure of the solvent, which allows the solvent to pass through while rejecting the solute, thereby achieving separation, purification, and concentration of the mixture solutions [21]. In addition, RO with a pore size of less than 1nm is capable of removing all impurities from water, including trace organics as well

as inorganic [22]. RO is regarded as one of the most promising technologies in the 21st century, including the merits of no phase change, simple process, and low energy consumption. Nowadays, RO membranes are developing rapidly in fields such as the preparation of ultrapure water and pharmaceutical water, food processing, municipal wastewater, electroplating, printing and dyeing, papermaking wastewater treatment and reuse, and desalination of seawater and brackish water. However, membrane fouling would become the main factor hindering the further application of RO membranes because it leads to increased chemical cleaning frequency, higher operating costs, and reduced membrane separation performance [23].

1.2.4 Nanofiltration membrane

Nanofiltration (NF) is an emerging pressure-driven membrane separation technology between UF and RO [24]. NF membranes are a valuable tool in a wide range of applications, thanks to their ability to selectively separate substances and improve water quality with relatively low energy consumption and environmental impact. In addition, NF is one of the promising and practical membrane treatment technologies in wastewater treatment and has attracted widespread attention in the field of seawater desalination. The operating pressure and pore size of NF are between those of UF and RO, which indicates that NF could effectively separate divalent salts while maintaining excellent permeance at relatively low operating pressure [25-27]. Since the flux of NF membrane is higher than that of RO membrane and its rejection is better than that of UF membrane, it has achieved satisfactory development and application in the fields of desalination, screening, and purification. At present, the NF separation membranes generally have shortcomings including low flux, poor anti-fouling ability, and short service life. Therefore, the development and preparation of advanced NF membranes with high flux, high rejection, and long service life have become important research directions in water treatment membrane technology.

The purpose of this dissertation is to improve the performance of NF membranes, especially graphene oxide-based NF membranes. Thus, the following sections provide

a more detailed explanation of the NF membrane.

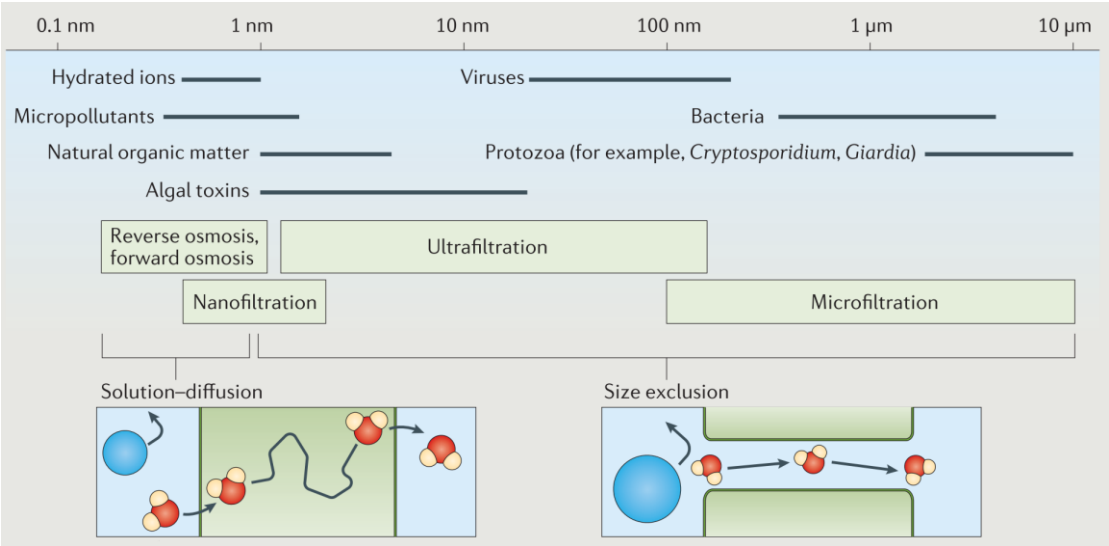

Fig. 1.3 Schematic diagram of the membrane separation technology [28].

1.3 Nanofiltration membrane categories

In 1984, NF membranes were applied industrially for the first time to solve the problem of offshore oil field water treatment [29]. These experimental results indicate that the NF membrane could selectively remove sulfate in seawater at high flux, thereby eliminating the expansion problem of $BaSO_4$ downhole. Subsequently, NF membranes gradually entered the historical stage of seawater desalination and wastewater treatment due to their low operating pressure, high flux, and acceptable salt rejection rate. To date, NF technology has been widely used in the purification and concentration of chemicals, beverages, medicine, food, potable water deep purification, water softening, brackish water desalination, wastewater treatment and other fields. After nearly 40 years of development, the research on NF membranes has entered a stage of rapid development, and membrane materials have also been greatly expanded. At present, the superiority of inorganic NF membranes is gradually emerging although organic polymer membranes still occupy a dominant position. The following are brief exploration of different separation membrane materials.

1.3.1 Traditional polymeric NF membranes [30-32]

Based on the membrane structure, traditional organic polymer NF membranes are commonly classified into two distinct types: symmetric (isotropic) and asymmetric (anisotropic) structure, as illustrated in **Figure 1.4**. Symmetric membranes maintain a consistent and uniform composition across their entire membrane thickness. Conversely, asymmetric membranes exhibit a structural gradient. In symmetric membranes, the separation properties are influenced by the entire structure, offering consistent filtration characteristics throughout the membrane. However, for asymmetric membranes, the separation properties predominantly hinge on the densest region within the membrane—the selective layer. This selective layer acts as the primary filtration barrier, while the accompanying support layer contributes to the durability and structural integrity of membranes. This structural asymmetry provides enhanced selectivity and efficiency in separation processes, particularly beneficial in precision-demanding NF applications. Nowadays, commercial organic NF membranes are mainly composed of aromatic polyamide, cellulose acetate, polysulfone, melamine/phenolic resin, polyethersulfone, polyacrylonitrile, melamine/polypropylene, etc. Therein, cellulose acetate possesses the advantages of readily available raw materials, low cost, high water permeability, and good chlorine resistance. However, the application of this membrane is limited due to its poor oxidative resistance, resistance to biodegradation, resistance to organic solvents, pH resistance, and mechanical properties. In addition, polysulfone NF membranes exhibit excellent mechanical stability and outstanding resistance to acid-base corrosion and temperature. However, their limited hydrophilicity, poor biological stability, and susceptibility to fouling impose certain limitations on their application. Furthermore, the modification of membrane materials by coupler with appropriate charges (such as sulfonated polysulfone, etc.) is a common method applied to enhance the anti-fouling properties of membranes. Typically, this method not only improves the anti-fouling of membranes but also exhibits obvious advantages in terms of water permeability and selective permeability. In summary, organic NF membranes are characterized by a wide variety of raw materials, simple preparation processes, and

affordability, leading to significant development in recent years. However, these NF membranes are confronted with challenges in terms of mechanical stability, temperature resistance, chlorine resistance, acid-base corrosion resistance, biodegradability, and solvent resistance.

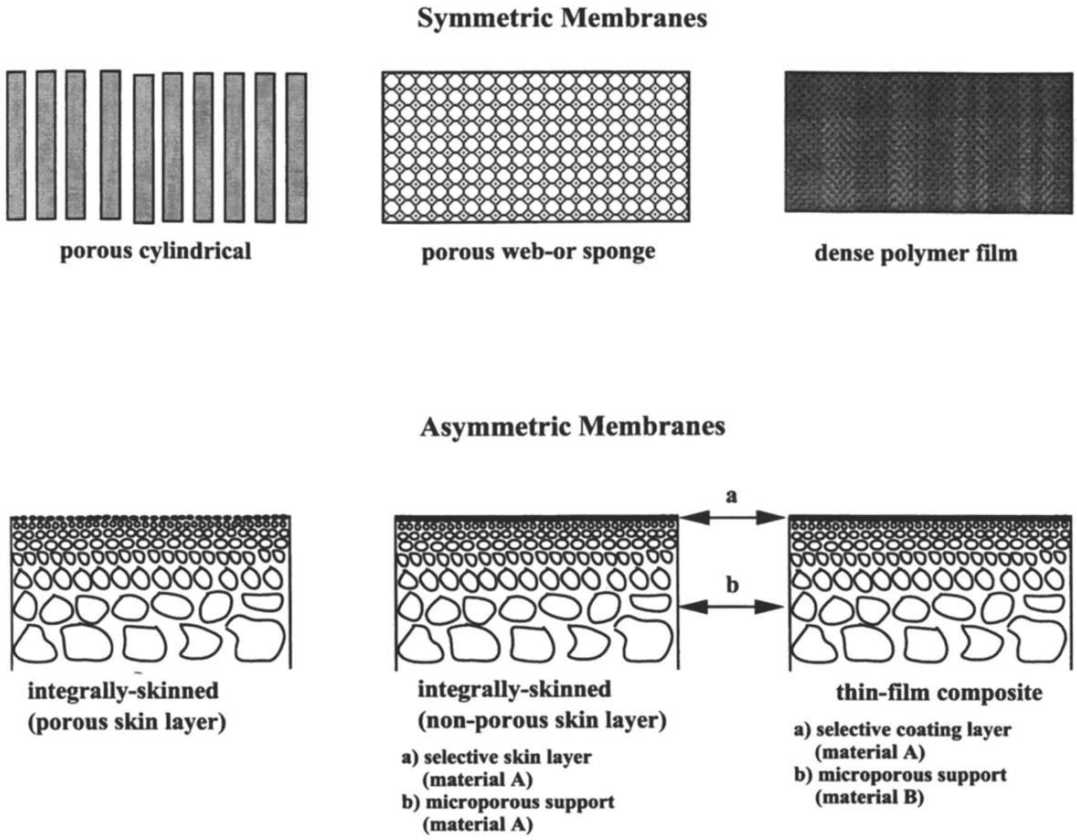

Fig. 1.4 Schematic representation of symmetric and asymmetric membrane structures [33].

1.3.2 Inorganic nanofiltration membranes

In order to overcome the inherent drawbacks of traditional organic polymer NF membranes, various ceramic materials such as SiO_2 [34], TiO_2 [35], and ZrO_2 [36] are used to prepare porous inorganic NF membranes. Initially, ceramic materials are hydrolyzed to form sol, then the sol-gel method is employed to coat the surface of support materials. Finally, inorganic NF membranes with pore sizes smaller than 4 nm are prepared through high-temperature calcination methods. The NF membranes fabricated by this method exhibited uniform pore size distribution and reliable

performance (**Fig. 1.5**). It is worth mentioning that although inorganic NF membranes overcome the stability drawbacks of organic NF membranes, their further development is hindered due to the complex prepare technology, the repeated coating and sintering are required, and achieving narrower pore sizes is difficult.

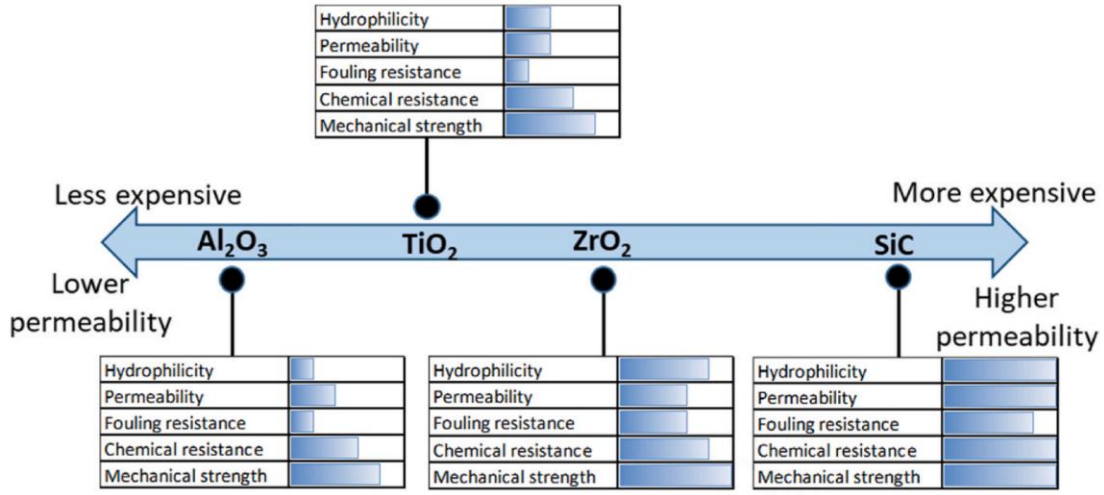

Fig. 1.5 Relative properties of ceramic membrane fabricated using alumina, titania, zirconia, and silicon carbide [36].

1.3.3 Two-dimensional (2D) laminar NF membranes

Recently, multitudinous 2D materials have been adopted as building blocks for the preparation of high-performance membranes, including graphene and its derivatives [37], layered metal dichalcogenides (LMDCs) [38], metal oxides and 2D zeolites [39], metal-organic framework (MOF) nanosheets [40], 2D covalent organic frameworks (2D-COFs) [41] and so on. Among these, in addition to the price advantage due to the continuously expanding production scale of GO [42], its impermeability to gases and liquids other than water molecules, as well as the rapid transport of molecules within the two-dimensional channels between layers, cause GO-based NF membranes expected to become the next generation mainstream NF membranes. Compared to the complexity of the sol-gel preparation method and the difficulty of adjusting pore size, 2D laminar NF membranes with controllable nanochannels and high performance have gradually attracted the attention of researchers [43]. The membrane treated in this dissertation, GO-based NF membrane, is one of two-dimensional membranes.

As shown in **Fig. 1.6**, the 2D graphene oxide (GO) membrane is deposited on the surface of the PES substrate through simple vacuum filtration method, thereby forming the layered stacked structure [44]. Among them, by introducing in-plane nanopores into graphene oxide (GO) nanosheets, more transmission paths and shorter transport distances could be obtained, thus enhancing membrane flux. Meanwhile, the controllable sub-nanometer channels of 2D laminar membranes present significant advantages for achieving ion separation. Compared with the porous inorganic NF membranes, 2D membranes have great potential to be powerful and scalable [45].

The following sections provide a more detailed explanation on GO-based NF membrane.

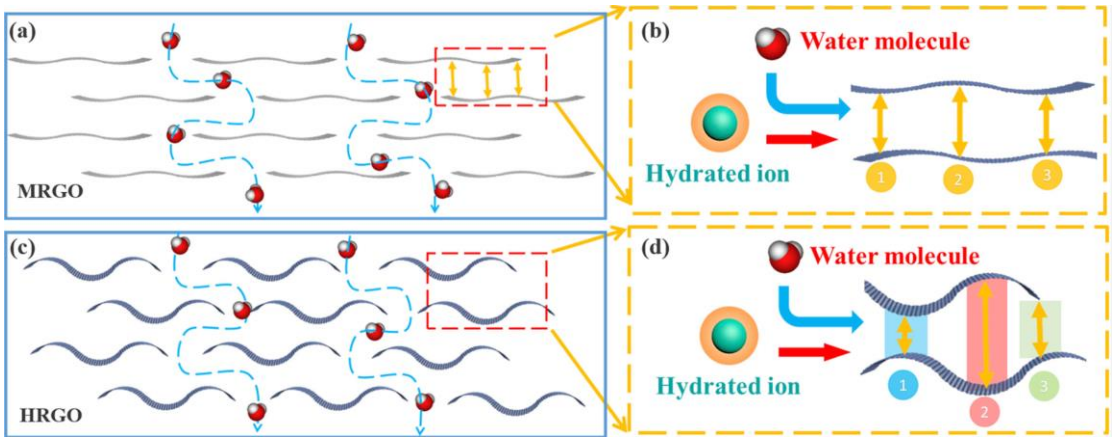

Fig. 1.6 Schematic of water transport and salt rejection through 2D nanochannels.

1.4 Two-dimensional graphene oxide based nanofiltration membranes

1.4.1 Graphene and its derivatives

Graphene is a single-layer, two-dimensional crystal formed by carbon atoms connected through sp^2 hybridization, where carbon atoms are arranged regularly within a hexagonal honeycomb lattice structure (**Fig. 1.7**) [46]. Each carbon atom in graphene is bonded to three neighboring carbon atoms by σ bond. The remaining p electrons tend to form π bonds of orbitals perpendicular to the plane with the surrounding atoms. This allows the π electrons to move freely in these long-range π orbitals, endowing graphene with excellent electrical conductivity. Furthermore, graphene exhibits excellent mechanical properties due to each carbon atom in graphene forms strong σ bonds with

three adjacent carbon atoms [47]. Recently, scientists at Columbia University used atomic force microscopy to directly test the mechanical properties of single-layer graphene and found that its Young modulus is approximately 1100 GPa, with a breaking strength reaching 130 GPa, which is 100 times higher than the superb steel materials [48]. In addition, graphene possesses the ability for high thermal conductivity while having an ultra-high electrical conductivity [49]. The thermal conductivity of a single-layer of defect-free graphene is as high as 5300 W m^{-1} K^{-1}, which is one of the highest thermal conductivity among known materials [50, 51]. It is worth noting that graphene has an extremely high theoretical specific surface area (2630 m^2 g^{-1}) due to its unique single atomic layer structure [52]. The above-mentioned properties impart graphene broad prospects for applications in important fields such as nanodevices, sensors, hydrogen storage materials, composite materials, and more.

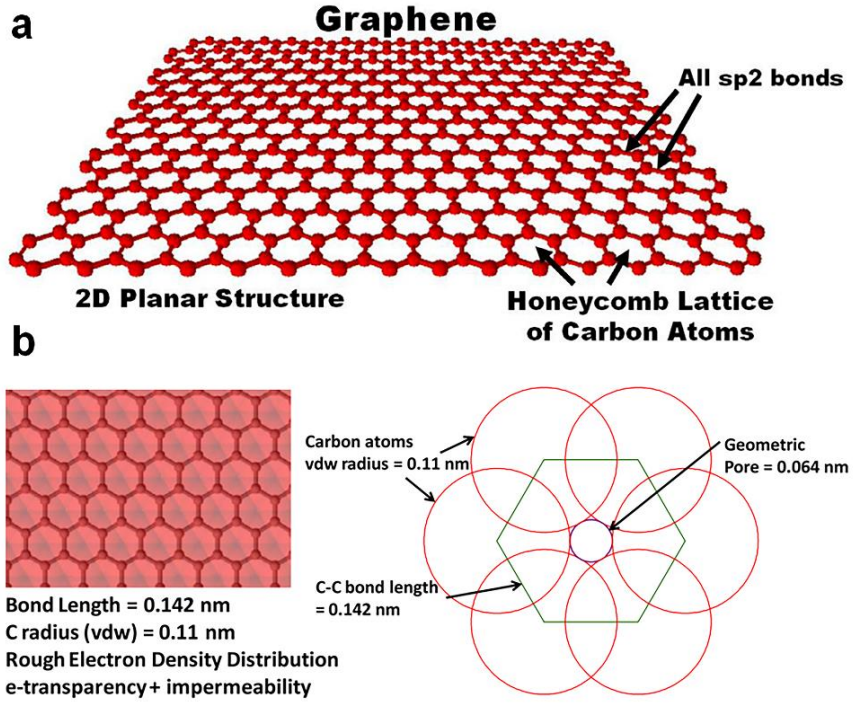

Fig. 1.7 (a) Graphene lattice structure: sp^2 hybridized carbon atoms arranged in a 2D honeycomb lattice, (b) the molecular structure with rough electronic density distribution: while graphene is relatively transparent to electrons, it is practically impermeable to all molecules at room temperature. Geometric pore (0.064 nm) is also small enough not to allow molecules to pass through [53].

As an important derivative of graphene, graphene oxide (GO) also possesses atomic thickness, nearly frictionless surface, and excellent tensile strength, which endows it lower transmission resistance and higher flux in practical applications [54-56]. Similar to graphite, GO is a 2D laminate structure and could be stacked layer by layer through hydrogen bonding and other forces between layers [57]. Unlike hydrophobic graphene, GO is the oxidized form of graphene and contains abundant oxygen-containing functional groups on the basal planes and edges of nanosheets including epoxy groups, hydroxyl groups, carbonyl groups, and carboxyl groups, which imparts it with satisfactory hydrophilicity (**Fig. 1.8**) [58]. These oxygen-containing functional groups create electrostatic repulsion between GO sheets and expand the interlayer spacing, which not only acts as a water permeation channel but also complements any existing pores on the basal plane or grain boundaries between GO flakes [59]. Furthermore, these functional groups enhance the hydrophilicity of GO, allowing for the design of GO microstructures and properties [60]. Additionally, GO can be produced on a large scale through cost-effective methods [61]. The solution synthesis method provides the opportunity for surface functionalization, thereby conferring diverse functions to GO.

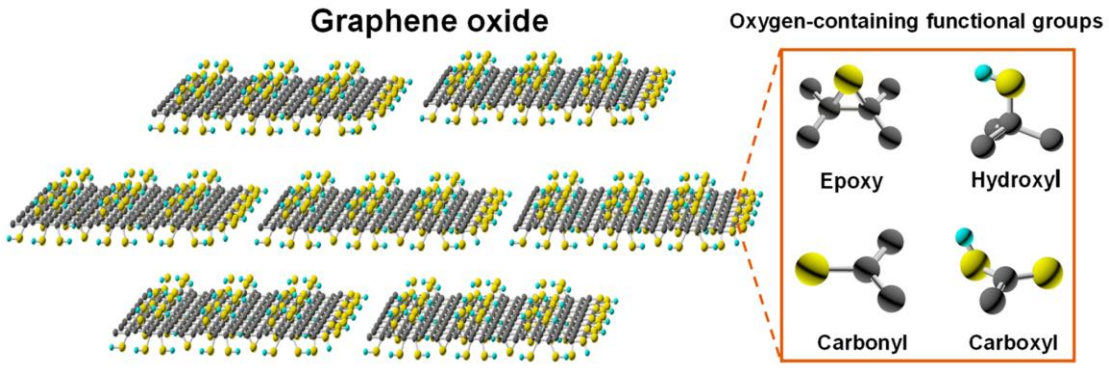

Fig. 1.8 Schematics of the molecular structure of graphene oxide [59].

1.4.2 Structure and separation mechanism of graphene oxide membranes

Graphene oxide membranes are mainly divided into graphene oxide-based hybrid membranes and graphene oxide laminate membranes. Among them, graphene oxide-

based hybrid membranes typically involve the auxiliary modification of polymeric membrane materials based on the excellent properties of graphene oxide, such as hydrophilicity, mechanical strength, and antifouling properties. Graphene oxide laminate membranes exhibit superb permeability to water molecules and can selectively separate solutes based on their nanoscale interlayer spacing. Furthermore, graphene oxide laminate membranes with ultrathin layered structures would be obtained due to their excellent dispersibility. This property allows for the preparation of uniform graphene oxide laminate membranes. However, different support substrates are required for the fabrication of graphene oxide laminate membranes due to their extremely thin intrinsic thickness.

The water transport pathways of the GO membrane are depicted in **Fig. 1.9**. According to the fluid transport pathways, the transport channels within the GO separation layer could be divided into two parts [62]. On the one hand, there are porous structures formed by the defects on the basal plane and interedge gap between horizontally aligned GO nanosheets. On the other hand, there are 2D nanocapillaries between vertically stacked GO nanosheets. These transmission paths, which are composed of physical structures, obey the steric hindrance effect. In addition, graphene oxide exhibits electronegativity due to the presence of oxygen-containing functional groups, which triggers electrostatic interactions between charged molecules and ions and the membrane surface, known as the Donnan effect [63].

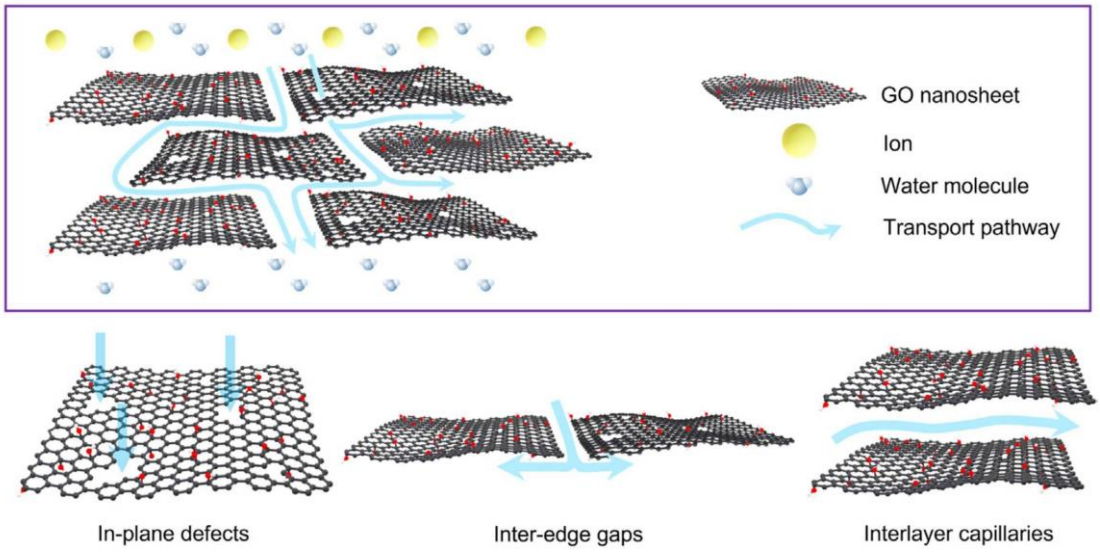

Fig. 1.9 Schematic illustration of water transport pathways across GO membranes, including in-plane defects in GO, interedge gaps between horizontally aligned GO, and interlayer nanocapillaries between vertically stacked GO [64].

(1) Size exclusion

Based on the different size between the diameter of the target substances and the membrane pore sizes, larger substances are difficult to pass through the separation membrane and are rejected, while relatively small substances could easily pass through the pores and narrow gaps of the separation membrane (**Fig. 1.10**). This physical size sieving can be applied to all solute systems.

(2) Donnan equilibrium theory

The Donnan equilibrium theory refers to the membrane rejection induced by electrostatic repulsion between the charge on the membrane surface and substances in the solution with the same charge (**Fig. 1.10**). Meanwhile, in order to maintain the electroneutrality conditions of the bulk solutions, substances with opposite charges are also rejected [65]. It is worth noting that the Donnan theory is applicable to charged separation membranes, allowing interaction with charged particles in the solution, such as sodium salts, magnesium salts, potassium salts, and so on.

(3) Ionization

Inoization refers to the deprotonation of carboxylic acid and other functional groups on the surface of the separation membrane to produce a certain electrostatic force (**Fig. 1.10**). The presence of electrostatic repulsion prevents contaminants with the same charge in the solution is different to approaching the membrane surface, thus impeding the passage of such substances through the separation membrane. In addition, the hydrophilicity of the membrane surface is generally enhanced due to the functional groups on the membrane surface with highly hydrophilic [66]. This exceptional hydrophilicity promotes the tight adsorption of water molecules on the membrane surface, forming a shielding layer [67], leading to hydrophobic organic compounds (such as antibiotics, pesticides, etc.) having difficulty approaching the surface of the

separation membrane.

(4) Others such as the dehydration effect and π-π effect

Generally, the "real" size of the ions is revealed when they are transferred across the narrow nanochannels of the GO membrane. Dehydration and rearrangement appeared to be ubiquitous during filtration using subnanometer porous membranes. Water molecules were easily removed from the solvation shell when hydrated ions entered narrow pores [68]. In addition, organic macromolecules containing benzene rings could form π-π interactions with the π-bonds of GO, which lead to organic macromolecules being constrained between the GO layers and hinder their transport within the separation membrane, thereby achieving the separation of the target substances (**Fig. 1.10**). Additionally, heavy metal ions can also interact with the π-bonds of GO and thus be removed.

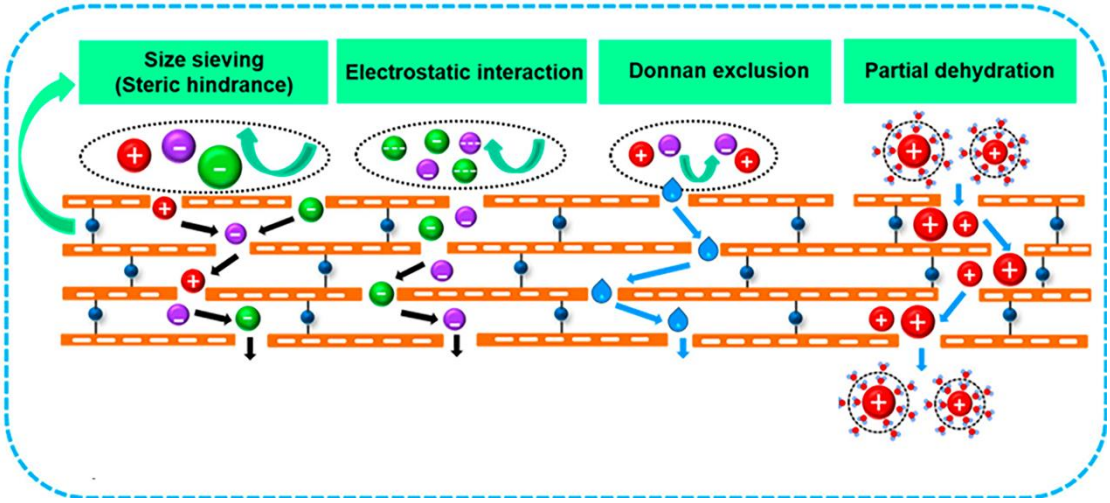

Fig. 1.10 Schematic diagrams of the purposed separation mechanisms of GO membranes [69].

1.5 Preparation methods of graphene oxide membranes

The potential of high selectivity and permeability of GO separation membrane endow it become ideal separation membrane material for water purification. Nowadays, GO laminar membranes can be prepared by vacuum filtration [70], drop-casting [71], spin-coating [72], and layer-by-layer (LBL) assembly [73] and other ways.

1.5.1 Vacuum filtration

Vacuum filtration is one of the most common methods for preparing 2D GO membranes (**Fig. 1.11a**). Dikin et al. [67] were the first to report the vacuum filtration method to prepare GO membranes with thicknesses ranging from 1 to 30 μm. The fabricated GO membranes exhibited tensile modulus as high as 32 GPa, demonstrating mechanical properties superior to traditional membranes. Additionally, vacuum filtration could induce ordered deposition of GO on the substrate by pressing water molecules out from between the nanosheets. Subsequently, the GO membrane with a dense structure is formed on the substrate and relies on hydrogen bonding forces and π-π interactions between the nanosheets. Finally, GO membranes with different thicknesses are obtained by adjusting the concentration or volume of GO.

This method is widely applied in the large-scale preparation of layered GO membranes due to its advantages including simplicity of operation, ease of control, flat membrane formation, and stable performance [74]. However, GO laminate membranes prepared by the vacuum filtration method are challenging to completely separate from the substrate due to strong physical interlocking and intermolecular forces between them.

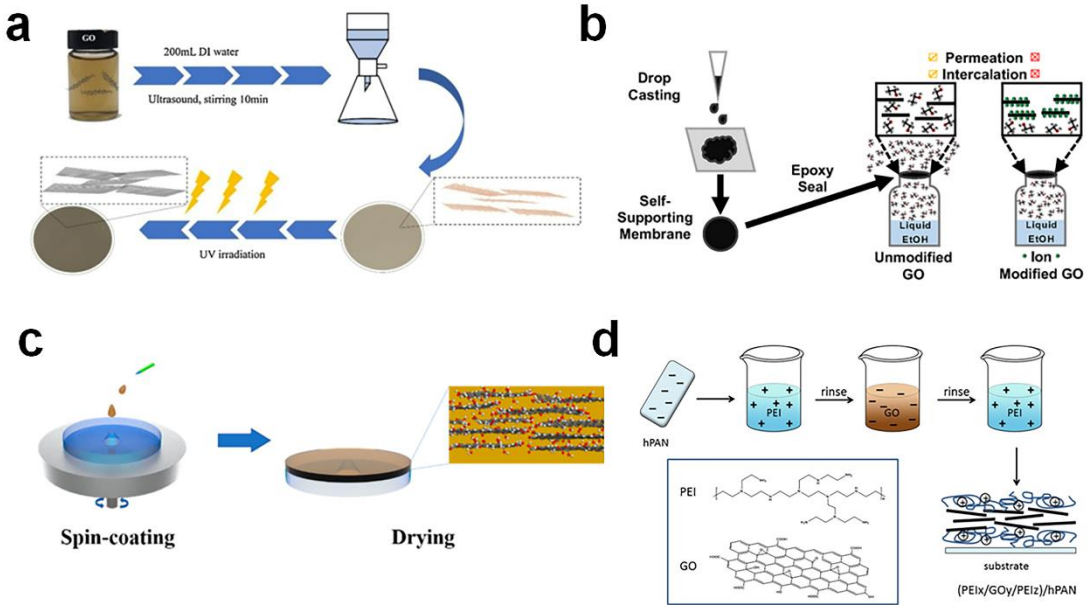

Fig. 1.11 (a) Preparation of GO membranes by vacuum filtration [75], (b) preparation of GO membranes by drop-casting [76], (c) preparation of GO membranes by spin-

coating [77], and (d) preparation of GO membranes by layer-by-layer (LBL) assembly [78].

1.5.2 Drop-casting

Drop-casting is another basic method commonly applied for preparing GO membranes (**Fig. 1.11b**) [79]. This process involves directly dropping a prepared dispersion of GO at a specific concentration onto a smooth substrate and then allowing it to dry either by air drying or through exposure to light. After that, the GO layered membrane can be fully and successfully separated from the substrate [80]. It is worth mentioning that this method is simple to operate and possesses high utilization rate of raw materials. However, the prepared membrane is prone to defects like wrinkles and breaks after drying. In addition, the expansion of membrane dimensions is a difficult task as solvent evaporation hinders rapid processing of the membrane.

1.5.3 Spin-coating

The spin-coating method is to first apply the prepared GO solution onto the substrate, and then uniformly disperse the solution on the surface of the substrate by rotating at a certain speed and temperature (**Fig. 1.11c**) [81]. Finally, the 2D GO membranes are obtained after drying. This type of GO membrane is very uniform, dense, and regular due to the spin-coating method primarily relying on centrifugal force. However, it is inevitable that there are errors in dosage and concentration. Therefore, the GO membranes prepared by this method are characterized by uniformity but low concentration accuracy.

1.5.4 Layer-by-layer assembly

Layer-by-layer (LBL) assembly is also a common method for depositing GO materials onto substrates (**Fig. 1.11d**) [82]. During the assembly process, adjacent nanosheets are stably held together by various forces, including covalent bonding, electrostatic forces, or both. Therefore, some functional molecules can be introduced

for constructing modified membranes during the membrane fabrication process. Compared to the spin-coating method, layer-by-layer assembly focuses on the interaction between layers and the design of interlayer structures. The thickness of GO membranes can be controlled at the molecular level by adjusting the number of deposition cycles. However, this process is relatively complex as it usually requires pre-treatment of GO. Furthermore, compared to the vacuum filtration method, the surfaces of GO membranes obtained through layer-by-layer assembly are very rough because the assembly process is random, which hinders the migration of water molecules [73, 83].

1.6 Challenges faced by graphene oxide membranes

1.6.1 The improvement of structural stability

The great potential of GO laminate NF membranes in the field of separation has been confirmed through significant progress in material preparation, synthesis, and separation. However, the stability of stacked GO membranes in water environments is challenging to maintain in the long term due to the abundant hydrophilic functional groups of nanochannels [84]. Furthermore, the precise control of the nanoscale interlayer spacing of GO membranes is highly challenging in actual aqueous separation processes due to the hydration interactions between the layers. Research has exhibited that the interlayer spacing of dry GO membranes is approximately 0.8 ± 0.1 nm [85]. After prolonged wetting, the interlayer spacing increased significantly due to the intercalation of water molecules. Based on the above, the separation performance of GO membranes suffers a great loss due to the swelling phenomenon. Therefore, it is necessary to develop effective methods to enhance the stability and selectivity of graphene oxide nanochannels in water environments.

1.6.2 The improvement of separation performance

The water permeability and solute retention are crucial performance parameters for evaluating separation membranes in water treatment applications, which are

primarily influenced by the stacking behavior and interlayer spacing of GO nanosheets [86]. For separation layers consisting solely of GO nanosheets, the degree of oxidation directly determines the interlayer spacing of the stacking nanochannels. On the one hand, the interlayer spacing of GO membranes could be supported by the inherent size of oxygen-containing functional groups. On the other hand, the unsatisfactory swelling of nanochannels in aqueous environments is primarily attributed to the hydrophilicity of oxygen-containing functional groups, which induces water molecules to remain within the nanochannels, thereby reducing stability and increasing interlayer spacing of the nanochannels. Nowadays, it is widely recognized to employ reduction methods to decrease the oxygen-containing functional groups on GO in order to narrow the interlayer spacing. The stronger π-π interactions between neighbor GO layers with lower oxidized degrees would reduce the interlayer space occupied by oxygen-containing functional groups while simultaneously hindering the swelling of nanochannels [87]. Therefore, retention could be enhanced by controlling the density of oxygen-containing functional groups on GO, but this often results in a significant compromise of permeance. To date, numerous methods have been successfully applied to the regulation and improvement of GO nanochannels. The separation layers of graphene oxide with different interlayer spacing can be prepared by intercalating nanoparticles with different sizes including TiO_2, SiO_2, Si_3N_4, etc. into the interlayer of graphene oxide, which leads to the expansion of nanochannels and the improvement of water flux [88]. In addition, the porous metal-organic framework (MOF) materials as intercalation materials coupled with graphene oxide also provide more transmission paths for the transmission of water molecules [89]. In addition to providing additional transport pathways for water molecules to enhance water permeance, some negatively charged materials (carbon nanotubes) also be introduced as intercalation materials into nanochannels, which will lead to a stronger Donnan effect and improve the retention of charged solutes [90]. However, the methods of introducing intercalation materials between the layers of graphene oxide would break the integrity and continuity of the nanochannel of graphene oxide, resulting in non-uniform performance and defects in

the separation layer. Furthermore, the enlarged interlayer spacing generally leads to the separation of relatively large-sized solutes (e.g., dye molecules) and is rarely able to remove small solutes (e.g., small salt solutes) from the water although there are significant improvements of water flux.

1.7 Purpose and overview of this dissertation

Graphene oxide (GO) has a wide range of applications and significant potential due to its unique two-dimensional structure and tunable chemical properties. Furthermore, GO membranes as selective barriers exhibit fascinating characteristics for precise sieving of solutes in aqueous solutions. However, the separation performance and stability of nanochannels, which are prerequisites for widespread application, have become a significant bottleneck for the development of GO membranes in water environment technologies. On the one hand, the abundant oxygen-containing functional groups on GO nanosheets strongly hydrate with water molecules, thereby enhancing electrostatic repulsion and limiting π-π attraction, which may cause swelling or even disintegrate the GO membrane in the water environment. On the other hand, the expansion of the interlayer spacing induced by the swelling phenomenon restricts the retention performance of the separation membrane. Therefore, it is crucial to enhance the stability of the graphene oxide structure while controlling the nanochannel size to optimize the desalination performance of nanochannels. Based on the above-mentioned matters, there are provided insights and considerations for constructing stable confined nanochannels, analyzing nanochannel deformations, and optimizing nanochannel properties.

This dissertation includes 5 chapters.

Chapter 1: The research background and purpose of this research are generally introduced.

Chapter 2: Selective ion/ion transport is of great importance in environmental and energy applications. Nanofiltration membranes possessing sub-nanometer pore sizes and charge characteristics have garnered significant attention in effectively separating

target ions. Nevertheless, the contributions of pore size, charge, and their combined impact on ion/ion separation have remained relatively unexplored. In this chapter, a well-defined example is presented using multilayered graphene oxide membranes with ordered interlayer nanochannels. These membranes were utilized to prepare diverse nanochannel types, each possessing distinct channel sizes and charge properties. A systematic investigation was conducted to discern their separation selectivity for mono-/di-valent ion pairs. The dominant factor governing mono-/di-valent ion selectivity was not found to be the channel pore size within the sub-nanometer scale. This could be because nanochannels are flexible and cannot strictly sieve ions based on their specific size. Instead, the difference in electrostatic effects between mono- and di-valent ions plays a more significant role in enhancing ion/ion selectivity within the subnanometer channel. This study offers certain insights into selective ion transport in two-dimensional membrane nanochannels, potentially assisting in the design of nanochannels with single-ion selectivity.

Chapter 3: Chemically converted graphene oxide laminate membranes, which exhibit stable interlayered nanochannels in water environments, are receiving growing attention for their potential in selective water and ion permeation. However, how the molecule properties of conversion agents influence the stabilization of nanochannels and how effectively the nanochannel be stabilized accordingly are rarely studied. In this study, the mono-, di-, and tri-saccharide molecules of glucose (Glu), maltose (Glu2), and maltotriose (Glu3) are utilized respectively to chemically modify graphene oxide (GO). The aim was to create nanochannels with different levels of stability and investigate how the separation performance is affected by these functional conversion agents. The effects of property difference between different conversion agents on the nanochannel stabilization were evidenced. The agent with efficient chemical reduction of GO and limited intercalation effect in the resulting nanochannel ensured satisfactory nanochannel stability under desalination process. The optimal membrane nanochannel possessed significantly improved stability under various changing conditions (e.g., concentration, pressure, temperature, and flow rate) as compared to the original

GO. This study provides useful information in the design of chemical conversion agents for GO nanochannel stabilization and feasible development of the nanochannel membranes for precise separations.

Chapter 4: Multilayered graphene oxide (GO) membranes, featuring interlayered sub-nanometer channels, have garnered substantial attention for their potential in selective water and ion transport. However, the tortuous transport pathways within these GO laminates, coupled with their propensity to swell in water, have posed challenges to their desalination performance. Introducing modifications to the interlayer via nanoparticle intercalation stands as a widely employed method to widen the nanochannels for rapid transport. However, this approach generally leads to a considerable reduction in separation precision. This chapter presents a novel approach, confined interlayer modification with mediated nanoparticle intercalation, to precisely tailor GO membranes. This method ensured the improvement of water transport while retaining high ion retardation was achieved. The chapter delves into the crucial roles of confinement and mediation in the intercalation modification process of GO laminates. It underscores their essential contribution in establishing an efficient and effective desalination process. This strategic framework holds promise for extending its applicability to the precise control of the fine structure of other two-dimensional laminates, offering potential advancements in various fields beyond desalination.

Chapter 5: A summary of this dissertation is given.

References

[1] M. Issaoui, S. Jellali, A.A. Zorpas, P. Dutournie, Membrane technology for sustainable water resources management: Challenges and future projections, Sustainable Chemistry and Pharmacy 25 (2022).

[2] L. Guo, Y. Wang, M. Steinhart, Porous block copolymer separation membranes for 21st century sanitation and hygiene, Chem. Soc. Rev. 50(11) (2021) 6333-6348.

[3] C. Tortajada, Contributions of recycled wastewater to clean water and sanitation Sustainable Development Goals, npj Clean Water 3(1) (2020).

[4] B.S. Lal, Water for Life: Issues and Challenges, International Journal of Science and Research (IJSR) 8(6) (2019) 1949-1957.

[5] G.D. Kang, Y.M. Cao, Development of antifouling reverse osmosis membranes for water treatment: A review, Water Res. 46(3) (2012) 584-600.

[6] X. Qu, P.J. Alvarez, Q. Li, Applications of nanotechnology in water and wastewater treatment, Water Res. 47(12) (2013) 3931-46.

[7] A. Boretti, L. Rosa, Reassessing the projections of the World Water Development Report, npj Clean Water 2(1) (2019).

[8] M.A. Shannon, P.W. Bohn, M. Elimelech, J.G. Georgiadis, B.J. Marinas, A.M. Mayes, Science and technology for water purification in the coming decades, Nature 452(7185) (2008) 301-10.

[9] H. Abu Hasan, M.H. Muhammad, N.I. Ismail, A review of biological drinking water treatment technologies for contaminants removal from polluted water resources, Journal of Water Process Engineering 33 (2020).

[10] K. Zuo, K. Wang, R.M. DuChanois, Q. Fang, E.M. Deemer, X. Huang, R. Xin, I.A. Said, Z. He, Y. Feng, W. Shane Walker, J. Lou, M. Elimelech, X. Huang, Q. Li, Selective membranes in water and wastewater treatment: Role of advanced materials, Mater. Today 50 (2021) 516-532.

[11] B. Liang, X. He, J. Hou, L. Li, Z. Tang, Membrane Separation in Organic Liquid: Technologies, Achievements, and Opportunities, Adv. Mater. 31(45) (2019) e1806090.

[12] A. Gul, J. Hruza, F. Yalcinkaya, Fouling and Chemical Cleaning of Microfiltration

Membranes: A Mini-Review, Polymers (Basel) 13(6) (2021).

[13] N. Hampu, J.R. Werber, W.Y. Chan, E.C. Feinberg, M.A. Hillmyer, Next-Generation Ultrafiltration Membranes Enabled by Block Polymers, ACS Nano 14(12) (2020) 16446-16471.

[14] S. Shao, F. Zeng, L. Long, X. Zhu, L.E. Peng, F. Wang, Z. Yang, C.Y. Tang, Nanofiltration Membranes with Crumpled Polyamide Films: A Critical Review on Mechanisms, Performances, and Environmental Applications, Environ. Sci. Technol. 56(18) (2022) 12811-12827.

[15] R.H. Hailemariam, Y.C. Woo, M.M. Damtie, B.C. Kim, K.D. Park, J.S. Choi, Reverse osmosis membrane fabrication and modification technologies and future trends: A review, Adv. Colloid Interface Sci. 276 (2020) 102100.

[16] P. Bhol, S. Yadav, A. Altaee, M. Saxena, P.K. Misra, A.K. Samal, Graphene-Based Membranes for Water and Wastewater Treatment: A Review, ACS Applied Nano Materials 4(4) (2021) 3274-3293.

[17] J.P. Dijkshoorn, M.A.I. Schutyser, R.M. Wagterveld, C.G.P.H. Schroën, R.M. Boom, A comparison of microfiltration and inertia-based microfluidics for large scale suspension separation, Sep. Purif. Technol. 173 (2017) 86-92.

[18] R. Shoshaa, M.Y. Ashfaq, M.A. Al-Ghouti, Recent developments in ultrafiltration membrane technology for the removal of potentially toxic elements, and enhanced antifouling performance: A review, Environmental Technology & Innovation 31 (2023).

[19] D. Akhil, D. Lakshmi, P. Senthil Kumar, D.-V.N. Vo, A. Kartik, Occurrence and removal of antibiotics from industrial wastewater, Environmental Chemistry Letters 19(2) (2021) 1477-1507.

[20] X. Fan, Y. Su, X. Zhao, Y. Li, R. Zhang, J. Zhao, Z. Jiang, J. Zhu, Y. Ma, Y. Liu, Fabrication of polyvinyl chloride ultrafiltration membranes with stable antifouling property by exploring the pore formation and surface modification capabilities of polyvinyl formal, J. Membr. Sci. 464 (2014) 100-109.

[21] M. Qasim, M. Badrelzaman, N.N. Darwish, N.A. Darwish, N. Hilal, Reverse osmosis desalination: A state-of-the-art review, Desalination 459 (2019) 59-104.

[22] C. Skuse, A. Gallego-Schmid, A. Azapagic, P. Gorgojo, Can emerging membrane-based desalination technologies replace reverse osmosis?, Desalination 500 (2021).

[23] M. Asadollahi, D. Bastani, S.A. Musavi, Enhancement of surface properties and performance of reverse osmosis membranes after surface modification: A review, Desalination 420 (2017) 330-383.

[24] A.W. Mohammad, Y.H. Teow, W.L. Ang, Y.T. Chung, D.L. Oatley-Radcliffe, N. Hilal, Nanofiltration membranes review: Recent advances and future prospects, Desalination 356 (2015) 226-254.

[25] C. Zhang, K. Wei, W. Zhang, Y. Bai, Y. Sun, J. Gu, Graphene Oxide Quantum Dots Incorporated into a Thin Film Nanocomposite Membrane with High Flux and Antifouling Properties for Low-Pressure Nanofiltration, ACS Appl Mater Interfaces 9(12) (2017) 11082-11094.

[26] H. Zhang, L. Bin, J. Pan, Y. Qi, J. Shen, C. Gao, B. Van der Bruggen, Carboxyl-functionalized graphene oxide polyamide nanofiltration membrane for desalination of dye solutions containing monovalent salt, J. Membr. Sci. 539 (2017) 128-137.

[27] W.J. Lau, S. Gray, T. Matsuura, D. Emadzadeh, J.P. Chen, A.F. Ismail, A review on polyamide thin film nanocomposite (TFN) membranes: History, applications, challenges and approaches, Water Res. 80 (2015) 306-24.

[28] J.R. Werber, C.O. Osuji, M. Elimelech, Materials for next-generation desalination and water purification membranes, Nature Reviews Materials 1(5) (2016).

[29] M. Boczkowski, P. Eriksson, M. Simionato, Water Injection and Sulfate Removal in the Offshore Oil & Gas Industry, GE Power & Water, Water & Process Technologies (2015).

[30] X. He, H. Sin, B. Liang, Z.A. Ghazi, A.M. Khattak, N.A. Khan, H.R. Alanagh, L. Li, X. Lu, Z. Tang, Controlling the Selectivity of Conjugated Microporous Polymer Membrane for Efficient Organic Solvent Nanofiltration, Adv. Funct. Mater. 29(32) (2019).

[31] Z. Yang, Y. Zhou, Z. Feng, X. Rui, T. Zhang, Z. Zhang, A Review on Reverse Osmosis and Nanofiltration Membranes for Water Purification, Polymers (Basel) 11(8)

(2019).

[32] G.M. Geise, H.B. Park, A.C. Sagle, B.D. Freeman, J.E. McGrath, Water permeability and water/salt selectivity tradeoff in polymers for desalination, J. Membr. Sci. 369(1-2) (2011) 130-138.

[33] I. Pinnau, B.D. Freeman, Formation and modification of polymeric membranes: overview, American Chemical Society Symposium (1999) 1-22.

[34] Y. Hu, Z. Lü, C. Wei, S. Yu, M. Liu, C. Gao, Separation and antifouling properties of hydrolyzed PAN hybrid membranes prepared via in-situ sol-gel SiO2 nanoparticles growth, J. Membr. Sci. 545 (2018) 250-258.

[35] Y. Lu, T. Chen, X. Chen, M. Qiu, Y. Fan, Fabrication of TiO2-doped ZrO2 nanofiltration membranes by using a modified colloidal sol-gel process and its application in simulative radioactive effluent, J. Membr. Sci. 514 (2016) 476-486.

[36] F.E. Bortot Coelho, G. Magnacca, V. Boffa, V.M. Candelario, M. Luiten-Olieman, W. Zhang, From ultra to nanofiltration: A review on the fabrication of ZrO2 membranes, Ceram. Int. 49(6) (2023) 8683-8708.

[37] J. Zhao, Z. Wang, J.C. White, B. Xing, Graphene in the aquatic environment: adsorption, dispersion, toxicity and transformation, Environ. Sci. Technol. 48(17) (2014) 9995-10009.

[38] S.Z. Butler, S.M. Hollen, L. Cao, Y. Cui, J.A. Gupta, H.R. Gutierrez, T.F. Heinz, S.S. Hong, J. Huang, A.F. Ismach, E. Johnston-Halperin, M. Kuno, V.V. Plashnitsa, R.D. Robinson, R.S. Ruoff, S. Salahuddin, J. Shan, L. Shi, M.G. Spencer, M. Terrones, W. Windl, J.E. Goldberger, Progress, Challenges, and Opportunities in Two-Dimensional Materials Beyond Graphene, ACS Nano 7(4) (2013) 2898-2926.

[39] C.J. Heard, J. Cejka, M. Opanasenko, P. Nachtigall, G. Centi, S. Perathoner, 2D Oxide Nanomaterials to Address the Energy Transition and Catalysis, Adv. Mater. 31(3) (2019) e1801712.

[40] A. Dhakshinamoorthy, A.M. Asiri, H. Garcia, 2D Metal-Organic Frameworks as Multifunctional Materials in Heterogeneous Catalysis and Electro/Photocatalysis, Adv. Mater. 31(41) (2019) e1900617.

[41] S.B. Alahakoon, S.D. Diwakara, C.M. Thompson, R.A. Smaldone, Supramolecular design in 2D covalent organic frameworks, Chem. Soc. Rev. 49(5) (2020) 1344-1356.

[42] W. Ren, H.M. Cheng, The global growth of graphene, Nat Nanotechnol 9(10) (2014) 726-30.

[43] G. Liu, W. Jin, N. Xu, Two-Dimensional-Material Membranes: A New Family of High-Performance Separation Membranes, Angew. Chem. Int. Ed. 55(43) (2016) 13384-13397.

[44] Y. Li, S. Yuan, Y. Xia, W. Zhao, C.D. Easton, C. Selomulya, X. Zhang, Mild annealing reduced graphene oxide membrane for nanofiltration, J. Membr. Sci. 601 (2020).

[45] S. Hong, F. Ming, Y. Shi, R. Li, I.S. Kim, C.Y. Tang, H.N. Alshareef, P. Wang, Two-Dimensional Ti(3)C(2)T(x) MXene Membranes as Nanofluidic Osmotic Power Generators, ACS Nano 13(8) (2019) 8917-8925.

[46] M. Xu, T. Liang, M. Shi, H. Chen, Graphene-like two-dimensional materials, Chem. Rev. 113(5) (2013) 3766-98.

[47] A. Ibrahim, A. Klopocinska, K. Horvat, Z. Abdel Hamid, Graphene-Based Nanocomposites: Synthesis, Mechanical Properties, and Characterizations, Polymers (Basel) 13(17) (2021).

[48] C. Lee, X. Wei, J.W. Kysar, J. Hone, Measurement of the Elastic Properties and Intrinsic Strength of Monolayer Graphene, Science 321(5887) (2008) 385-388.

[49] L. Zhong, L. Guo, J. Wang, Q. Song, H. Li, Y. Li, Excellent heat transfer and mechanical properties of graphite material with rolled-up graphene layers, Carbon 208 (2023) 123-130.

[50] X. Meng, H. Pan, C. Zhu, Z. Chen, T. Lu, D. Xu, Y. Li, S. Zhu, Coupled Chiral Structure in Graphene-Based Film for Ultrahigh Thermal Conductivity in Both In-Plane and Through-Plane Directions, ACS Appl Mater Interfaces 10(26) (2018) 22611-22622.

[51] L.L. Cullari, S. Ligati Schleifer, D. Kogan, G. Ziskind, O. Regev, Down the Dimensionality Lane: Thermal Conductivity Enhancement in Carbon-Based Liquid

Dispersions, ACS Appl Mater Interfaces 14(7) (2022) 9844-9854.

[52] E. Svinterikos, I. Zuburtikudis, M. Al-Marzouqi, Carbon Nanomaterials for the Adsorptive Desulfurization of Fuels, Journal of Nanotechnology 2019 (2019) 1-13.

[53] V. Berry, Impermeability of graphene and its applications, Carbon 62 (2013) 1-10.

[54] G. Liu, W. Jin, N. Xu, Graphene-based membranes, Chem. Soc. Rev. 44(15) (2015) 5016-30.

[55] Y. You, V. Sahajwalla, M. Yoshimura, R.K. Joshi, Graphene and graphene oxide for desalination, Nanoscale 8(1) (2016) 117-9.

[56] Q. Wang, C. Aubry, Y. Chen, H. Song, L. Zou, Insights on Tuning the Nanostructure of rGO Laminate Membranes for Low Pressure Osmosis Process, ACS Appl Mater Interfaces 9(27) (2017) 22509-22517.

[57] N.V. Medhekar, A. Ramasubramaniam, R.S. Ruoff, V.B. Shenoy, Hydrogen bond networks in graphene oxide composite paper: structure and mechanical properties, ACS Nano 4(4) (2010) 2300-2306.

[58] Y. Zhu, S. Murali, W. Cai, X. Li, J.W. Suk, J.R. Potts, R.S. Ruoff, Graphene and graphene oxide: synthesis, properties, and applications, Adv. Mater. 22(35) (2010) 3906-24.

[59] T. Yang, H. Lin, K.P. Loh, B. Jia, Fundamental Transport Mechanisms and Advancements of Graphene Oxide Membranes for Molecular Separation, Chem. Mater. 31(6) (2019) 1829-1846.

[60] T. Yu, Z. Xu, S. Liu, H. Liu, X. Yang, Enhanced hydrophilicity and water-permeating of functionalized graphene-oxide nanopores: Molecular dynamics simulations, J. Membr. Sci. 550 (2018) 510-517.

[61] S. Pei, H.-M. Cheng, The reduction of graphene oxide, Carbon 50(9) (2012) 3210-3228.

[62] J. Guo, H. Bao, Y. Zhang, X. Shen, J.-K. Kim, J. Ma, L. Shao, Unravelling intercalation-regulated nanoconfinement for durably ultrafast sieving graphene oxide membranes, J. Membr. Sci. 619 (2021).

[63] Z. Wang, C. Xu, Q. Fu, S. Nair, Transport properties of graphene oxide

nanofiltration membranes: Electrokinetic modeling and experimental validation, AlChE J. 68(11) (2022).

[64] H. Zhang, X. Li, T. Xu, Two-dimensional graphene oxide nanochannel membranes for ionic separation, Current Opinion in Chemical Engineering 39 (2023).

[65] T. Zhang, W. Zheng, Q. Wang, Z. Wu, Z. Wang, Designed strategies of nanofiltration technology for Mg2+/Li+ separation from salt-lake brine: A comprehensive review, Desalination 546 (2023).

[66] D.R. Dreyer, A.D. Todd, C.W. Bielawski, Harnessing the chemistry of graphene oxide, Chem. Soc. Rev. 43(15) (2014) 5288-301.

[67] D.A. Dikin, S. Stankovich, E.J. Zimney, R.D. Piner, G.H. Dommett, G. Evmenenko, S.T. Nguyen, R.S. Ruoff, Preparation and characterization of graphene oxide paper, Nature 448(7152) (2007) 457-60.

[68] C. Lu, C. Hu, C.L. Ritt, X. Hua, J. Sun, H. Xia, Y. Liu, D.W. Li, B. Ma, M. Elimelech, J. Qu, In Situ Characterization of Dehydration during Ion Transport in Polymeric Nanochannels, J. Am. Chem. Soc. 143(35) (2021) 14242-14252.

[69] B. Yuan, M. Wang, B. Wang, F. Yang, X. Quan, C.Y. Tang, Y. Dong, Cross-linked Graphene Oxide Framework Membranes with Robust Nano-Channels for Enhanced Sieving Ability, Environ. Sci. Technol. 54(23) (2020) 15442-15453.

[70] Y. Han, Z. Xu, C. Gao, Ultrathin Graphene Nanofiltration Membrane for Water Purification, Adv. Funct. Mater. 23(29) (2013) 3693-3700.

[71] P. Sun, M. Zhu, K. Wang, M. Zhong, J. Wei, D. Wu, Z. Xu, H. Zhu, Selective Ion Penetration of Graphene Oxide Membranes, ACS Nano 7(1) (2013) 428-437.

[72] R.R. NAIR, H.A. WU, P.N. JAYARAM, I.V. GRIGORIEVA, A.K. GEIM, Unimpeded Permeation of Water Through Helium-Leak–Tight Graphene-Based Membranes, Science 335(6067) (2012) 442-444.

[73] M. Hu, B. Mi, Enabling graphene oxide nanosheets as water separation membranes, Environ. Sci. Technol. 47(8) (2013) 3715-23.

[74] G. Eda, G. Fanchini, M. Chhowalla, Large-area ultrathin films of reduced graphene oxide as a transparent and flexible electronic material, Nat Nanotechnol 3(5) (2008)

270-4.

[75] H. Yu, Y. He, G. Xiao, Y. Fan, J. Ma, Y. Gao, R. Hou, J. Chen, Weak-reduction graphene oxide membrane for improving water purification performance, Journal of Materials Science & Technology 39 (2020) 106-112.

[76] R.B. Church, K. Hu, G. Magnacca, M. Cerruti, Cations Block Hydrogen-Bonding-Driven Ethanol Permeation through Disordered Drop-Cast Graphene Oxide Membranes, ACS Applied Nano Materials 2(9) (2019) 5389-5398.

[77] Y. Dong, Y. Cheng, G. Xu, H. Cheng, K. Huang, J. Duan, D. Mo, J. Zeng, J. Bai, Y. Sun, J. Liu, H. Yao, Selectively Enhanced Ion Transport in Graphene Oxide Membrane/PET Conical Nanopore System, ACS Appl Mater Interfaces 11(16) (2019) 14960-14969.

[78] Q. Nan, P. Li, B. Cao, Fabrication of positively charged nanofiltration membrane via the layer-by-layer assembly of graphene oxide and polyethylenimine for desalination, Appl. Surf. Sci. 387 (2016) 521-528.

[79] O. Kwon, Y. Choi, E. Choi, M. Kim, Y.C. Woo, D.W. Kim, Fabrication Techniques for Graphene Oxide-Based Molecular Separation Membranes: Towards Industrial Application, Nanomaterials (Basel) 11(3) (2021).

[80] C. Zhao, L. Xing, J. Xiang, L. Cui, J. Jiao, H. Sai, Z. Li, F. Li, Formation of uniform reduced graphene oxide films on modified PET substrates using drop-casting method, Particuology 17 (2014) 66-73.

[81] Y. Guo, C. Di, H. Liu, J. Zheng, L. Zhang, G. Yu, Y. Liu, General Route toward Patterning of Graphene Oxide by a Combination of Wettability Modulation and Spin-Coating, ACS Nano 4(10) (2010) 5749-5754.

[82] B. Mi, Graphene Oxide Membranes for Ionic and Molecular Sieving, Science 343(6172) (2014) 740-742.

[83] L. Wang, N. Wang, J. Li, J. Li, W. Bian, S. Ji, Layer-by-layer self-assembly of polycation/GO nanofiltration membrane with enhanced stability and fouling resistance, Sep. Purif. Technol. 160 (2016) 123-131.

[84] S. Zheng, Q. Tu, J.J. Urban, S. Li, B. Mi, Swelling of graphene oxide membranes

in aqueous solution: Characterization of interlayer spacing and insight into water transport mechanisms, ACS Nano 11(6) (2017) 6440-6450.

[85] D.C. Marcano, D.V. Kosynkin, J.M. Berlin, A. Sinitskii, Z. Sun, A. Slesarev, L.B. Alemany, W. Lu, J.M. Tour, Improved Synthesis of Graphene Oxide, ACS Nano 4(8) (2010) 4806-4814.

[86] B. Li, C.G. Wang, N.E. Surat'man, X.J. Loh, Z. Li, Microscopically tuning the graphene oxide framework for membrane separations: a review, Nanoscale Adv 3(18) (2021) 5265-5276.

[87] S. Wang, S. Liang, L. Chen, H. Fang, Realizing ultrahigh nanofiltration performance based on small flake reduced graphene oxide membranes, Desalination 528 (2022).

[88] Z.-y. Han, L.-j. Huang, H.-j. Qu, Y.-x. Wang, Z.-j. Zhang, Q.-l. Rong, Z.-q. Sang, Y. Wang, M.J. Kipper, J.-g. Tang, A review of performance improvement strategies for graphene oxide-based and graphene-based membranes in water treatment, Journal of Materials Science 56(16) (2021) 9545-9574.

[89] Y. Mao, J. Xu, H. Chen, G. Liu, Z. Liu, L. Cheng, Y. Guo, G. Liu, W. Jin, Hydrophobic metal-organic framework@graphene oxide membrane with enhanced water transport for desalination, J. Membr. Sci. 669 (2023).

[90] W.-L. Jiang, M.R. Haider, J.-L. Han, Y.-C. Ding, X.-Q. Li, H.-C. Wang, H.M. Adeel Sharif, A.-J. Wang, N.-Q. Ren, Carbon nanotubes intercalated RGO electro-Fenton membrane for coenhanced permeability, rejection and catalytic oxidation of organic micropollutants, J. Membr. Sci. 623 (2021).

Chapter 2

Nanochannel characteristics contributing to ion/ion selectivity in two-dimensional graphene oxide membranes

2.1. Introduction

Recovery of valuable solutes from domestic wastewater is an important strategy to achieve a circular economy [1]. Specifically, achieving solute/solute separation plays a critical role in breaking down mixtures into individual components, thereby enabling more value-added water treatment processes [2], including the isolation and concentration of valuable resources [3], water softening [4], and industrial wastewater reuse [5]. Membrane technologies are considered as a chemical-free, energy-saving method with the potential to enable precise separations and important economic value [6, 7]. Reverse osmosis (RO) and nanofiltration (NF) have gained widespread application in seawater desalination and advanced water purification [8]. However, achieving solute/solute selectivity in RO membranes is challenging owing to their overly dense polymer matrix, which almost completely hinders a wide range of solutes [9, 10]. In contrast, the NF process, utilizing membranes with pores slightly larger than those of RO, possesses promising potential for solute/solute selectivity [11, 12]. In addition, NF membranes offer a diverse range of molecular weight cut-off (MWCO) values (ranging from 200 to 1000 Da) and abundant charge characteristics (e.g., positive, negative, or zwitterionic) [13-15], providing satisfactory feasibility for selectively targeting various specific solutes.

Concentrated NaCl solutions from high-salinity solutions in chlor-alkali factories [16] and the recovery of lithium from salt-lake brines and seawater for resource recovery have garnered widespread attention [17]. The demand for ion/ion separation

of Cl^-/SO_4^{2-} (anion pair) and Li^+/Mg^{2+} (cation pair) is robust in the market. NF membranes play a crucial role in achieving ion/ion selectivity by exhibiting both low and high rejection for monovalent and divalent ions, respectively [18]. The selectivity of mono/divalent ions can be attributed to certain key characteristics of NF membranes. First, a size difference exists between monovalent and divalent ions [19]. Second, ion diffusion through the membrane is significantly influenced by electrostatic interactions, and monovalent and divalent ions exhibit different sensitivities to these interactions [20]. Generally, the ion/ion separation mechanism of NF membranes is primarily driven by steric hindrance (resulting from the size difference between the nanochannel and ions) and electrostatic effects (involving repulsion or attraction between the membrane and charged ions) [16, 21]. Consequently, the enhanced selectivity for these species is mainly attributed to the well-controlled pore size and charge of the NF membrane [22]. However, some ambiguities regarding selectivity may hinder the development of satisfactory NF membranes. Typically, ion/ion separation of NF membranes is evaluated using ideal selectivity [23], which measures the permeability ratio of monovalent to divalent ions in individual solutions. However, there has been limited demonstration of the divergence between ideal and true selectivities, where the latter measures the permeability ratio of monovalent to divalent ions in their binary solution [24]. The discrepancy between ideal selectivity and true selectivity primarily arises from ion competition [25] in specific transporting channels. Compared with ideal selectivity, true selectivity is defined as the ratio of permeabilities for both ions measured in their binary mixture solution. Therefore, the presence of both monovalent and divalent ions leads to competitive transport of ions, with those having lower charge and higher mobility being more likely to pass through the membrane. This difference may lead to inconsistencies in membrane performance evaluation as well as inaccuracies in membrane structure optimization. Therefore, it is necessary to simultaneously analyze the difference of ion transport behavior between ideal and true selectivity, which would be more conducive to promoting the preparation of high-performance separation membranes. Furthermore, although ion/ion selectivity is

typically attributed to a combination of steric exclusion and charge interactions [21, 26], it is crucial to note that the greater significance between these factors has not been thoroughly established in the existing literature.

The suitability of two-dimensional graphene oxide (GO) laminate membranes for ion/ion separation stems from the presence of relatively uniform and tunable nanochannels within GO laminates. This characteristic also offers a intuitive and conducive approach to control ion transport characteristics. Generally, the interlayer spacing in the nanochannels of GO membranes can be controlled within the sub-nanometer range [27-29]. In addition, the negatively charged GO sheets provide abundant and tunable charged sites for NF separation [30, 31]. The charge and interlayer spacing of GO membranes can be readily adjusted by altering the oxygenation degree of GO [32, 33], thereby facilitating the correlation of different nanochannel characteristics with their corresponding ion transport behaviors. Commonly, there exists a delicate balance between membrane charge and pore size. The higher charge density of the nanosheets or polymer chains typically results in enlarged nanopores or nanochannels due to the swelling of the membrane materials by increased charge content [34]. Therefore, exploring the respective contributions of steric exclusion and electrostatic effects to the ion/ion selectivity is important for the nanochannel design.

In this study, appropriate nanochannels within GO membranes with different subnanometer channels and charge characteristics were successfully prepared by changing the oxygenation degree of GO. Subsequently, the ion/ion selectivity under the effects of different nanochannel properties of the GO membrane and external feed mixture compositions was analyzed (**Fig. 2.1**). The correlation between channel characteristics and ion-selective transport is expected to yield significant insights into the effective factors contributing to the ion/ion selectivity of the two-dimensional nanochannles.

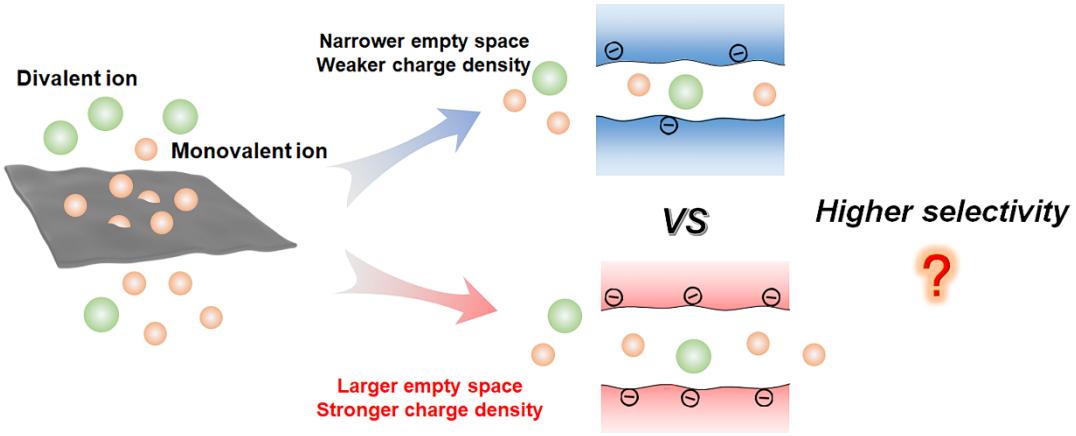

Fig. 2.1 Schematic of the influence of different GO nanochannels on selectivity.

2.2. Experimental

2.2.1. Materials

A commercial nylon membrane (hydrophilic, 0.2 μm pore size, 47 mm diameter), purchased from Merck Millipore (St. Louis, MO, USA), was applied as substrates of GO and GO-PAA membrane. An aqueous GO suspension (4 mg mL^{-1}) was obtained from Sigma-Aldrich Co., LLC (St. Louis, MO, USA). D-(+)-glucose (> 98.0%) was obtained from Tokyo Chemical Industry (TCI) Co., Ltd., Japan. Polyallylamine (PAA; MW = 15000 g/mol; 15% aqueous solution), used for the positively charged modification of the GO membrane surface, was purchased from Polysciences, Inc. (USA). Sodium chloride (NaCl, 99.5%), sodium sulfonate (Na_2SO_4, 99.0%), magnesium chloride ($MgCl_2$, 99.0%), and ammonia solution (NH_3H_2O, 28%) were obtained from FUJIFILM Wako Pure Chemical Industries Co. Ltd. (Osaka, Japan). Anhydrous lithium chloride (LiCl, > 98.0%) was obtained from Tokyo Chemical Industry (TCI) Co., Ltd., Japan.

2.2.2. Preparation of GO and GO-PAA membranes

Glucose was utilized as a reducing agent to functionalize GO at various O/C ratios. Initially, a 10 mL aqueous solution containing 0.15 mg GO, 1.5 mg glucose, and 40 μL ammonia solution was thoroughly blended. Subsequently, the above dispersions were heated in a water bath at 94.5 °C for 0, 20, 40, and 60 min, respectively, to obtain

precursor suspensions of GO membranes. The preparation of different GO membranes was accomplished through vacuum filtration [35]. The precursor suspensions were diluted with ultrapure water to a volume of 300 mL, sonicated for 5 min, and vacuum filtered onto a nylon substrate. The GO membranes with different O/C ratios were dried in a desiccator for 24 h at room temperature. In addition, the GO-PAA membranes were fabricated using a simple coating method. The prepared GO membranes were immersed in a 0.1% PAA aqueous solution for 30 min, subsequently removed, and dried at room temperature.

2.2.3. Characterization

The O/C ratios of the GO membranes were characterized using X-ray photoelectron spectroscopy (XPS) (JPS-9010MC, JEOL, Tokyo, Japan). The interlayer spacings of the GO membranes under dry and wet conditions were estimated through X-ray diffraction (XRD; RINT 2500 VHF, Rigaku Corp., Tokyo, Japan). The surface charges of the GO membranes were observed using a zeta potential analyzer (SurPASSTM3, Anton Paar, Graz, Austria). The concentrations of Mg^{2+} and Li^{+} were measured using inductively coupled plasma atomic emission spectroscopy (ICP, Optima 7000 DV ICP-OES, Perkin Elmer, USA). The concentration of SO_4^{2-} and Cl^{-} were determined through ion chromatography using a Shim-pack IC-A3 column (IC; Shimadzu Co., Kyoto, Japan).

2.2.4 Membrane performance

The membrane performance of the GO and GO-PAA membranes was assessed using a cross-flow device with a flow rate of 9.9 mL min^{-1} and an effective membrane surface area of 7.06 cm^2, as reported previously [36]. Once the resultant membranes were pre-compacted under a pressure of 10 bar until reaching steady water permeance, a transmembrane pressure of 10 bar was applied.

The ion/ion selectivity of the GO and GO-PAA membranes was evaluated by testing the anion pairs (NaCl and Na_2SO_4) and cation pairs (LiCl and $MgCl_2$) at an

equivalent total charge concentration of the target ions (0.05 equivalent per liter). For single salts, the 0.05 equivalent per liter of NaCl, Na_2SO_4, LiCl, and $MgCl_2$ were determined as 0.05 mol/L, 0.025 mol/L, 0.05 mol/L, and 0.025 mol/L, respectively. For binary solutions, the concentrations of monovalent (Cl^- or Li^+) and divalent (SO_4^{2-} or Mg^{2+}) ions were set to 0.025 mol/L and 0.0125 mol/L, respectively, when the equivalent ratio was 1/1. In addition, a series of equivalent ratios (9/1, 4/1, 1/1, 1/4, and 1/9) of the target ions were prepared to investigate the selectivity mechanism.

Herein, the use of permeability instead of permeance, as well as selectivity rather than rejection, would offer clearer comparisons of performance, relying solely on the fundamental transport characteristics [37-39]. The specific calculations are as follows:

The transport of water and salt across membranes was determined based on the solution–diffusion model. The water flux, J_W (g cm^{-2} s^{-1}), can be calculated using Equation 2.1:

$$J_W = \frac{D_W}{L}\left(C_{W,F}^m - C_{W,P}^m\right) = \frac{D_W C_{W,F}^m}{L}\left(1 - \frac{C_{W,P}^m}{C_{W,F}^m}\right) \quad (2.1)$$

where D_W (cm^2 s^{-1}) is the average water diffusion coefficient in the membrane; L (cm) is the membrane thickness; and $C_{W,F}^m$ and $C_{W,P}^m$ (g cm^{-3}) are water concentrations in the membrane on the feed and permeate side, respectively.

Due to the pressure and osmotic pressure difference between the feed and permeate sides of the membrane, Equation 2.1 was written as follows:

$$J_W = \frac{D_W C_{W,F}^m}{L}\frac{\bar{V}}{RT}(\Delta P - \Delta\pi) \quad (2.2)$$

where $\bar{V}$ (cm^3 mol^{-1}) is the partial molar volume of water, which is typically well approximated by the molar volume of pure water when the water uptake varies little with salt concentration over the salt concentration range of interest; R (83.1 cm^3 bar mol^{-1} K^{-1}) is the gas constant, T (K) is the absolute temperature; ΔP (bar) is the pressure difference across the membrane, and $\Delta\pi$ (bar) is the osmotic pressure.

The K_W is the water partition (or solubility) coefficient, which is defined as the ratio of water concentration in the membrane to that in the contiguous solution:

$$K_W = \frac{C_{W,F}^m}{C_{W,F}} \tag{2.3}$$

For relatively dilute solutions, $C_{W,F}$ can be approximately equal to the density of pure water, ρ_W (g cm^{-3}).

Combine with Equation 2.2 and Equation 2.3,

$$J_W = \frac{P_W}{L}\frac{\rho_W \bar{V}}{RT}(\Delta P - \Delta\pi) = \frac{P_W}{L}\frac{M_W}{RT}(\Delta P - \Delta\pi) = A(\Delta P - \Delta\pi) \tag{2.4}$$

where A is the effective membrane permeance to water, and P_W is the membrane permeability to water.

Based on Equation 2.4, the relationship between A and Pw is as follows:

$$A = \frac{P_W}{L}\frac{M_W}{RT} \tag{2.5}$$

Based on the solution–diffusion model, the salt flux through membrane, J_S (g cm^{-2} s^{-1}), can be calculated as:

$$J_S = \frac{P_S}{L}\left(C_{S,F} - C_{S,P}\right) = \frac{P_S}{L}\Delta C_S = B\Delta C_S \tag{2.6}$$

where P_S (cm^2 s^{-1}) is the salt permeability; $C_{S,F}$ and $C_{S,P}$ (g cm^{-3}) are the salt concentrations in the solution on the feed and permeate sides of the membrane, respectively; ΔC_S is the difference between salt concentration.

It is worth mentioning that our target is on the transport properties of salt and water through the membrane and therefore concentration polarization is not considered. Additionally, $B = P_S/L$ is salt flux and $\Delta\pi = \Delta C_S RT$.

Generally, the ability of the membrane to separate salt from the feed solution is usually observed by the salt rejection R (%), which can be expressed based on the above-mentioned solution–diffusion model as follows:

$$R = \frac{(P_W/P_S)(\bar{V}/PT)(\Delta P - \Delta\pi)}{1 + (P_W/P_S)(\bar{V}/PT)(\Delta P - \Delta\pi)} \times 100 = \frac{(A/B)(\Delta P - \Delta\pi)}{1 + (A/B)(\Delta P - \Delta\pi)} \times 100\% \tag{2.7}$$

Therefore, water permeability and salt permeability were calculated as follows:

$$P_W = K_W D_W \tag{2.8}$$

$$P_S = K_S D_S \tag{2.9}$$

The ideal water/salt selectivity, $\alpha_{w/s}$ was determined by Equation 2.10:

$$\alpha_{W/S} = \frac{K_W}{K_S} \times \frac{D_W}{D_S} = \frac{P_W}{P_S} \quad (2.10)$$

The salt/salt selectivity, $\alpha_{s1/s2}$ was determined by Equation 2.11:

$$\alpha_{s1/s2} = \frac{P_{S1}}{P_{S2}} \quad (2.11)$$

where P_{S1} is the salt permeability (cm^2/s) of monovalent ions (Cl^- or Li^+) and P_{S2} is the salt permeability (cm^2/s) of divalent ions (SO_4^{2-} or Mg^{2+}).

2.3 Results and discussion

2.3.1 Characterization of GO membranes with different O/C ratios

GO with functional groups, including carboxylic, hydroxyl, and epoxy groups, demonstrates excellent multifunctionality, enabling easy assembly into a laminate membrane. As the O/C ratio decreased, the GO membranes exhibited similar laminate structures **(Fig. 2.2)**. The interlayered nanochannels in the laminates exhibit distinct ion transport properties [40]. In addition, GO membrane nanochannels can exclude various ions by tuning the interlayer spacing between the stacked GO sheets and the charged functional groups (**Fig. 2.3a**) [41, 42]. Specifically, with decreasing O/C ratio, the interlayer spacing and electronegativity of the GO membrane become narrower and weaker, respectively, owing to the removal of oxygen-containing functional groups. As **Fig. 2.3b** shows, the reduction time directly correlates with a decrease in the specific peak area of C-O, indicating an effective removal of partial oxygen-containing functional groups. Therefore, the O/C ratio of GO decreased from 0.60 to 0.20 owing to prolonged chemical reduction (**Fig. 2.3c**). Meanwhile, GO membranes with O/C ratios of 0.60, 0.41, 0.29, and 0.20 are defined as GO60, GO41, GO29, and GO20, respectively. In addition, the surface zeta potential weakened (**Fig. 2.3d**), and the interlayer spacing narrowed (**Fig. 2.3e**) (evident from the characteristic peaks of GO in the XRD spectra shifting slightly to larger *2θ*, **Fig. 2.3f**), as the O/C ratio decreased. Wetting the GO samples with water caused the characteristic peaks of all GO membranes to shift significantly to smaller 2θ, indicating that the interlayer spacing in the wet state expanded (**Fig. 2.3g**) owing to the intercalation of water molecules [43].

In addition, a decrease in the O/C ratio reduced the swelling (difference in interlayer spacing between dry and wet conditions) of the GO membrane, as oxygen-containing functional groups that induced hydrogen bonding with water molecules decreased in abundance [44]. As the interlayer spacing between two GO planes decreases with a lower O/C ratio in both dry and wet conditions, there will be an increasing steric hindrance for mass transport in the interlayered nanochannels of GO laminates. It is important to note that the calculated interlayer spacing value mainly represents the average for the entire sample, and it may slightly deviate from the actual interlayer spacing during separation conditions. However, these calculated values can give a rough idea of the range of sizes for membrane pores. Based on the confinement of the subnanometer sized channels of GO membrane, the cation pair (Li^+ and Mg^{2+}) and anion pair (Cl^- and SO_4^{2-}) having different sizes and valences were likely to be selectively separated by the membrane nanochannels. Hence, separation of the anion or cation pairs by these membrane nanochannels were performed to explore the contributions of electrostatic interactions and steric hindrance to selectivity.

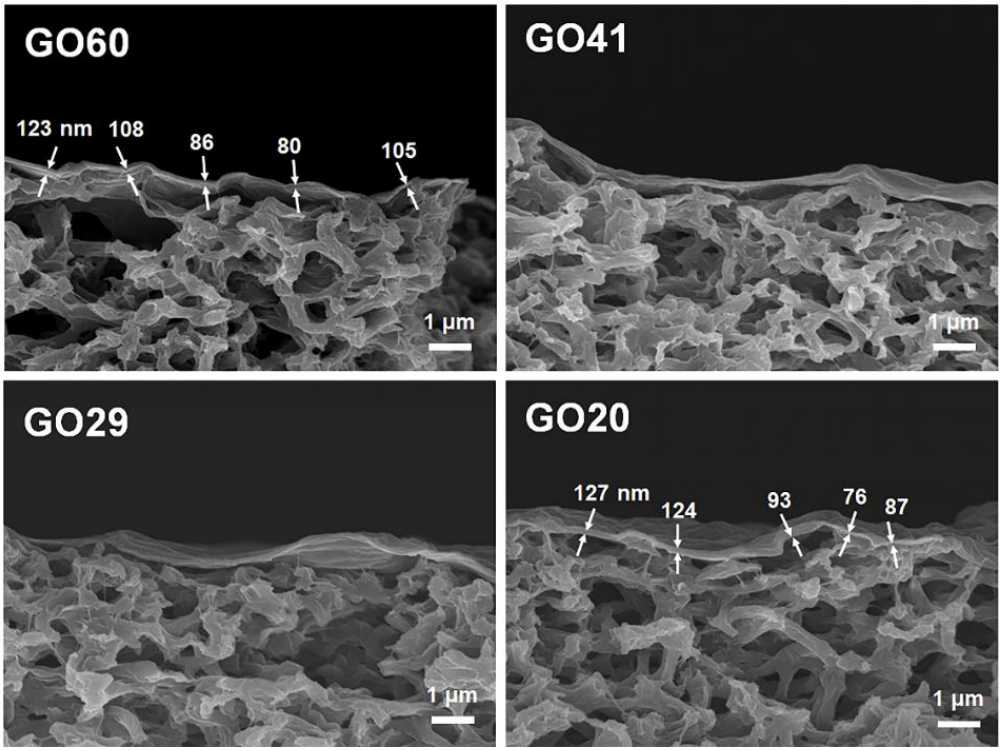

Fig. 2.2 SEM cross-sectional view of GO membranes with different O/C ratios.

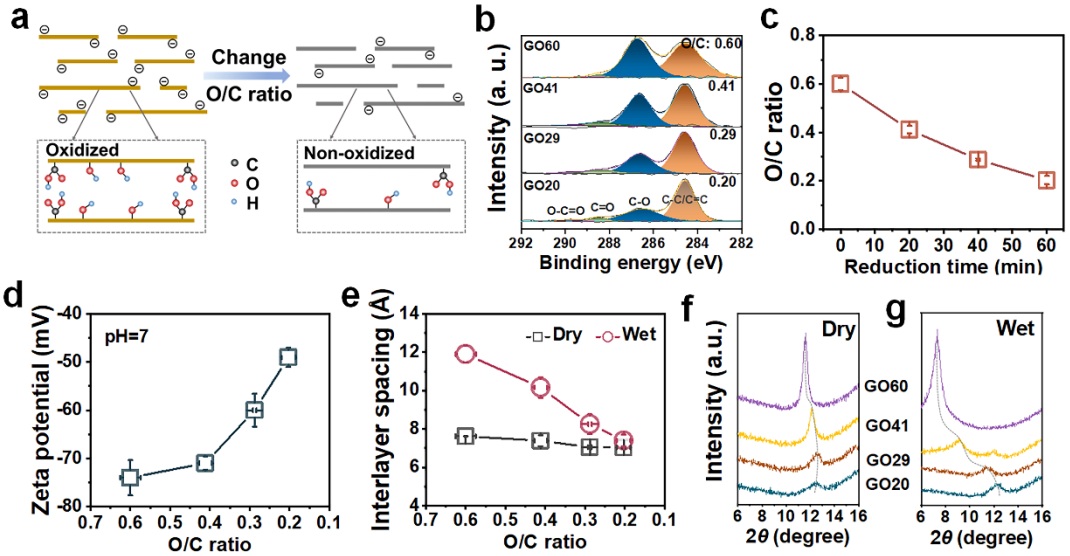

Fig. 2.3 (a) Schematic of GO membranes with different O/C ratios, (b) C1s of XPS spectra of GO membranes with different O/C ratios, (c) O/C ratio of GO membranes with different oxygenated degrees, (d) surface zeta potentials of GO membranes at pH = 7, (e) interlayer spacing of different GO membranes at dry and wet states, and (f-g) XRD spectra of different GO membranes at dry and wet states.

2.3.2 Selective water and salt permeation in GO membrane nanochannels

The selective transport pathway for the separation of water and ions was influenced by the constitution of different underwater nanochannels as the O/C ratio changed. The change in O/C ratio also affects the hydrophilicity of GO membranes. As shown in **Fig. 2.4a,** the water contact angles measured for GO60, GO41, GO29, and GO20 were 53°, 57 °, 64 °, and 67 °, respectively. The surface of the membrane with different O/C ratios still remain wettable ($\theta < 90°$), despite a slight increase in water contact angle [45]. According to the permeance and rejection of different GO membranes in single salt solutions, the permeability and water/salt selectivity of the GO membranes were obtained (**Table 2.1**). In addition, despite potential variations in the O/C ratio among different GO membranes, the permeability order of different salt solutes remained consistent ($MgCl_2 > LiCl \approx NaCl > Na_2SO_4$), as shown in **Fig. 2.4b**. This order mainly depended on the influence of the Donnan effect, indicating that the salt with a larger valence ratio of cation and anion (Z^+/Z^-) was more favorable to

permeate [35]. Therefore, for SO_4^{2-} and Cl^-, the decrease in electronegativity of the GO membranes weakens electrostatic repulsion, enhancing anion transport. In contrast, the transport of Mg^{2+} and Li^+ tends to be hindered due to weaker electrostatic attraction. If only electrostatic interactions were considered, it would observe different trends in the change of water/salt selectivity for Na_2SO_4 and $MgCl_2$. However, in reality, the water/salt selectivity increases for all types of salts as the O/C ratio decreases (**Fig. 2.4c**). Thus, it can be concluded that the reduced interlayer spacing has a significant impact on enhancing the water/salt selectivity for all types of salts. Meanwhile, the change in the O/C ratio had a greater influence on the decrease in *Ps* than on that in *Pw*, which led to improved water/solute selectivity. While decreased hydrophilicity can impact water permeability and, consequently, ion permeability, it is not directly linked to ion/ion selectivity. Therefore, the focus lies on nanochannel size and charge as these factors significantly influence specific ion transport, ultimately affecting ion/ion selectivity. As the effects of charge and size of nanochannels are different for specific ions, for the following analysis of ion/ion selectivity, a series of binary solutions as target solutions were further tested using GO membranes with different O/C ratios to explore the significant role of charge or size in enhancing ion/ion selectivity.

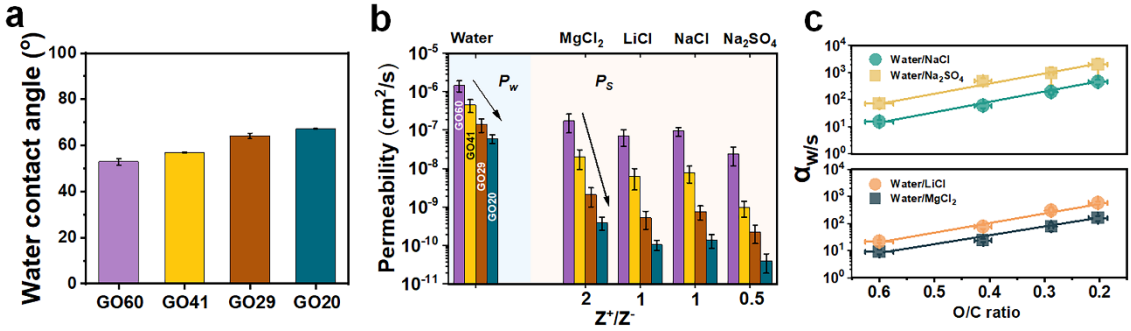

Fig. 2.4 (a) Water contact angle, (b) permeability, and (c) water/salt selectivity of single salts of different GO membranes.

Table 2.1 Summary of permeance and rejection of different GO membranes in single salt solutions.

Membrane	Permeance [L m^{-2} h^{-1} bar^{-1}]	Na_2SO_4 rejection ratio [%]	NaCl rejection ratio [%]	$MgCl_2$ rejection ratio [%]	LiCl rejection ratio [%]
GO60	3.78±1.21	32.35±7.25	9.76±1.27	6.04±1.14	13.12±1.45
GO41	1.18±0.42	74.88±4.53	28.67±3.58	14.31±1.70	33.49±3.61
GO29	0.39±0.17	85.15±8.26	55.41±5.04	35.23±8.28	64.80±7.11
GO20	0.14±0.02	91.34±4.25	72.59±4.74	50.66±5..81	77.00±2.23
GO60-PAA	0.46±0.05	46.69±9.06	25.44±1.27	86.65±3.64	42.29±2.84
GO41-PAA	0.41±0.02	67.88±8.75	34.94±1.80	91.35±3.18	48.1±4.97
GO29-PAA	0.30±0.08	72.75±5.79	44.12±1.94	84.85±38.11	54.93±2.47
GO20-PAA	0.24±0.17	75.85±9.89	51.33±14.52	86.99±1.96	53.05±8.80

2.3.3 Ion-ion selectivity of co-ions

First, the co-ion pair (Cl^- and SO_4^{2-}) separation by the different GO membrane nanochannels was evaluated. Generally, ion/ion selectivity is determined by the permeabilities [38, 46]. The ratio of the permeabilities of the two ions measured from their pure single-salt solutions is defined as the ideal selectivity, whereas the ratio of the permeabilities of the two ions measured from their binary mixture solution is defined as the true selectivity. For example, the ideal selectivity of the Cl^-/SO_4^{2-} pair is the ratio of the permeability of Cl^- to SO_4^{2-} measured separately from pure NaCl and pure Na_2SO_4 solutions, respectively. In contrast, the true selectivity is the ratio of permeabilities measured from a binary salt solution of NaCl and Na_2SO_4. Subsequently, the contribution of electrostatic interactions and steric hindrance to the selectivity was evaluated by exploring the effect of the nanochannel properties on the permeation behavior of the co-ions (Cl^- and SO_4^{2-}). As shown in **Fig. 2.5a**, the ion permeability of the binary-salt solution decreased with decreasing O/C ratio, which is consistent with that of the single-salt solutions. Contrary to Cl^-, which exhibited only slight differences in *Ps* in the single (NaCl) and binary (NaCl + Na_2SO_4) salt solutions, the *Ps* of SO_4^{2-} in the binary-salt solution was consistently lower than that in the single-salt solution. A

decrease in the O/C ratio influenced SO_4^{2-} more significantly than Cl^-, which could be attributed to competition between anions [25]. Specifically, SO_4^{2-} with high valence and low mobility was more difficult to permeate than Cl^-, which could be attributed to the synergistic effect of the stronger transport resistance of SO_4^{2-} with a larger crystal diameter in the nanochannels and the preferential repulsion of divalent anions by the negatively charged GO membrane. A significant *Ps* decrease of SO_4^{2-} in the binary salt solution led to a higher selectivity for the binary salt than the ideal ion/ion selectivity of the single salts (**Fig. 2.5b**). Although the transport behavior of anions changed with the modification of nanochannel properties, the selectivity remained constant, owing to insufficient mutual compensation between electrostatic interactions and steric hindrance. As illustrated in the schematic in **Fig. 2.5c**, the ion/ion selectivity was reasonably maintained at a balance of narrower interlayer spacing and weaker electrostatic repulsion to impede and facilitate anion transport, respectively. However, the contributions of charge and size to the ion/ion selectivity must be determined.

Generally, if the ion/ion selectivity is dominated by steric hindrance, there would be a weak influence on the true selectivity by changing the composition of ions with different charges (concentrations of Cl^- and SO_4^{2-}) of the feed solution. Conversely, the true selectivity varies with changes in the composition of the feed solution when the selectivity is controlled by electrostatic interactions between the nanochannels and ions. In this regard, the same total equivalent charge concentration is maintained in order to minimize the effect of changes in coexisting ions on the target ion transport behavior. Meanwhile, various binary solutions with different equivalent ratios (the total charge of Cl^- relative to the total charge of SO_4^{2-} in binary solutions was 9/1, 4/1, 1/1, 1/4, and 1/9) were employed as feed solutions to further explore the importance of electrostatic interactions or size. For evaluation, two typical nanochannel membranes were selected, GO60 (O/C ratio of 0.60) and GO20 (O/C ratio of 0.20). The former had a higher charge density but larger interlayer spacing, while the latter had a lower charge density but smaller interlayer spacing. The transport of anions in the nanochannels of the GO60 membrane was easier because of the larger interlayer spacing and lower transport

resistance (**Fig. 2.5d**). In addition, the permeabilities of SO_4^{2-} and Cl^- of the GO60 membrane exhibited opposite trends with a larger SO_4^{2-} fraction (increasing the charge-equivalent concentrations of SO_4^{2-}, $C_{eq,\ SO_4^{2-}}$), leading to a gradual increase in the permeability difference. The interaction between the membrane surface and Na^+ was similar because binary salt solutions of different equivalent ratios maintained the same equivalent concentration, which means that the transport behavior of Na^+ through the GO membranes is consistent. Cl^- and SO_4^{2-} were passively passed through the membrane to maintain electroneutrality conditions [47]. However, the transport of divalent SO_4^{2-} was more difficult, attributed to its higher electric charge density and size [7] compared to monovalent Cl^-, leading to a lower permeability of SO_4^{2-}. Therefore, electroneutrality of the permeate side was achieved by the faster permeation of Cl^-. In contrast, the permeability difference of SO_4^{2-} and Cl^- through GO20 with a narrower interlayer spacing was almost consistent regardless of the change in the equivalence ratio, possibly due to the steric hindrance effect.

The true selectivities of co-ions with different equivalence ratios were determined based on their corresponding permeabilities (**Fig. 2.5e**). The selectivity of GO60 gradually increased with an increasing SO_4^{2-} fraction in the binary salt solution, suggesting that the negatively charged membrane preferentially hindered the migration of high-valence SO_4^{2-} because of electrostatic repulsion. In other words, anions with a low valence and high permeability were prone to permeate through GO60 when there was a competition between Cl^- and SO_4^{2-}. However, the Cl^-/SO_4^{2-} selectivity of GO20 with smaller interlayer spacing was constant regardless of changes in equivalent ratios of Cl^- and SO_4^{2-}. Therefore, the higher charge density from the GO60 membrane was more effective than the narrower interlayer spacing of GO20, contributing to the Cl^-/SO_4^{2-} selectivity (**Fig. 2.5f**). It is concluded that nanochannels with appropriately large interlayer spacing coupled with high charge density may be more beneficial for the separation of co-ions of Cl^- and SO_4^{2-}, considering the low transport resistance and high selectivity.

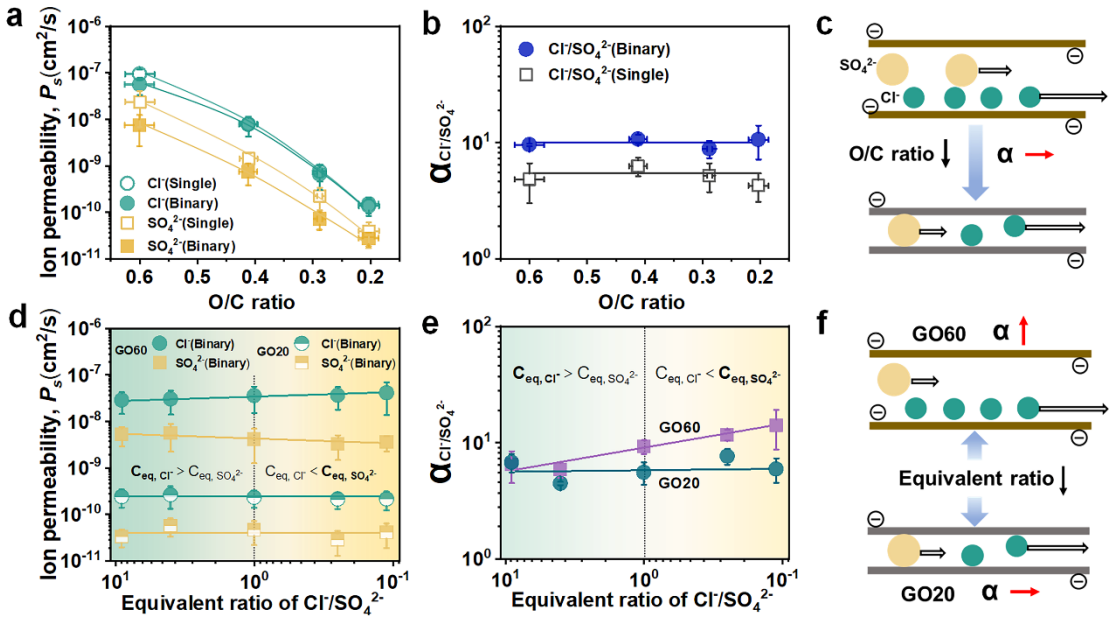

Fig. 2.5 (a) Ion permeability, (b) solute/solute selectivity, and (c) schematic of anion pair of GO membranes with different O/C ratios; (d) ion permeability, (e) solute/solute selectivity, and (f) schematic of GO60 and GO20 membranes with various feed solutions. The charge-equivalent concentration ratios of Cl^- and SO_4^{2-} ($C_{eq,Cl^-}/C_{eq,SO_4^{2-}}$) are 9/1, 4/1, 1/1, 1/4, and 1/9.

2.3.4 Selectivity of GO membranes for counter-ions

The effects of nanochannel properties on counter-ion selectivity were observed through the transport behavior of the cation pair (Li^+/Mg^{2+}). Similar to the Cl^-/SO_4^{2-} pair, the permeation resistances of Mg^{2+} and Li^+ increased with decreasing O/C ratio (**Fig. 2.6a**). Interestingly, the permeabilities of Mg^{2+} and Li^+ in the single- and binary-salt solutions between GO sheets exhibited opposite trends. Under single-salt conditions, the permeability of Mg^{2+} was larger than that of Li^+ owing to the GO membrane's emerging electrostatic attraction [48] with cations, preferentially enhancing the transport of divalent Mg^{2+} rather than monovalent Li^+. However, the permeability of Mg^{2+} in a binary salt solution was lower than that of Li^+, indicating ion competition between Li^+ and Mg^{2+}. When fed with a counter-ion solution, it neutralizes or reversal [49] the membrane charge. Subsequently, in the case of the binary-salt

solution, the transfer resistance of high-valence Mg^{2+} was stronger than that of low-valence Li^+ owing to electrostatic repulsion, resulting in a lower permeability for Mg^{2+}.

The true selectivity from the binary salt solution and ideal selectivity from the single-salt solutions of Li^+/Mg^{2+} consistently showed values > 1 (Li^+ was selectively transported over Mg^{2+}) and < 1(Mg^{2+} was selectively transported over Li^+), respectively (**Fig. 2.6b**). This highlighted the divergence between the ideal and true selectivities (**Fig. 2.6c**). Moreover, as the O/C ratio decreased, the selectivity under both ideal and true conditions continuously decreased and increased, respectively. The distinction between ideal and true selectivities was mainly attributable to the exclusion of ion competition in single-salt solutions. In contrast, the enhanced true selectivity was attributed to divalent Mg^{2+} with high valence and larger size, which was more susceptible to changes in the nanochannel properties than Li^+ [50]. Consequently, with weakened electronegativity and narrowed interlayer spacing of the nanochannels, the permeability of Mg^{2+} was more significantly hindered than that of Li^+, leading to a widening difference between the permeabilities of Mg^{2+} and Li^+.

Binary salt solutions with a series of equivalent ratios of Li^+ to Mg^{2+} were prepared to observe the dominant role of the electrostatic effects or steric hindrance. The permeabilities of Mg^{2+} and Li^+ exhibited a slight increase simultaneously with the increased fraction of Mg^{2+}, owing to ion competition between Li^+ and Mg^{2+} (**Fig. 2.6d**). As the electrostatic attraction of Mg^{2+} with negatively charged nanochannels was stronger than that of Li^+, the ion permeability increased when the composition of the binary-salt solution approached that of a single-salt solution of Mg^{2+} (the equivalent ratio of Li^+/Mg^{2+} from 9/1→1/9), and vice versa. In addition, although the change in the equivalent ratio was nearly a hundred times (from 9/1 to 1/9), the ion/ion selectivity of the different nanochannels of GO20 and GO60 was almost constant (**Fig. 2.6e**). Except for the relatively weak electrostatic interactions, the slightly higher selectivity of GO20 compared to that of GO60 could be attributed to steric hindrance (**Fig. 2.6f**). These results indicated that negatively charged membrane nanochannels could selectively filter Li^+ over Mg^{2+}, similar to the transport behavior of positively charged

membranes [51]. Additionally, constructing narrower nanochannels is more beneficial for realizing enhanced selectivity of counter-ions of Li^+/Mg^{2+}.

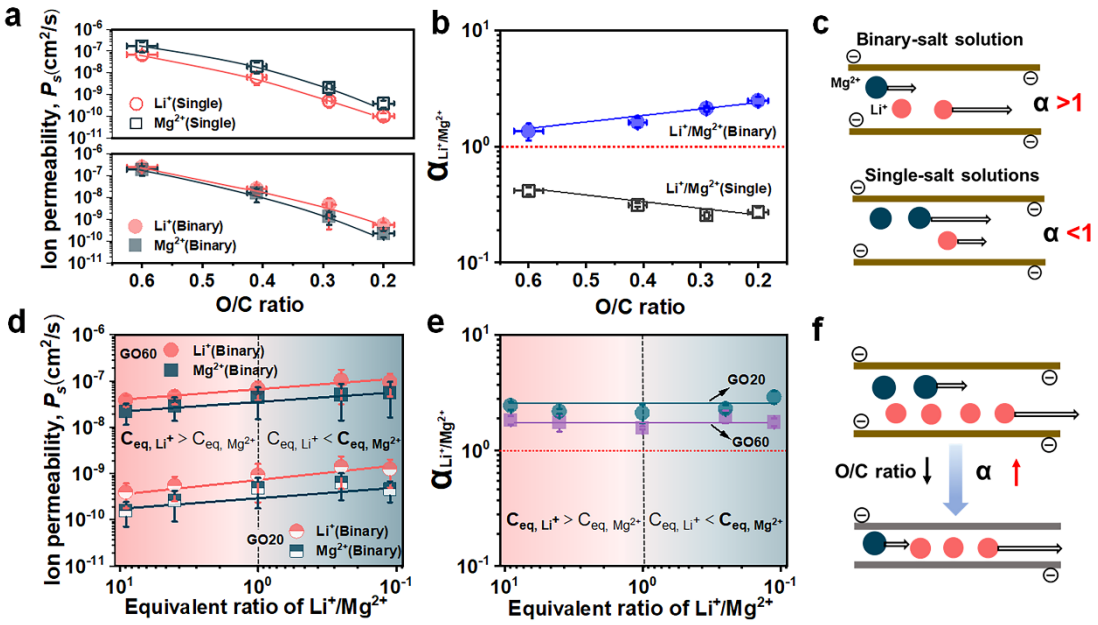

Fig. 2.6 (a) Ion permeability, (b) solute/solute selectivity, and (c) schematic diagram of cation pair of GO membranes with different O/C ratios; (d) ion permeability, (e) solute/solute selectivity, and (f) schematic of GO60 and GO20 membranes with various feed solutions. The charge-equivalent concentration ratios of Li^+ and Mg^{2+} ($C_{eq,\ Li^+}/C_{eq,Mg^{2+}}$) are 9/1, 4/1, 1/1, 1/4, and 1/9.

Based on the separation results of the negatively charged nanochannels transporting co-ions and counter-ions, it was observed that the true selectivity of counter-ions was generally lower than that of co-ions (**Fig. 2.7**). In the case of co-ions, the reduction of interlayer spacing induced by decreased O/C is beneficial to the improvement of Cl^-/SO_4^{2-} selectivity, whereas the concurrent weakening of electronegativity had an adverse effect. For counter ions, although the reduction in interlayer spacing and electronegativity caused by the reduction of O/C were both beneficial for improving Li^+/Mg^{2+} selectivity, the selectivity of counter-ions was lower than that of the co-ions. This finding suggests that the valence and concentration of co-ions exerted a more significant impact on ion transport compared to counter-ions,

indicating that the selectivity of different nanochannels was predominantly determined by the distinctive properties of co-ions and, to a lesser extent, by counter-ions.

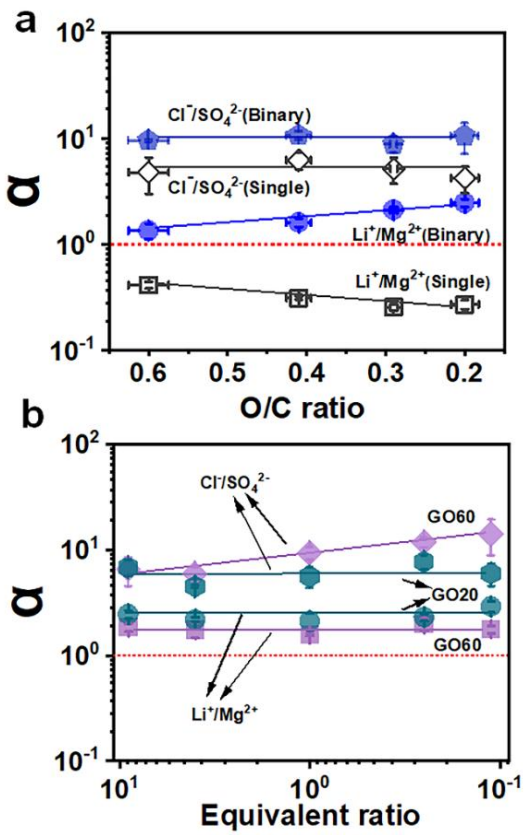

Fig. 2.7 Comparison of co-ions (Cl^-/SO_4^{2-}) and counter-ions (Li^+/Mg^{2+}) selectivity of (a) GO membranes with different O/C ratios, and (b) GO60 and GO20 membranes with various feed solutions. The charge-equivalent concentration ratios are 9/1, 4/1, 1/1, 1/4, and 1/9.

2.3.5 Single-salt performance of GO-PAA membrane with surface charge modification

To investigate the contribution of the charge and size of the nanochannels on ion/ion selectivity, the modification on the GO membranes was performed to introduce a positive surface charge to explore the ion transport behavior in the modified membranes. Poly (allylamine) (PAA), a common polycation [52], was deposited on the surface of the GO60 (GO60-PAA) and GO20 (GO20-PAA) membranes as a charge modification layer through a simple soaking method, in contrast to the pristine GO60

and GO20 membranes. As shown in **Fig. 2.8a**, successful surface modification of the membranes with a positive charge was achieved using PAA. The GO-PAA exhibited satisfactory structure stability due to strong electrostatic interaction and hydrogen bonds between GO and PAA. In addition, the average thickness of the GO-PAA membranes changed from approximately 106 nm to 106.4 nm after soaking in PAA. It was also demonstrated that PAA was successfully loaded onto the surface of the GO membranes, owing to the slightly increased thickness of the GO-PAA membranes (**Fig. 2.9**). Similar to the GO membrane-repelling anions, the surfaces of the GO-PAA membrane acted as barriers for co-ions (cations) [53] owing to electrostatic repulsion (**Fig. 2.8b**). Specifically, cations were propelled through the negatively charged GO membrane owing to electrostatic attraction, while the GO-PAA membrane considerably hindered the transport of cations, especially high-valence cations, owing to surface charge repulsion. Therefore, significant differences were found in the order of salt permeability before and after the electropositive modification of the GO membranes (**Fig. 2.8c-d**). For the GO-PAA membrane that suppressed the co-ions (cation) while attracting counter-ions (anion), the salt permeability order was $LiCl \approx NaCl > Na_2SO_4 > MgCl_2$. Compared to the GO membrane with the highest salt permeability for $MgCl_2$, the GO-PAA membrane was tremendously impeded by its permeation owing to electrostatic repulsion. Generally, the salt with lower Z^+/Z^- would transport faster within the positive membrane. However, the permeability of Na_2SO_4 was lower than that of LiCl and NaCl because of its larger diameter and/or repulsion by the underlying GO membrane [54], indicating that the underlayer GO membrane still played a role in transporting ions. The order of salt permeability was consistent for both GO60-PAA and GO20-PAA, suggesting that electrostatic effects played a more important role than size. By assessing the ion/ion separation performance of the PAA-modified membranes, it is necessary to further explore the properties of the membrane nanochannels to achieve ion/ion selectivity.

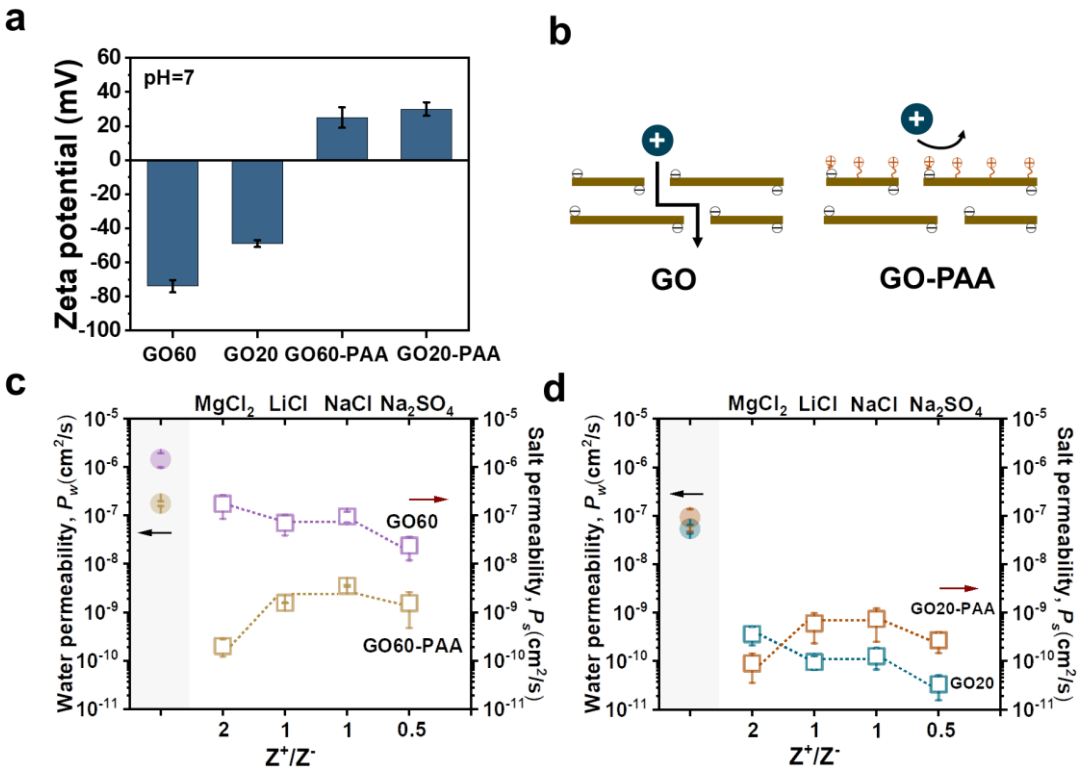

Fig. 2.8 (a) Zeta potential, (b) schematization of electrostatic interaction, and (c-d) permeability of single salts of GO60 and GO20 before and after modification by PAA.

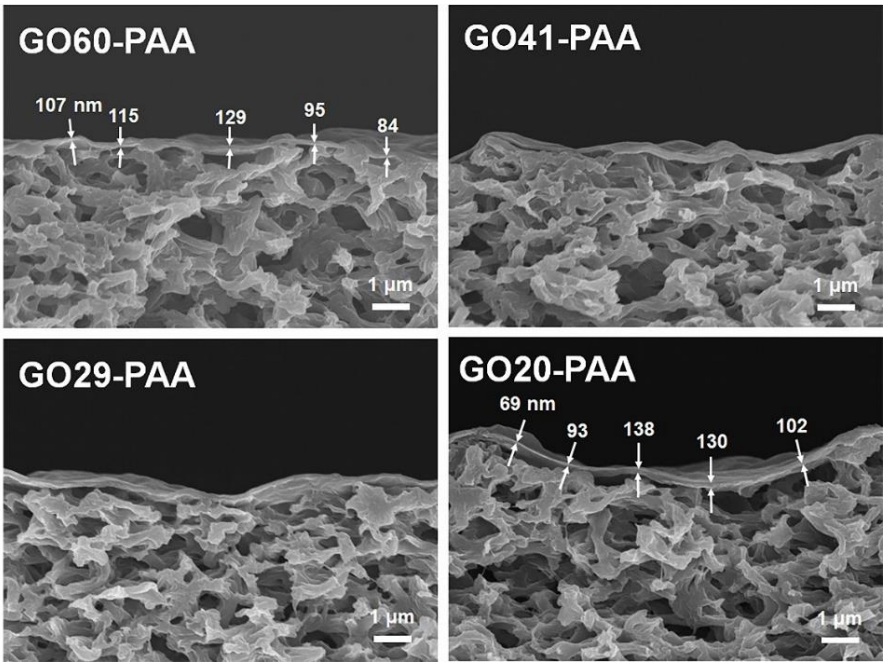

Fig. 2.9 SEM cross-sectional view of GO-PAA membranes with different O/C ratios.

2.3.6 Selectivity of GO-PAA membranes for co-ions (Li^+/Mg^{2+}) and counter-ions (Cl^-/SO_4^{2-})

The Li^+/Mg^{2+} selectivity of GO-PAA remained relatively constant regardless of the property changes of the underlying GO nanochannels and was significantly higher than that of the GO membrane (**Fig. 2.10a-b**). Therefore, membrane selectivity was strongly associated with the surface modification and valence of co-ions, and the introduction of electrostatic repulsion between ions and the membrane surface proved advantageous for enhancing selectivity. Meanwhile, the trend of the selectivity change of the GO-PAA membrane to co-ions of Li^+/Mg^{2+} with different equivalent ratios (**Fig. 2.10c-d**) was consistent with that of the GO membrane to the co-ions of Cl^-/SO_4^{2-}. The ion competition was confirmed by the improved selectivity of the GO-PAA membrane with a larger Mg^{2+} fraction. Therefore, the transport of high-valent ions across the charged membrane was more severely restrained than that of low-valent ions. In conclusion, the construction of charge-enhanced nanochannels and/or charge-modified membrane surfaces improved the selectivity for co-ions.

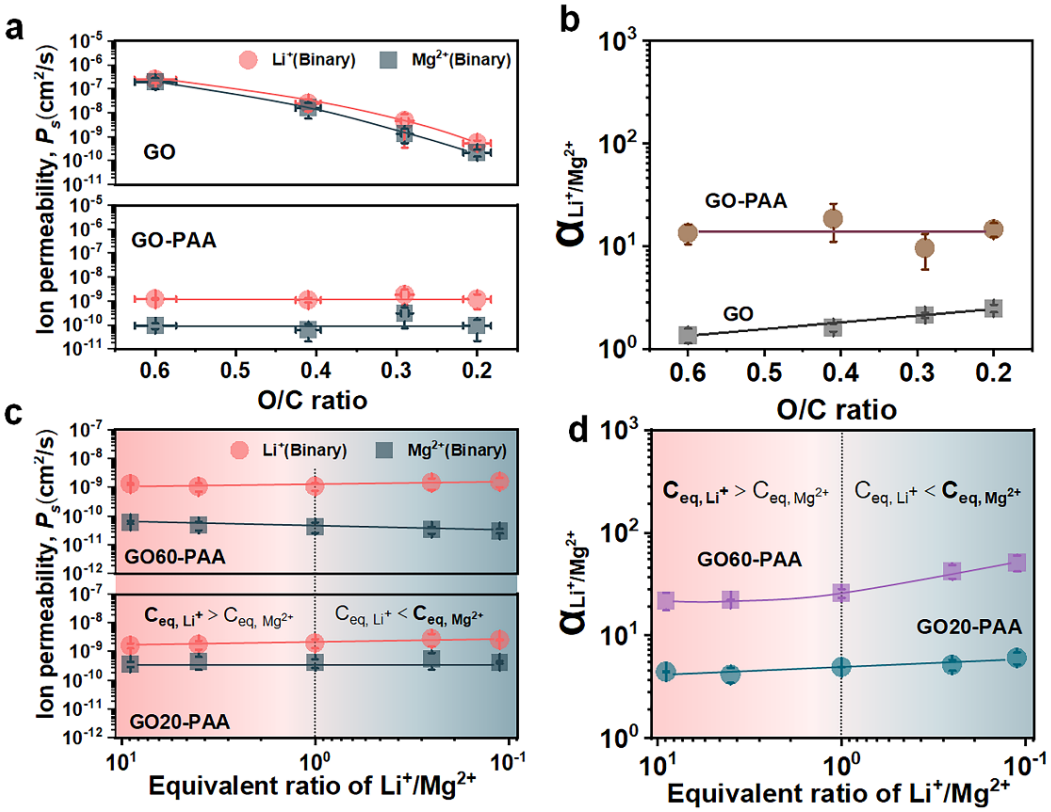

Fig. 2.10 (a) Ion permeability, and (b) ion/ion selectivity of cation pair of different GO-

PAA membranes; (c) Ion permeability, and (d) ion/ion selectivity of cation pair of GO60-PAA and GO20-PAA membranes with various feed solutions (the charge-equivalent concentration ratios of Li^+ and Mg^{2+} ($C_{eq,\ Li^+}/C_{eq,Mg^{2+}}$) are 9/1, 4/1, 1/1, 1/4, and 1/9).

The underlying ion/ion selectivity mechanism of the GO-PAA membranes was further confirmed using counter-ions (SO_4^{2-} and Cl^-). The SO_4^{2-}/Cl^- selectivity sharply decreased with a decrease in the O/C ratio of the nanochannel, which could be attributed to the adverse effects of electrostatic attraction [51] on selectivity (**Fig. 2.11a-b**). Positively charged GO-PAA membranes attracted counter-ions (SO_4^{2-} and Cl^-) via electrostatic interactions, compromising the selectivity of Cl^-/SO_4^{2-} [48]. A decreased O/C ratio led to a more significant decrease in SO_4^{2-}/Cl^- selectivity. Since PAA was coated for all GO-PAA membranes, the difference of SO_4^{2-}/Cl^- selectivity would be due to the varied interlayered nanochannels of the GO with different O/C ratios.

Separation of Cl^-/SO_4^{2-} by GO20-PAA and GO60-PAA using different ion compositions was then evaluated. GO60-PAA exhibited increased selectivity when the equivalent concentration of SO_4^{2-} became higher while the GO20-PAA remained relatively constant (**Fig. 2.11c-d**). Cl^-/SO_4^{2-} selectivity would be further hindered ascribed to the narrowed interlayer spacing, leading to the largely increased transport resistance for both Cl^- and SO_4^{2-}. Hence the differentiation of Cl^- and SO_4^{2-} was further weakened. In contrast, for the GO60-PAA with larger interlayer spacing, ion competition was emphasized, leading to faster permeation of Cl^- with a low valence and smaller size in the nanochannel compared to SO_4^{2-} [49]. Therefore, the GO60-PAA membrane with larger interlayer spacing exhibited increasing ion/ion selectivity with decreasing equivalent ratio of Cl^-/SO_4^{2-}, highlighting the contributive of a relatively large interlayer spacing in the nanochannel for the enhancement of ion/ion selectivity. It was concluded that the appropriate expansion of the subnanometer channel with a favorable charge density achieved efficient mass transfer and promising ion/ion selectivity.

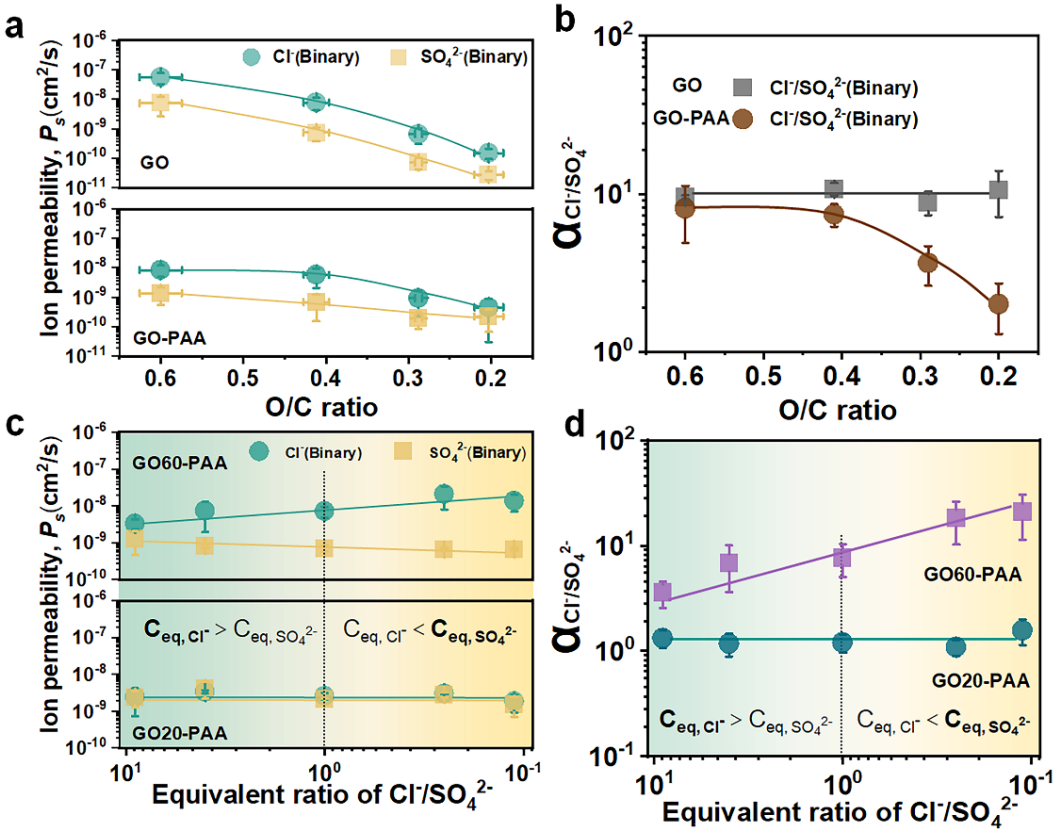

Fig. 2.11 (a) Ion permeability, and (b) ion/ion selectivity of anion pair of different GO-PAA membranes; (c) Ion permeability, and (d) ion/ion selectivity of anion pair of GO60-PAA and GO20-PAA membranes with various feed solutions (the charge-equivalent concentration ratios of Cl^- and SO_4^{2-} ($C_{eq,Cl^-}/C_{eq,SO_4^{2-}}$) are 9/1, 4/1, 1/1, 1/4, and 1/9).

The performance of different GO nanochannels for co-ion separation was summarized. The ion/ion selectivity versus permeability was plotted to indicate the favorable characteristics of the nanochannels for separation (**Fig. 2.12**). When more charged groups were introduced to the nanochannels (GO membrane with higher O/C ratio), the co-ions (Cl^-/SO_4^{2-}) selectivity was almost constant along with the water permeability improvement due to the accompanied channel size expanding, implying more target solutions could be processed without compromising ion/ion selectivity. In addition, applying a surface coating with abundant positively charged groups (PAA modification) is a simple strategy to significantly improve counter-ion (Li^+/Mg^{2+} for

GO membrane) selectivity. After oppositely charged modification of the membrane surface, the co-ion selectivity was enhanced. Therefore, it is concluded that the difference in electrostatic effects for mono- and di-valent ions plays a more important role and is more effective in enhancing their ion/ion selectivity within the subnanometer channel.

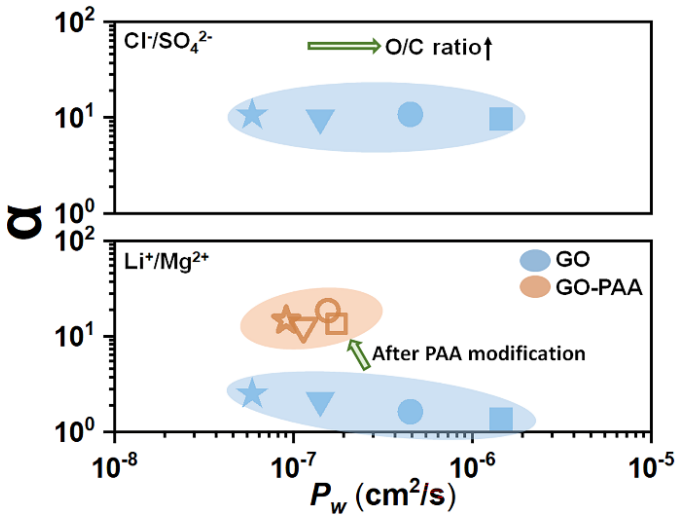

Fig. 2.12 Summary of water permeability and ion/ion selectivity of GO and GO-PAA membranes.

2.4 Conclusions

In this chapter, there are explored the correlation between nanochannel properties and the selectivity of single-salt solutes. By manipulating the charge and interlayer spacing of GO membrane nanochannels, it is investigated that the impact of electrostatic interactions and steric hindrance on the separation of ion pairs such as SO_4^{2-}/Cl^- and Li^+/Mg^{2+}. The key findings are as follows: (1) The nanochannel size of the GO membrane exhibited limited ability to differentiate between hydrated mono- and di-valent ions, possibly due to the flexibility of nanochannel that cannot strictly sieve ions based on specific sizes; (2) Electrostatic interactions between mono- and di-valent ions played a more substantial role within the subnanometer channels, surpassing the influence of size, thereby enhancing ion/ion selectivity significantly; (3) Emphasis was placed on the contribution of ion competition in binary solutions to selectivity. Binary solutions with high concentrations of high-valent ions were observed to be

selectively separated more easily. This study highlighted the dominance of electrostatic interactions over the channel size effect in enhancing ion/ion selectivity. Designing nanochannels with larger interlayer spacing and an abundance of charges proved advantageous for efficient single-salt selective processes. These findings not only contribute to a better understanding of nanochannel selectivity but also provide valuable insights for the design of two-dimensional membranes, enhancing their performance across various separation applications.

References

[1] Y. Zhao, X. Tong, J. Kim, T. Tong, C.H. Huang, Y. Chen, Capillary-Assisted Fabrication of Thin-Film Nanocomposite Membranes for Improved Solute-Solute Separation, Environ. Sci. Technol. 56(9) (2022) 5849-5859.

[2] R. Epsztein, R.M. DuChanois, C.L. Ritt, A. Noy, M. Elimelech, Towards single-species selectivity of membranes with subnanometre pores, Nat Nanotechnol 15(6) (2020) 426-436.

[3] C. Zhao, Y. Zhang, Y. Jia, B. Li, W. Tang, C. Shang, R. Mo, P. Li, S. Liu, S. Zhang, Polyamide membranes with nanoscale ordered structures for fast permeation and highly selective ion-ion separation, Nat Commun 14(1) (2023) 1112.

[4] L. Wang, S. Lin, Mechanism of Selective Ion Removal in Membrane Capacitive Deionization for Water Softening, Environ. Sci. Technol. 53(10) (2019) 5797-5804.

[5] M.A. Halakarni, A. Samage, A. Mahto, V. Polisetti, S.K. Nataraj, Forward osmosis process for energy materials recovery from industrial wastewater with simultaneous recovery of reusable water: a sustainable approach, Materials Today Sustainability 22 (2023).

[6] Y. Zhao, X. Tong, Y. Chen, Fit-for-Purpose Design of Nanofiltration Membranes for Simultaneous Nutrient Recovery and Micropollutant Removal, Environ. Sci. Technol. 55(5) (2021) 3352-3361.

[7] Y. Li, S. Wang, H. Li, G. Kang, Y. Sun, H. Yu, Y. Jin, Y. Cao, Preparation of highly selective nanofiltration membranes by moderately increasing pore size and optimizing microstructure of polyamide layer, J. Membr. Sci. 643 (2022).

[8] I. Shefer, K. Lopez, A.P. Straub, R. Epsztein, Applying Transition-State Theory to Explore Transport and Selectivity in Salt-Rejecting Membranes: A Critical Review, Environ. Sci. Technol. 56(12) (2022) 7467-7483.

[9] G.D. Kang, Y.M. Cao, Development of antifouling reverse osmosis membranes for water treatment: A review, Water Res. 46(3) (2012) 584-600.

[10] M. Zhang, W. Jin, F. Yang, M. Duke, Y. Dong, C.Y. Tang, Engineering a Nanocomposite Interlayer for a Novel Ceramic-Based Forward Osmosis Membrane

with Enhanced Performance, Environ. Sci. Technol. 54(12) (2020) 7715-7724.
[11] L. Yang, J. Zhou, Q. She, M.P. Wan, R. Wang, V.W. Chang, C.Y. Tang, Role of calcium ions on the removal of haloacetic acids from swimming pool water by nanofiltration: mechanisms and implications, Water Res. 110 (2017) 332-341.
[12] Z. Lu, Y. Wu, L. Ding, Y. Wei, H. Wang, A Lamellar MXene (Ti3 C2 Tx)/PSS Composite Membrane for Fast and Selective Lithium-Ion Separation, Angew. Chem. Int. Ed. Engl. 60(41) (2021) 22265-22269.
[13] K. Wang, X. Wang, B. Januszewski, Y. Liu, D. Li, R. Fu, M. Elimelech, X.J.C.S.R. Huang, Tailored design of nanofiltration membranes for water treatment based on synthesis–property–performance relationships, 51(2) (2022) 672-719.
[14] H.B. Park, J. Kamcev, L.M. Robeson, M. Elimelech, B.D. Freeman, Maximizing the right stuff: The trade-off between membrane permeability and selectivity, Science 356(6343) (2017).
[15] K. Gu, S. Wang, Y. Li, X. Zhao, Y. Zhou, C. Gao, A facile preparation of positively charged composite nanofiltration membrane with high selectivity and permeability, J. Membr. Sci. 581 (2019) 214-223.
[16] Q. Wang, Y. Wang, B.-Z. Chen, T.-D. Lu, H.-L. Wu, Y.-Q. Fan, W. Xing, S.-P. Sun, Designing High-Performance Nanofiltration Membranes for High-Salinity Separation of Sulfate and Chloride in the Chlor-Alkali Process, Industrial & Engineering Chemistry Research 58(27) (2019) 12280-12290.
[17] Y. Zhang, L. Wang, W. Sun, Y. Hu, H. Tang, Membrane technologies for Li+/Mg2+ separation from salt-lake brines and seawater: A comprehensive review, Journal of Industrial and Engineering Chemistry 81 (2020) 7-23.
[18] A.W. Mohammad, Y.H. Teow, W.L. Ang, Y.T. Chung, D.L. Oatley-Radcliffe, N. Hilal, Nanofiltration membranes review: Recent advances and future prospects, Desalination 356 (2015) 226-254.
[19] E. Nightingale, Jr, Phenomenological theory of ion solvation. Effective radii of hydrated ions, J. Phys. Chem. A 63(9) (1959) 1381– 1387.
[20] Y. Kang, Y. Xia, H. Wang, X. Zhang, 2D Laminar Membranes for Selective Water

and Ion Transport, Adv. Funct. Mater. 29(29) (2019).

[21] Z.L. Qiu, L.F. Fang, Y.J. Shen, W.H. Yu, B.K. Zhu, C. Helix-Nielsen, W. Zhang, Ionic Dendrimer Based Polyamide Membranes for Ion Separation, ACS Nano 15(4) (2021) 7522-7535.

[22] Y. Zhao, T. Tong, X. Wang, S. Lin, E.M. Reid, Y. Chen, Differentiating Solutes with Precise Nanofiltration for Next Generation Environmental Separations: A Review, Environmental Science & Technology 55(3) (2021) 1359-1376.

[23] H. Peng, Q. Tang, S. Tang, J. Gong, Q. Zhao, Surface modified polyamide nanofiltration membranes with high permeability and stability, J. Membr. Sci. 592 (2019).

[24] Z. He, K. Wang, The 'ideal selectivity' vs 'true selectivity' for permeation of gas mixture in nanoporous membranes, IOP Conference Series: Materials Science and Engineering 323 (2018).

[25] J. Luo, Y. Wan, Effects of pH and salt on nanofiltration—a critical review, J. Membr. Sci. 438 (2013) 18-28.

[26] H. Zhang, Q. He, J. Luo, Y. Wan, S.B. Darling, Sharpening Nanofiltration: Strategies for Enhanced Membrane Selectivity, ACS Appl Mater Interfaces 12(36) (2020) 39948-39966.

[27] J. Lyu, X. Wen, U. Kumar, Y. You, V. Chen, R.K. Joshi, Separation and purification using GO and r-GO membranes, RSC Adv 8(41) (2018) 23130-23151.

[28] R.K. Joshi, P. Carbone, F.C. Wang, V.G. Kravets, Y. Su, I.V. Grigorieva, H.A. Wu, A.K. Geim, R.R. Nair, Precise and Ultrafast Molecular Sieving Through Graphene Oxide Membranes, Science 343 (2014).

[29] K. Guan, S. Wang, Y. Ji, Y. Jia, L. Zhang, K. Ushio, Y. Lin, W. Jin, H.J.J.o.M.C.A. Matsuyama, Nanochannel-confined charge repulsion of ions in a reduced graphene oxide membrane, J. Mater. Chem. A 8(48) (2020) 25880-25889.

[30] L. Xie, J. Tang, R. Qin, Q. Zhang, J. Liu, Y. Jin, H. Wang, Surface Charge Modification on 2D Nanofluidic Membrane for Regulating Ion Transport, Adv. Funct. Mater. 33(4) (2022).

[31] K. Guan, Z. Mai, S. Zhou, S. Fang, Z. Li, P. Xu, Y.H. Chiao, M. Hu, P. Zhang, G. Xu, K. Nakagawa, H. Matsuyama, Side-Chain-Dependent Functional Intercalations in Graphene Oxide Membranes for Selective Water and Ion Transport, Nano Lett. 23(13) (2023) 6095-6101.

[32] M. Sun, J. Li, Graphene oxide membranes: Functional structures, preparation and environmental applications, Nano Today 20 (2018) 121-137.

[33] Y. Li, S. Yuan, Y. Xia, W. Zhao, C.D. Easton, C. Selomulya, X. Zhang, Mild annealing reduced graphene oxide membrane for nanofiltration, J. Membr. Sci. 601 (2020).

[34] M. Paul, S.D. Jons, Chemistry and fabrication of polymeric nanofiltration membranes: A review, Polymer 103 (2016) 417-456.

[35] K. Guan, Y. Jia, Y. Lin, S. Wang, H. Matsuyama, Chemically Converted Graphene Nanosheets for the Construction of Ion-Exclusion Nanochannel Membranes, Nano Lett. 21(8) (2021) 3495-3502.

[36] S. Zhou, K. Guan, Z. Wang, Q. Song, Z. Li, P. Xu, L. Deng, S. Xiang, H. Matsuyama, Confined and mediated intercalation of nanoparticles in graphene oxide membrane to fine-tune desalination performance, Chem. Eng. J. 465 (2023).

[37] Z. Yang, R. Takagi, X. Zhang, T. Yasui, L. Zhang, H. Matsuyama, Engineering a dual-functional sulfonated polyelectrolyte-silver nanoparticle complex on a polyamide reverse osmosis membrane for robust biofouling mitigation, J. Membr. Sci. 618 (2021).

[38] G.M. Geise, H.B. Park, A.C. Sagle, B.D. Freeman, J.E. McGrath, Water permeability and water/salt selectivity tradeoff in polymers for desalination, J. Membr. Sci. 369(1-2) (2011) 130-138.

[39] M. Zhang, K. Guan, Y. Ji, G. Liu, W. Jin, N. Xu, Controllable ion transport by surface-charged graphene oxide membrane, Nature Communications 10(1) (2019).

[40] K. Raidongia, J. Huang, Nanofluidic ion transport through reconstructed layered materials, J. Am. Chem. Soc. 134(40) (2012) 16528-31.

[41] Y.-L. Xing, G.-R. Xu, Z.-H. An, Y.-H. Liu, K. Xu, Q. Liu, H.-L. Zhao, R. Das, Laminated GO membranes for water transport and ions selectivity: Mechanism,

synthesis, stabilization, and applications, Sep. Purif. Technol. 259 (2021).

[42] W.-S. Hung, S.-M. Chang, R.L.G. Lecaros, Y.-L. Ji, Q.-F. An, C.-C. Hu, K.-R. Lee, J.-Y. Lai, Fabrication of hydrothermally reduced graphene oxide/chitosan composite membranes with a lamellar structure on methanol dehydration, Carbon 117 (2017) 112-119.

[43] S. Zheng, Q. Tu, J.J. Urban, S. Li, B. Mi, Swelling of graphene oxide membranes in aqueous solution: Characterization of interlayer spacing and insight into water transport mechanisms, ACS Nano 11(6) (2017) 6440-6450.

[44] A. Iakunkov, A.V. Talyzin, Swelling properties of graphite oxides and graphene oxide multilayered materials, Nanoscale 12(41) (2020) 21060-21093.

[45] H. Yu, Y. He, G. Xiao, Y. Fan, J. Ma, Y. Gao, R. Hou, X. Yin, Y. Wang, X. Mei, The roles of oxygen-containing functional groups in modulating water purification performance of graphene oxide-based membrane, Chem. Eng. J. 389 (2020).

[46] Parna Mukherjee, A.K. SenGupta, Ion Exchange Selectivity as a Surrogate Indicator of Relative Permeability of Ions in Reverse Osmosis Processes, Environmental Science & Technology 37(7) (2003) 1432-1440.

[47] T. Zhang, W. Zheng, Q. Wang, Z. Wu, Z. Wang, Designed strategies of nanofiltration technology for Mg2+/Li+ separation from salt-lake brine: A comprehensive review, Desalination 546 (2023).

[48] D. Lu, T. Ma, S. Lin, Z. Zhou, G. Li, Q. An, Z. Yao, Q. Sun, Z. Sun, L. Zhang, Constructing a selective blocked-nanolayer on nanofiltration membrane via surface-charge inversion for promoting Li+ permselectivity over Mg2+, J. Membr. Sci. 635 (2021).

[49] J. Garcia-Aleman, J.M. Dickson, Permeation of mixed-salt solutions with commercial and pore-filled nanofiltration membranes: membrane charge inversion phenomena, J. Membr. Sci. 239(2) (2004) 163-172.

[50] R. He, C. Dong, S. Xu, C. Liu, S. Zhao, T. He, Unprecedented Mg2+/Li+ separation using layer-by-layer based nanofiltration hollow fiber membranes, Desalination 525 (2022).

[51] Y. Li, S. Wang, W. Wu, H. Yu, R. Che, G. Kang, Y. Cao, Fabrication of positively charged nanofiltration membrane with uniform charge distribution by reversed interfacial polymerization for Mg2+/Li+ separation, J. Membr. Sci. 659 (2022).

[52] R. He, S. Xu, R. Wang, B. Bai, S. Lin, T. He, Polyelectrolyte-based nanofiltration membranes with exceptional performance in Mg2+/Li+ separation in a wide range of solution conditions, J. Membr. Sci. 663 (2022).

[53] D. Rana, T. Matsuura, Surface Modifications for Antifouling Membranes, Chem. Rev. 110(4) (2010) 2448–2471.

[54] S. Déon, Z. Koubaa, E. Korzhova, A. Airoudj, P. Fievet, V. Roucoules, Understanding the impact of poly(allylamine) plasma grafting on the filtration performances of a commercial polymeric membrane, Sep. Purif. Technol. 212 (2019) 30-39.

Chapter 3

Nanochannel stability of chemically converted graphene oxide membranes

3.1. Introduction

Recently, multitudinous two-dimensional (2D) materials have been widely applied to sustainable energy technology and environmental remediation, including graphene and its derivatives [1], layered metal dichalcogenides (LMDCs) [2], metal oxides and 2D zeolites [3], metal-organic framework (MOF) nanosheets [4], 2D covalent organic frameworks (2D-COFs) [5] and so on. By tailoring the in- and out-of-plane nanostructures, 2D materials receive growing interests in many application areas, including electronic/optical [6], catalysis [7], energy storage [8], and membrane separation [9]. 2D materials are considered as ideal building blocks to construct membranes with layered structures owing to the distinct and tunable physiochemical properties [10]. The interlayered nanoscale space with between stacked nanosheets in the 2D laminates is ultilized as nanochannels for separation of desired molecules or ions [11]. In addition, the interlayered nanochannels are facile for implementing modification and thereby promoting the interactions of the membrane with the separable contaminants, which induces superb prospects in customizing high-quality modified membranes [12].

Although the introduction of modifications onto 2D materials potentially allows for turning the nanochannel performance, the instability of nanochannel membranes would be unfortunately induced [13], especially in liquid environments. The modification agents in the laminates may change the intra- or inter-molecule interactions in the modified nanochannel membranes, leaving impacts on the structure

stability in liquids. For instance, the modification with higher water affinity would lead to swelling of laminate structure in aqueous environments [14], weakening the nanochannel separation precision. Additionally, the uncertainty of external conditions (e.g., pressure, temperature, and target solution properties) when transporting fluids may further aggravate the instability of the nanochannels [15]. Therefore, it significantly restricts the available separation scenarios for nanochannel membranes to function effectively [16].

Graphene oxide (GO) is one of the most widely used building blocks for nanochannel membranes [17]. It has been widely demonstrated that GO laminar membranes contain two main kinds of transport channels: plane-to-plane interlayer galleries and edge-to-edge slit-like pores [18]. Meanwhile, these transport channels could be feasibly modified by altering the oxygen-containing functional groups between GO sheets [19]. Despite the intense study of GO nanochannel membranes for water purifications, similar to most 2D membranes, the water-instability frustrates the separation precision of the nanochannels [20]. In general, the swelling phenomenon of the GO membranes in water originates from the insertion of water molecules that weaken the hydrogen bonding and π-π interactions between adjacent layers [21]. To relieve this instability, chemically converting GO to modify its original oxygenated functional groups and to introduce is a feasible strategy [22, 23]. Different converted GO membranes have been reported possessing the precisely manipulated nanochannels for high-performance separation [24]. Nevertheless, how the molecule properties of conversion agents would affect the stabilization of nanochannels and how effectively the nanochannel could be stabilized accordingly are rarely studied. Gaining relevant insights of these would benefit the molecular design of modification agents for feasible construction of stable GO nanochannel membranes.

In order to systematically investigate the relationships between nanochannel stability and separation performance rendered by functional conversion agents, there is report the use of a series of saccharide molecules as agents to chemically modify GO for the construction of stable nanochannels. Monosaccharide glucose (Glu),

disaccharide maltose (Glu2), and trisaccharide maltotriose (Glu3) are chosen because they can function as reducing agents with the same reducing end in their molecules. They can convert GO with controlled reduction of oxygenated functional groups. Meanwhile, the saccharide molecules would be possibly attached to GO nanosheets during chemical conversion process and retained in the stacked laminate membrane as an intercalating molecule, which may also induce effects on the stability state of nanochannels. Therefore, the conversion of GO nanosheets using these different reducing agents would possibly lead to different nanochannel environment. A series of GO membrane nanochannels with different reduction and intercalation were systematically analyzed and compared to relate the saccharide molecular properties with nanochannel stability. It is expected to provide certain insights into the stabilization process of nanochannels and the selection of modifying agents.

3.2 Experimental

3.2.1 Materials

Maltose monohydrate, and Maltotriose (＞90%) were obtained from Sigma-Aldrich Co. LLC (St. Louis, MO, USA). Glycerol (99.0%), D-(+)- sucrose (＞99.0%), and D-(+)-raffinose pentahydrate (＞98.0%) were obtained from Tokyo Chemical Industry (TCI) Co., Ltd., Japan. And other chemicals used in this work were same as Chapter 2.

3.2.2 Preparation of GO, Glu/GO, Glu2/GO, and Glu3/GO membranes

The GO, Glu/GO, Glu2/GO, and Glu3/GO membranes were prepared by vacuum filtration [25]. The precursor suspension of the GO membrane is a 10 mL aqueous suspension containing GO (0.15 mg) and 28% ammonia solution (40 μL). In addition, the pre-suspension of Glu/GO, Glu2/GO, and Glu3/GO membranes are 10 mL aqueous suspension including GO (0.15 mg), 28% ammonia solution (40 μL), and reducing sugar. After uniformly mixed, the suspensions were then placed in a water bath at 94.5 °C for 20 min. Subsequently, the precursor suspensions were diluted with deionized

water to 300 mL and sonicated in an ice-water bath for 5 min. Finally, the above solution was vacuum-filtered onto a nylon substrate to prepare the GO, Glu/GO, Glu2/GO, and Glu3/GO membranes. The fabricated membranes were then dried in a desiccator for 24 h at room temperature. Taking Glu as an example, Glu/GO-0.4, Glu/GO-2.1, Glu/GO-4.3, Glu/GO-8.5, and Glu/GO-17.0 represent the addition amounts of Glu as 0.4, 2.1, 4.3, 8.5, and 17.0 μmol.

3.2.3 Characterization

The retention of neutral molecules and intercalation amount were measured by total organic carbon (TOC) analyzer (TOC-VCSH, Shimadzu, Kyoto, Japan). The evaluation of chemical compositions and interlayer spacing of GO, Glu/GO, Glu2/GO, and Glu3/GO membranes were the same as in Chapter 2.

3.2.4 Membrane performance

The desalination performance of GO, Glu/GO, Glu2/GO, and Glu3/GO membranes were determined by a cross-flow device (flow rate: 10 mL min^{-1}, effective membrane surface area 7.06 cm^2), as reported previously [26]. The deionized water used in the experiment was provided by a Milli-Q water system (Merck Millipore, Darmstadt, Germany). Subsequently, the GO membranes were pre-compacted to stability at a pressure of 10 bar and then tested at a transmembrane pressure of 10 bar. Finally, the water permeance (A, L m^{-2} h^{-1} bar^{-1}) was calculated by Equation 3.1:

$$A = \frac{\Delta V}{A_m \times \Delta t \times \Delta P} \tag{3.1}$$

where ΔV is permeated volume (L), A_m is the effective membrane area (m^2), Δt is test time, and ΔP indicates transmembrane pressure (bar).

NaCl and Na_2SO_4 aqueous solution at the same concentration (2000 ppm) were prepared to evaluate the separation performance of GO, Glu/GO, Glu2/GO, and Glu3/GO membranes. In addition, the electrical conductivity of the samples on the feed and permeate sides were measured using a conductivity meter (Ultrameter IITM 4P,

Myron L Company, Japan). The retention of the salts (R) was determined using Equation 3.2:

$$R(\%) = \left(1 - \frac{C_p}{C_f}\right) \times 100\% \tag{3.2}$$

where C_p and C_f represent the solute concentrations of the permeate and feed sides.

3.2.5 Determination of molecular weight cutoff (MWCO) values and pore size distribution

The separation of neutral molecules of the GO, Glu/GO, Glu2/GO, and Glu3/GO membranes was evaluated using glycerol (92 Da), glucose (180 Da), sucrose (342 Da), and raffinose (504 Da) with the same concentration (1000 ppm). The experimental conditions and retention calculations same as those for retention tests for single salts were followed. Here, C_p and C_f are the neutral molecule concentrations (determined by a total organic analyzer, TOC-VCSH, Shimadzu, Japan) of the permeate and feed sides, respectively.

According to some assumptions, the pore size distribution curve is represented as a probability density function: (1) there are no steric or hydrodynamic interactions between the solute and the nanochannels; (2) the mean pore size (μ_p, nm) of membranes is equal to the Stokes radius (d_p, nm) of the organic solute when the retention is 50%; (3) the distribution of membrane pore size is expressed by the geometric standard deviation of the probability density function curve, as shown in Equation 3.3 [27]:

$$\frac{\mathrm{d}R(d_p)}{\mathrm{d}d_p} = \frac{1}{d_p \ln \sigma_p \sqrt{2\pi}} \exp\left[-\frac{(\ln d_p - \ln \mu_p)^2}{2(\ln \sigma_p)^2}\right] \tag{3.3}$$

where the geometric standard deviation (σ_p) is determined by the ratio of the Stokes radius (d_s, nm) at a retention of 84.13% to the mean pore size (d_p, nm) with a retention is 50%.

The Stokes radii (r_p) of different neutral organic solutes related to their molecular weights (M_W) was obtained by Equation 3.4:

$$\log(r_p) = -1.4962 + 0.4654 \log(M_W) \tag{3.4}$$

According to the above, the Stokes radii of glycerol, glucose, sucrose, and raffinose were approximately 0.261, 0.359, 0.462, and 0.538 nm, respectively.

3.3 Results and discussion

3.3.1 Characterization of GO membranes reduced with different reducing sugars

The nanochannels of GO membranes could be chemically modified by glucose (Glu), maltose (Glu2), and maltotriose (Glu3), respectively. The modification of GO nanochannel membranes is mainly attributed to the chemical properties (as reducing agents) and physical properties (as intercalation materials) of Glu, Glu2, and Glu3 (**Fig. 3.1a**). On the one hand, the oxygen-containing functional groups on the GO nanosheets would be removed due to Glu, Glu2, and Glu3 possessing a similar reducing end of the hemiacetal groups [9, 28]. On the other hand, reducing sugars may serve as intercalation materials to stay between adjacent GO nanosheets due to hydrogen bonding [29] and confined nanochannels [30]. After the reduction process, the O/C ratios of Glu/GO, Glu2/GO, and Glu3/GO were decreased to 0.47, 0.38, and 0.40, respectively (**Fig. 3.1b**). Compared with pristine GO membranes, the reduced O/C ratios and weakened C-O peaks are attributed to the removal of oxygen-containing functional groups [31], which proves that GO nanochannels are modified successfully by different reducing sugars. Meanwhile, the discrepancy in the O/C ratio values of Glu/GO, Glu2/GO, and Glu3/GO membranes is mainly owed to the different modifications of oxygen-containing functional groups in the nanochannels [32] by various reducing sugars. In addition, the deformation of the nanochannels was observed through the XRD patterns of different GO membranes (**Fig. 3.1c**). After the treatment with reducing sugars, the laminar nanochannels became narrower based on the shift of characteristic peaks toward a higher degree [33]. According to Bragg's law [34], the interlayer spacings of GO, Glu/GO, Glu2/GO, and Glu3/GO membranes are 7.8, 7.4, 7.3, and 7.7 Å, respectively (**Fig. 3.1d**). The interlayer spacings of GO membranes introduced with reducing sugars are narrower compared with pristine GO membranes, which is ascribed to the reduced number density of functional groups in the plane and edges of nanosheets [35].

Compared with Glu/GO and Glu3/GO membranes, the Glu2/GO membrane reasonably possesses the narrower interlayer spacing due to its relatively low O/C ratio. However, the interlayer spacing of Glu3/GO is slightly larger than that of Glu/GO, an opposite trend to the O/C ratios, which may be due to the stay of maltotriose with larger molecular size in the neighbor GO nanosheets would hinder the shrinkage of the nanochannel. It can be concluded that Glu, Glu2 and Glu3 achieved chemical modification of GO nanochannels successfully. However, the reduction ability and intercalation behaviors of Glu, Glu2, and Glu3 are different although their have the same equivalent reducing end.

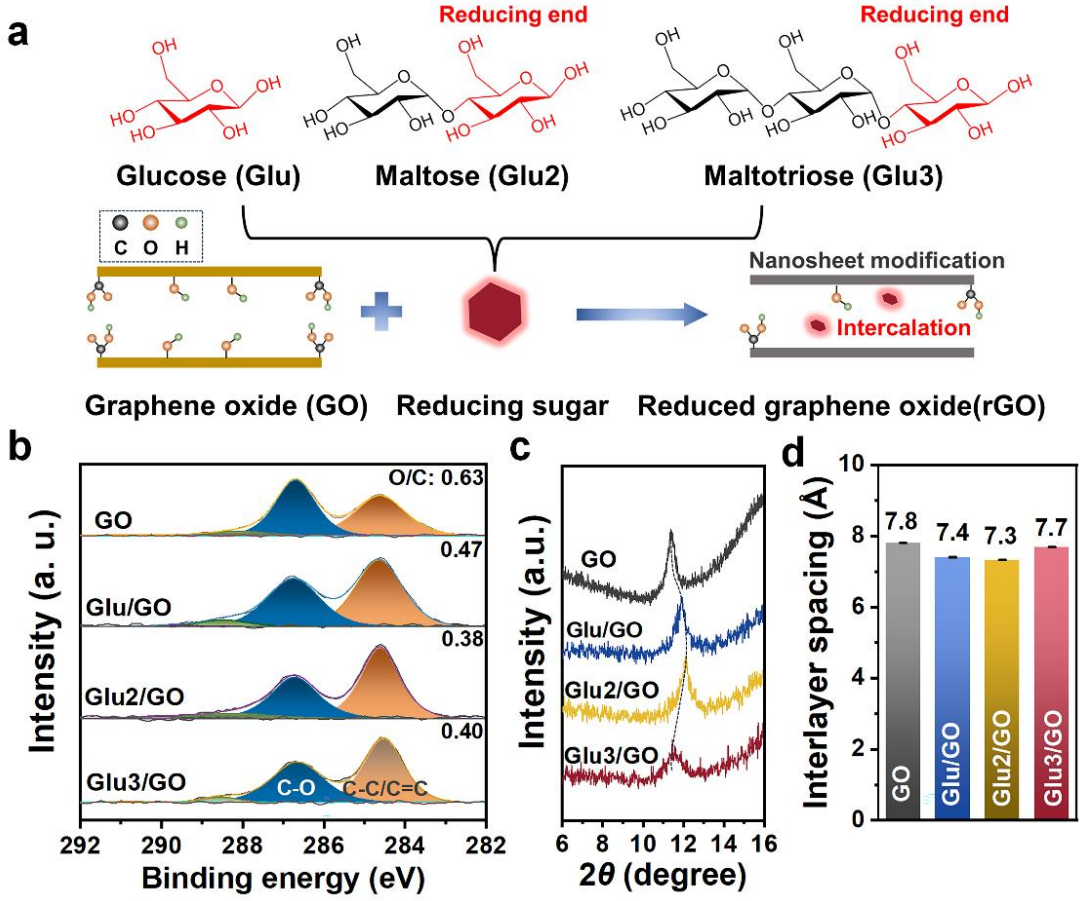

Fig. 3.1 (a) Schematic of GO nanochannels modified with glucose (Glu), maltose (Glu2), and maltotriose (Glu3); (b) C1s of XPS spectra, (c) XRD diffraction patterns, and (d) interlayer spacing of GO, Glu/GO, Glu2/GO, and Glu3/GO membranes. The additional amounts of glucose, maltose, and maltotriose are uniformly 2.1 μmol.

3.3.2 Stability of GO, Glu/GO, Glu2/GO and Glu3/GO membranes

To investigate the structural stability of nanochannels, the permeance of GO, Glu/GO, Glu2/GO, and Glu3/GO membranes during the operating process was evaluated. Generally, the GO membranes cannot maintain stability underwater mainly originating from the interaction between oxygen-containing functional groups and water molecules/ions, which leads to the laminate being rather sensitive to external conditions [23]. As shown in **Fig. 3.2a**, the GO membranes will undergo swelling induced by cations when the external solution changes from DI water to salt solutions, resulting in a sharp expansion of the nanochannels. Subsequently, the instability of the nanochannel is gradually mitigated due to the compaction of the membrane structure under the driving pressure. As displayed in **Fig. 3.2b**, the permeance of the pristine GO membrane increases significantly after the feed solution is changed to Na_2SO_4 because the cation-π interactions between Na^+ and oxygen-containing functional groups were generated once hydrated Na enters the nanochannels [36]. This unfavorable strong interaction results in expanded interlayer spacing and allows water molecules to transport with lower resistance. Immediately, there was almost no fluctuation in permeance when the target solution was replaced with NaCl since the interlayer spacing of the GO membrane was not affected by different anions (Cl^- and SO_4^{2-}) [37]. Therefore, the stability of the GO nanochannels could be reflected to a certain extent by changes in permeance. In order to systematically explore the transition of nanochannels from unstable to stable states, GO membranes with a series of reducing sugar additions were measured (**Fig. 3.2c-e**). In general, the transition of permeance from water to salt solution gradually weakens as the amount of reducing sugar increases, indicating that the Na-induced swelling of the nanochannels could be effectively impeded. For the Glu/GO membrane, the swelling of the nanochannels was effectively inhibited when the amount of glucose exceeded 4.3 μmol, which may be attributed to the appropriate reduction of oxygen-containing functional groups on the GO nanosheets (**Fig. 3.2c**) [38]. Glu2/GO obtained satisfactory and stable water and salt permeance when the addition amount was 2.1 μmol, which was earlier than that of Glu/GO

membrane (**Fig. 3.2d**). Surprisingly, the Glu3/GO membrane has reached a stable permeance at the amount of maltotriose is 0.4 μmol (**Fig. 3.2e**). However, the instability of the Glu3/GO nanochannel membrane reappeared when the amount of maltotriose was 17 μmol. Therefore, although glucose, maltose, and maltotriose possess the same equivalent of reducing ends, the permeance of Glu/GO, Glu2/GO, and Glu3/GO membranes exhibit different changing trends. It is concluded that the properties of reducing sugars including reducing ability, molecular size, and interaction with GO nanosheets need to be considered for the construction of stable nanochannels.

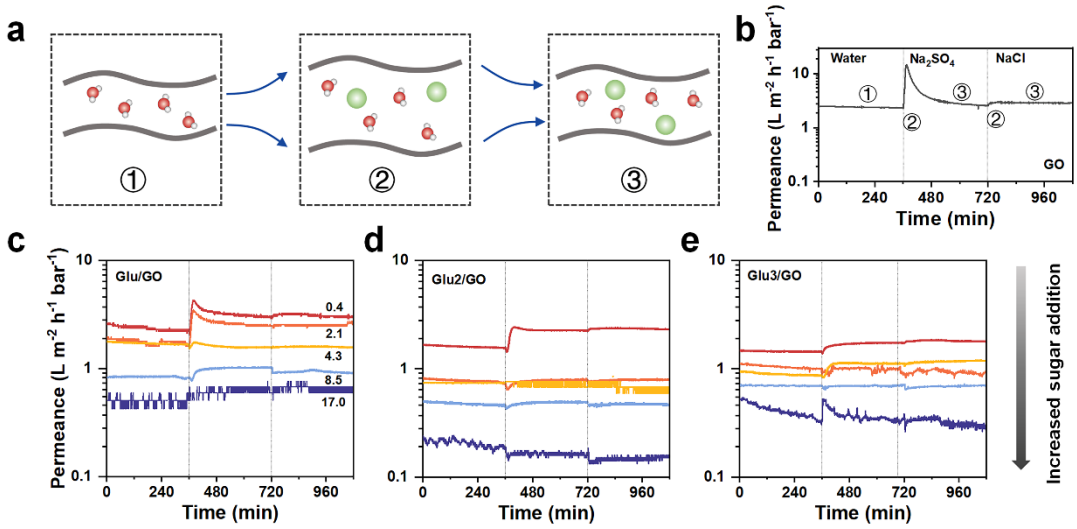

Fig. 3.2 (a) Schematic of nanochannel deformation of GO membranes during operating, (b) permeance of pristine GO membrane, (c-e) permeance of Glu/GO, Glu2/GO, and Glu3/GO membranes with different reducing sugar additions.

3.3.3 Performance of GO, Glu/GO, Glu2/GO and Glu3/GO membranes

In addition to stability, separation performance is an important index to evaluate the nanochannels. As the amount of reducing sugar increases, the water permeance decreases reasonably due to the oxygen components being removed continuously [39]. The water permeance of Glu/GO membrane decreased slightly with the increase of reducing sugar introduction attributed to the mild reductive ability of glucose (**Fig. 3.3a**) [40]. Meanwhile, the retention of salts are improved especially for NaCl due to the narrower nanochannels. In addition, Glu2/GO and Glu3/GO membranes also revealed a similar tendency, which proves that Glu, Glu2, and Glu3 with the potential to regulate

nanochannels and thereby improve separation performance (**Fig. 3.3b-c**). However, there are differences in the modification of nanochannels by Glu, Glu2, and Glu3. For Glu/GO and Glu3/GO membranes, the water permeance decreased weakly in the initial stage when the amount of reducing sugar was less than 8.5 μmol, and then decreased significantly when the amount reached 17 μmol. Different from them, the water permeance of Glu2/GO membrane exhibits a continuous and significant decrease. This indicates that Glu2 could satisfactorily adjust the permeability properties of nanochannels, which may be due to its stronger reducing ability and appropriate molecular size. In addition to water permeance, the retention of Na_2SO_4 and NaCl is indispensable for evaluating membrane performance. Among them, the retention of Na_2SO_4 of Glu/GO and Glu3/GO membranes is always maintained at around 80 % as the amount of reducing sugar increases, while the retention of Glu2/GO membrane satisfactorily above 90%. Specifically, when the amount of Glu2 added exceeds 2.1 μmol, the Na_2SO_4 retention rate has been stably regulated to more than 91.2 % accompanied by changes of water permeance. In addition, the NaCl retention of different GO membranes gradually increased as well as Glu2/GO had a higher and rapidly enhanced retention. The progressive decrease in the retention difference between Na_2SO_4 and NaCl is attributed to improvements in steric hindrance that generally more severely impedes the transport of NaCl [9]. In addition, the salt retention of Glu2/GO membrane is always higher than that of the Glu/GO and Glu3/GO membranes, proving that Glu2 with the ability to adjust GO nanochannels stably and efficiently. Therefore, maltose with moderate size and two glucose units exhibits satisfactory feasibility in regulating nanochannels.

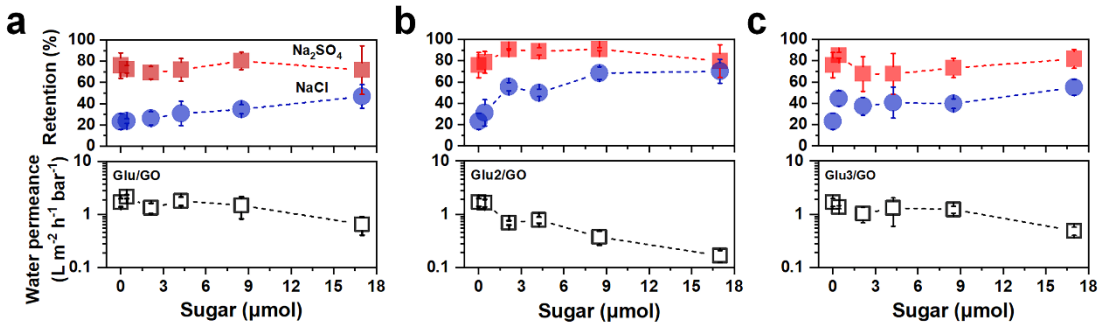

Fig. 3.3 Water permeance and salt retention of (a) Glu/GO, (b) Glu2/GO, and (c)

Glu3/GO membranes with different reducing sugar additions.

3.3.4 Nanochannel properties of GO, Glu/GO, Glu2/GO and Glu3/GO membranes

The specific behavior of nanochannel deformation induced by reducing sugars was analyzed for the construction of stable GO separation membranes. The O/C ratio decreases with the enrichment of reducing sugar content, proving the continued reduction of oxygen-containing functional groups (**Fig. 3.4a**) [41]. In addition, Glu2 and Glu3 would expose more reducing ends due to the possible partial hydrolysis of polysaccharides at high temperatures [42]. However, the sufficient reaction between large-sized Glu3 and GO nanosheets is limited due to the of more severe steric hindrance [43, 44]. Therefore, the O/C ratio of the Glu2/GO membrane is reasonably lower than that of the Glu/GO and Glu3/GO membranes, proving that Glu2 with a higher reducing ability and induces more oxygen-containing functional groups to be removed. Subsequently, the interlayer spacing as an important indicator for evaluating GO nanochannels was emphasized (**Fig. 3.4b**). With the amount of reducing sugar increases, the positions of the characteristic peak of Glu/GO, Glu2/GO, and Glu3/GO membranes shift to larger, unchanged, and smaller 2θ values, respectively (**Fig. 3.5**). According to Bragg's law [34], the interlayer spacing of Glu/GO, Glu2/GO, and Glu3/GO membranes decreases slightly, remains unchanged and increases significantly, respectively. Generally, the interlayer spacing gradually narrows with the removal of oxygen-containing functional groups. However, the interlayer spacing of Glu2/GO did not decrease although Glu2 exhibited significant reducing ability, which is attributed to the intercalation of reducing sugars within the nanochannel. Meanwhile, the interlayer spacing of Glu3/GO is gradually expanded due to the Glu3 with larger size inhibiting the shrinkage of the nanochannel severely. Additionally, the interlayer spacing of a GO membrane in a wet condition can be significantly larger than that in a dry condition because there is a high tendency to absorb water and swell in aqueous environments [37]. With the amount of reducing sugar increases, the difference of interlayer spacing between wet and dry conditions of the GO membranes reduction induced by different

reducing sugars gradually decreases, which indicates that the swelling phenomenon is gradually mitigated, especially for the Glu2/GO membrane. Furthermore, molecular weight cutoff (MWCO) curves of Glu/GO, Glu2/GO, and Glu3/GO membranes were obtained from the retention results of neutral organic solutes with varying molecular weights. Afterward, the probability density function curves were determined, representing the effective mean pore diameters of GO, Glu/GO-2.1, Glu2/GO-2.1 and Glu3/GO-2.1 membranes were 0.31, 0.31, 0.27 and 0.32 nm, respectively (**Fig. 3.4c**). Glu and Glu3 exhibit similar ability of nanochannel tuning according to nearly identical effective mean pore diameters of Glu/GO and Glu3/GO. Meanwhile, the pore sizes of Glu/GO and Glu3/GO are consistent with pristine GO membrane probably due to their weak reducing ability and intercalation within nanochannels. Compared with them, the effective mean pore diameter of Glu2/GO is significantly narrower, meaning that Glu2 can respond efficiently in regulating nanochannels. Glu2 not only ensures the effective adjustment of nanochannel size but also has satisfactory anti-swelling properties (**Fig. 3.4d**). With the enrichment of reducing sugars, the swelling ratio of the different membrane gradually decreases attribute to the reduction of oxygen-containing functional groups that induce the intercalation of water molecules [23]. The swelling ratio of the Glu2/GO membrane is obviously lower than that of Glu/GO and Glu3/GO membranes, certifying Glu2/GO with competitive and stable nanochannels. Although it has been demonstrated that reducing sugars serve as intercalation materials to stay between adjacent GO nanosheets, the effect of the intercalation amount of sugars on the nanochannels needs to be evaluated (**Fig. 3.4e**). With the addition amount increases, the intercalation amount slightly increases but is much less than complete intercalation, as well as the intercalation amounts of Glu, Glu2, and Glu3 are similar. Combined with changes of interlayer spacing, reducing sugar (Glu3) with larger molecular sizes would induce the expansion of the nanochannels and thus weaken the interlayer interactions, which may lead to the instability of the nanochannels. Therefore, Glu2 may be more appropriate and high-efficiency to be applied to construct stable and adjustable nanochannels compared with Glu and Glu3.

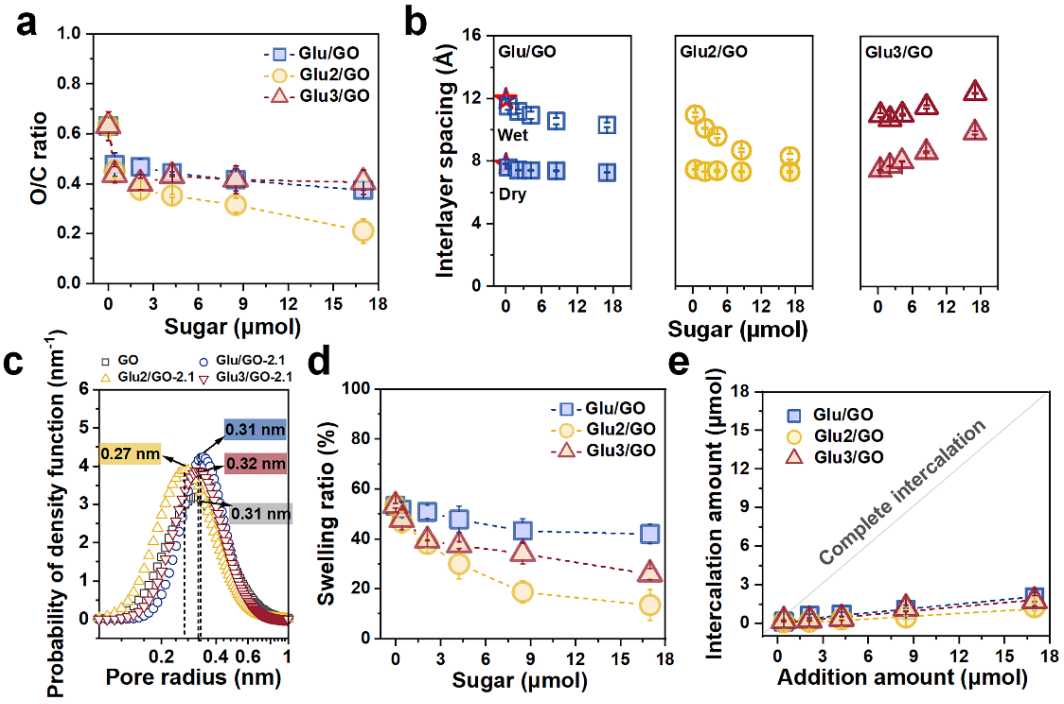

Fig. 3.4 (a) O/C ratios, (b) interlayer spacing, (c) pore size/pore size distribution, (d) swelling ratio, and (e) intercalation amount of Glu/GO, Glu2/GO, and Glu3/GO membranes with different reducing sugar additions.

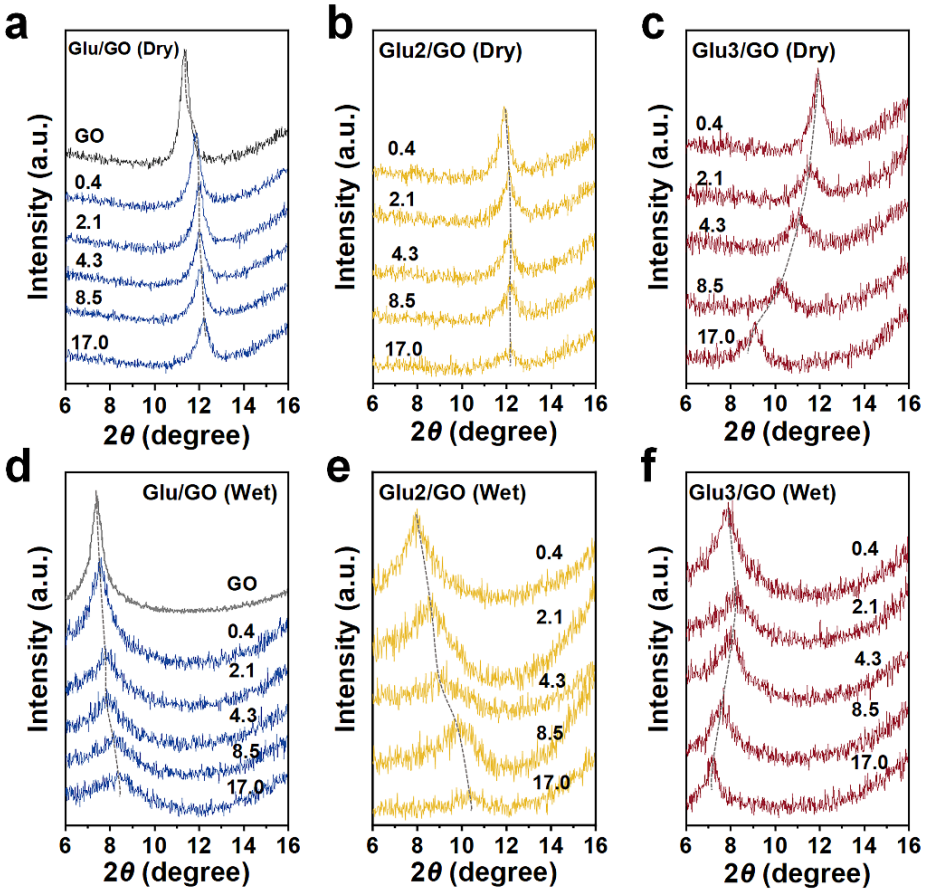

Fig. 3.5 XRD diffraction patterns of GO, Glu/GO, Glu2/GO, and Glu3/GO membranes under dry and wet conditions.

3.3.5 The stability of Glu2/GO membrane under different nanochannel environments

In order to further evaluate the stability of the nanochannels of the Glu2/GO membrane, different external environments were established. With the concentration of Na_2SO_4 increases from 500 ppm to 5000 ppm, the permeance and retention of the GO membrane decrease simultaneously (**Fig. 3.6a**). The decrease of permeance is attributed to the osmotic pressure of water increases, leading to aggravated concentration polarization and severely weakening the mass transfer driving force [45]. Meanwhile, the greater charge shield effect induced by Na^+ with the salt concentration increases, which would lessen the Donnan effect and thus reduce the retention of Na_2SO_4 [46]. In contrast, the introduction of Glu2 effectively prevents the serious loss of performance caused by the enhancement of concentration (**Fig. 3.6b**). Therefore, During the concentration range of 500-5000 ppm, the Glu2/GO-2.1 membrane was quite stable and without hysteresis curves [47]. The effect of operating pressure on the separation performance of the GO and Glu2/GO-2.1 membranes are presented in **Fig. 3.6c-d**. Glu2/GO revealed superb mechanical strength of nanochannels according to satisfactory robustness against high pressure [48]. This excellent pressure resistance originates from the mitigation of swelling and the intercalation of sugar within the nanochannels. Unfortunately, the desalination performance of GO membranes deteriorates sharply under high-pressure conditions due to the swelling of flexible GO nanochannels. Additionally, the temperature would also show an influence on GO membrane performance **(Fig. 3.6e-f)**. The retention of Na_2SO_4 improves with the increase of temperature primarily due to the degree of hydration of the functional groups on the membrane changing gradually. Specifically, the Stokes radius of the carboxyl group located at the edge of GO nanosheets increases with the higher temperature, which may be beneficial to promoting the separation of Na_2SO_4 [49]. Besides, the enhancement of permeance is accompanied by increased temperature,

which is mainly attributed to the strengthening of Brownian motion and the lower water viscosity [39]. As the temperature increases, GO and Glu2/GO membranes exhibit similar and reasonable performance trends. However, when the temperature decreases, the GO membrane exhibits an obvious hysteresis curve and the Glu2/GO membranes maintain excellent stability. Following this, the mechanical stability of GO membranes under different flow rates was evaluated. During the cycle of flow rate (10-50 mL min^{-1}), the permeance of the GO membrane first stabilized and then increased slightly (**Fig. 3.6g**). This instability may be due to the delamination of GO nanosheets by shear force in the cross-flow system [38]. In contrast, the Glu2/GO membrane exhibited excellent integrity while maintaining remarkable Na_2SO_4 retention and stable permeance in a flow rate of 50 mL min^{-1} (**Fig. 3.6h**). Therefore, the GO nanochannel regulated by Glu2 possesses satisfactory concentration, pressure, temperature and flow rate stability.

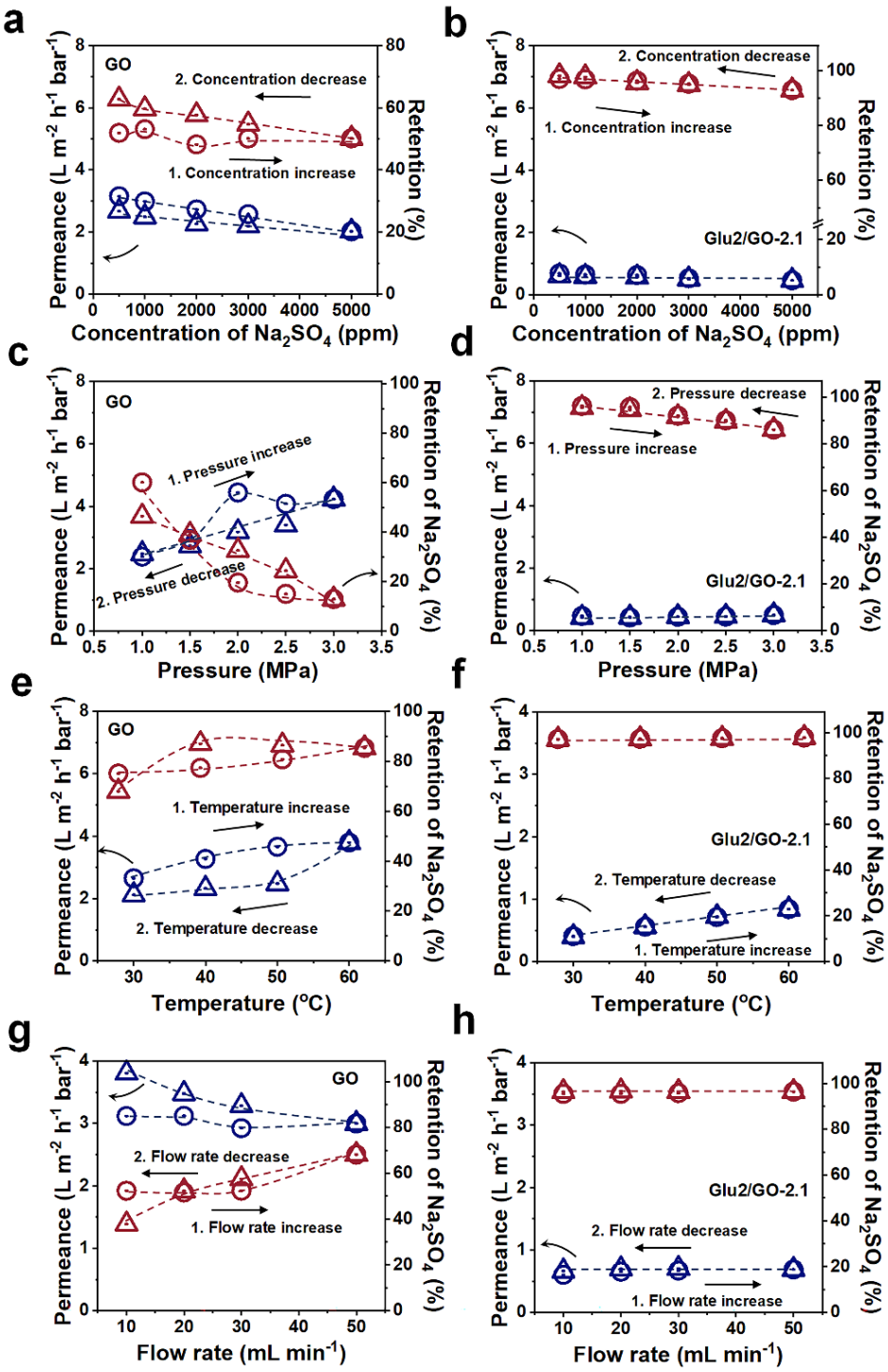

Fig. 3.6 Effect of (a-b) Na_2SO_4 concentration, (c-d) pressure, (e-f) temperature, and (g-h) flow rate on membrane stability.

To further evaluate the performance of the as-prepared Glu2/GO membrane, a long-term trial of 36 days was conducted to treat 2000 ppm Na_2SO_4 solution (**Fig. 3.7**).

As the operation time increases, both the permeance and retention change within a small range. In general, the permeance decreased slowly while the Na_2SO_4 retention increased slightly mainly due to compaction of the nanochannel and/or leakage of intercalation material (Glu2). Furthermore, the stable high value of the retention suggests that the Glu2-modified GO nanochannel could suppress swelling and enhance the rigidity of GO nanochannel, allowing it to withstand high operation pressure over one month without damage.

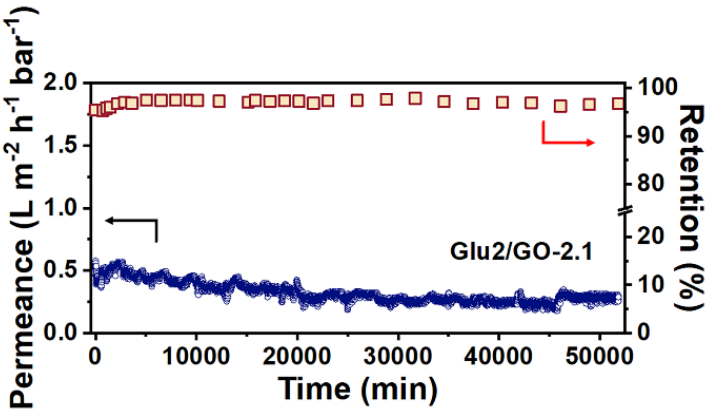

Fig. 3.7 Long-term stability of Glu2/GO-2.1 membrane.

3.4 Conclusions

Stable nanochannels were successfully constructed using a series of saccharide molecules as agents to chemically modify GO. The properties and concentration of reducing sugars were proved to be crucial factors in affecting the stability and nanochannel structure of GO membranes, thereby leading to the variation of desalination performance. It was proved that maltose (Glu2) exhibits satisfactory ability to regulate the stability and size of nanochannels. On the one hand, Glu2 with higher reducing ability could effectively control the density of oxygen-containing functional groups in the nanochannel. On the other hand, appropriate Glu2 as an intercalation material coupled with nanochannels ensures excellent Na_2SO_4 retention while maintaining stability. In addition, Glu2/GO nanochannel membranes have superb stability against different extreme external environments (concentration, pressure, temperature, flow rate). These promising results presented that the chemical molecules

with appropriate properties to mediate GO nanochannels have great potential and feasibility for the construction of 2D laminated membranes with stable and high separation performance.

References

[1] J. Zhao, Z. Wang, J.C. White, B. Xing, Graphene in the aquatic environment: adsorption, dispersion, toxicity and transformation, Environ. Sci. Technol. 48(17) (2014) 9995-10009.

[2] S.Z. Butler, S.M. Hollen, L. Cao, Y. Cui, J.A. Gupta, H.R. Gutierrez, T.F. Heinz, S.S. Hong, J. Huang, A.F. Ismach, E. Johnston-Halperin, M. Kuno, V.V. Plashnitsa, R.D. Robinson, R.S. Ruoff, S. Salahuddin, J. Shan, L. Shi, M.G. Spencer, M. Terrones, W. Windl, J.E. Goldberger, Progress, Challenges, and Opportunities in Two-Dimensional Materials Beyond Graphene, ACS Nano 7(4) (2013) 2898-2926.

[3] C.J. Heard, J. Cejka, M. Opanasenko, P. Nachtigall, G. Centi, S. Perathoner, 2D Oxide Nanomaterials to Address the Energy Transition and Catalysis, Adv. Mater. 31(3) (2019) e1801712.

[4] A. Dhakshinamoorthy, A.M. Asiri, H. Garcia, 2D Metal-Organic Frameworks as Multifunctional Materials in Heterogeneous Catalysis and Electro/Photocatalysis, Adv. Mater. 31(41) (2019) e1900617.

[5] S.B. Alahakoon, S.D. Diwakara, C.M. Thompson, R.A. Smaldone, Supramolecular design in 2D covalent organic frameworks, Chem. Soc. Rev. 49(5) (2020) 1344-1356.

[6] W.-g. Kim, S. Nair, Membranes from nanoporous 1D and 2D materials: A review of opportunities, developments, and challenges, Chem. Eng. Sci. 104 (2013) 908-924.

[7] X. Zhang, C. Li, J. Liang, S. Yang, F. Yuan, S. Zheng, J. Yi, Z. Sun, Catalytic membrane with multiscale iron-based catalysts anchored on 2D/2D hybrid g-C3N4/layered clay for pollutant removal, J. Membr. Sci. 685 (2023).

[8] J. Hu, X. Tang, Q. Dai, Z. Liu, H. Zhang, A. Zheng, Z. Yuan, X. Li, Layered double hydroxide membrane with high hydroxide conductivity and ion selectivity for energy storage device, Nat Commun 12(1) (2021) 3409.

[9] K. Guan, Y. Guo, Z. Li, Y. Jia, Q. Shen, K. Nakagawa, T. Yoshioka, G. Liu, W. Jin, H. Matsuyama, Deformation constraints of graphene oxide nanochannels under reverse osmosis, Nat Commun 14(1) (2023) 1016.

[10] L. Dai, K. Huang, Y. Xia, Z. Xu, Two-dimensional material separation membranes

for renewable energy purification, storage, and conversion, Green Energy & Environment 6(2) (2021) 193-211.

[11] P. Liu, J. Hou, Y. Zhang, L. Li, X. Lu, Z. Tang, Two-dimensional material membranes for critical separations, Inorganic Chemistry Frontiers 7(13) (2020) 2560-2581.

[12] L. Xie, J. Tang, R. Qin, Q. Zhang, J. Liu, Y. Jin, H. Wang, Surface Charge Modification on 2D Nanofluidic Membrane for Regulating Ion Transport, Adv. Funct. Mater. 33(4) (2022).

[13] T. Liu, X. Liu, N. Graham, W. Yu, K. Sun, Two-dimensional MXene incorporated graphene oxide composite membrane with enhanced water purification performance, J. Membr. Sci. 593 (2020).

[14] S. Kim, H. Wang, Y.M. Lee, 2D Nanosheets and Their Composite Membranes for Water, Gas, and Ion Separation, Angew. Chem. Int. Ed. Engl. 58(49) (2019) 17512-17527.

[15] Y. Wu, L. Ding, Z. Lu, J. Deng, Y. Wei, Two-dimensional MXene membrane for ethanol dehydration, J. Membr. Sci. 590 (2019).

[16] R. Rahighi, S.M. Hosseini-Hosseinabad, A.S. Zeraati, W. Suwaileh, A. Norouzi, M. Panahi, S. Gholipour, C. Karaman, O. Akhavan, M.A.R. Khollari, A. Vinu, A. Rashidi, A. Abdala, H. Karimi-Maleh, Y. Orooji, Two-dimensional materials in enhancement of membrane-based lithium recovery from metallic-ions-rich wastewaters: A review, Desalination 543 (2022).

[17] D.R. Dreyer, S. Park, C.W. Bielawski, R.S. Ruoff, The chemistry of graphene oxide, Chem. Soc. Rev. 39(1) (2010) 228-40.

[18] G. Liu, W. Jin, N. Xu, Two-Dimensional-Material Membranes: A New Family of High-Performance Separation Membranes, Angew. Chem. Int. Ed. 55(43) (2016) 13384-13397.

[19] H. Yu, Y. He, G. Xiao, Y. Fan, J. Ma, Y. Gao, R. Hou, X. Yin, Y. Wang, X. Mei, The roles of oxygen-containing functional groups in modulating water purification performance of graphene oxide-based membrane, Chem. Eng. J. 389 (2020).

[20] R.K. Joshi, S. Alwarappan, M. Yoshimura, V. Sahajwalla, Y. Nishina, Graphene oxide: the new membrane material, Applied Materials Today 1(1) (2015) 1-12.

[21] Y.C. An, X.X. Gao, W.L. Jiang, J.L. Han, Y. Ye, T.M. Chen, R.Y. Ren, J.H. Zhang, B. Liang, Z.L. Li, A.J. Wang, N.Q. Ren, A critical review on graphene oxide membrane for industrial wastewater treatment, Environ. Res. 223 (2023) 115409.

[22] S. Sharif, K.S. Ahmad, F. Rehman, Z. Bhatti, K.H. Thebo, Two-dimensional graphene oxide based membranes for ionic and molecular separation: Current status and challenges, Journal of Environmental Chemical Engineering 9(4) (2021).

[23] K. Guan, Y. Jia, Y. Lin, S. Wang, H. Matsuyama, Chemically Converted Graphene Nanosheets for the Construction of Ion-Exclusion Nanochannel Membranes, Nano Lett. 21(8) (2021) 3495-3502.

[24] W. Yu, L. Sisi, Y. Haiyan, L. Jie, Progress in the functional modification of graphene/graphene oxide: a review, RSC Adv 10(26) (2020) 15328-15345.

[25] M.A. Tofighy, T. Mohammadi, Divalent heavy metal ions removal from contaminated water using positively charged membrane prepared from a new carbon nanomaterial and HPEI, Chem. Eng. J. 388 (2020).

[26] K. Guan, Y. Jia, Y. Lin, S. Wang, H. Matsuyama, Chemically converted graphene nanosheets for the construction of ion-exclusion nanochannel membranes, Nano Lett. 21(8) (2021) 3495-3502.

[27] Q. Song, Y. Lin, T. Ueda, T. Istirokhatun, Q. Shen, K. Guan, T. Yoshioka, H. Matsuyama, Mechanism insights into the role of the support mineralization layer toward ultrathin polyamide nanofilms for ultrafast molecular separation, Journal of Materials Chemistry A 9(46) (2021) 26159-26171.

[28] H. Tao, N. Lavoine, F. Jiang, J. Tang, N. Lin, Reducing end modification on cellulose nanocrystals: strategy, characterization, applications and challenges, Nanoscale Horiz 5(4) (2020) 607-627.

[29] M. Fathizadeh, W.L. Xu, F. Zhou, Y. Yoon, M. Yu, Graphene oxide: A novel 2-dimensional material in membrane separation for water purification, Adv. Mater. Interfaces 4(5) (2017).

[30] J. Chen, Z. Yuan, X. Wu, J. Wang, Y. Yang, W. Li, Z. Jiang, Molecule stratification in 2D heterostructured nanochannels towards enhanced selective permeation, Chem. Eng. J. 440 (2022).

[31] S. Lin, J. Tang, K. Zhang, Y. Chen, R. Gao, H. Yin, L.C. Qin, Tuning oxygen-containing functional groups of graphene for supercapacitors with high stability, Nanoscale Adv 5(4) (2023) 1163-1171.

[32] H.-H. Huang, R.K. Joshi, K.K.H. De Silva, R. Badam, M. Yoshimura, Fabrication of reduced graphene oxide membranes for water desalination, J. Membr. Sci. 572 (2019) 12-19.

[33] Y. Li, S. Yuan, Y. Xia, W. Zhao, C.D. Easton, C. Selomulya, X. Zhang, Mild annealing reduced graphene oxide membrane for nanofiltration, J. Membr. Sci. 601 (2020).

[34] S. Li, J. Lu, D. Zou, L. Cui, B. Chen, F. Wang, J. Qiu, T. Yu, Y. Sun, W. Jing, Constructing reduced porous graphene oxide for tailoring mass-transfer channels in ultrathin MXene (Ti3C2T) membranes for efficient dye/salt separation, Chem. Eng. J. 457 (2023).

[35] S. Valizadeh, L. Naji, M. Karimi, S. Sarabadani Tafreshi, B. Heijman, N.H. de Leeuw, Experimental and density functional theory studies of laminar double-oxidized graphene oxide nanofiltration membranes, Chem. Eng. Res. Des. 188 (2022) 590-606.

[36] G. Zhao, K. Zhou, R. Hu, H. Zhu, Graphene oxide nanofiltration membranes with confined Na+ in two-dimensional nanochannels, Sep. Purif. Technol. 304 (2023).

[37] S. Zheng, Q. Tu, J.J. Urban, S. Li, B. Mi, Swelling of graphene oxide membranes in aqueous solution: Characterization of interlayer spacing and insight into water transport mechanisms, ACS Nano 11(6) (2017) 6440-6450.

[38] X. Chen, Z. Feng, J. Gohil, C.M. Stafford, N. Dai, L. Huang, H. Lin, Reduced Holey Graphene Oxide Membranes for Desalination with Improved Water Permeance, ACS Appl Mater Interfaces 12(1) (2020) 1387-1394.

[39] H. Chen, M. Wang, L. Wang, M. Zhou, H. Wu, H. Yang, Enhanced separation performance of Hg2+ in desulfurization wastewater using a tannin acid reduced

graphene oxide membrane, Sep. Purif. Technol. 274 (2021).

[40] C. Zhu, S. Guo, Y. Fang, S. Dong, Reducing Sugar: New Functional Molecules for the Green Synthesis of Graphene Nanosheets, ACS Nano 4(4) (2010) 2429-2437.

[41] A. Mohammadi, M.R. Daymond, A. Docoslis, New insights into the structure and chemical reduction of graphene oxide membranes for use in isotopic water separations, J. Membr. Sci. 659 (2022).

[42] X. Xiong, I.K.M. Yu, S.S. Chen, D.C.W. Tsang, L. Cao, H. Song, E.E. Kwon, Y.S. Ok, S. Zhang, C.S. Poon, Sulfonated biochar as acid catalyst for sugar hydrolysis and dehydration, Catal. Today 314 (2018) 52-61.

[43] Y. Chen, X. Liu, T.P. Labuza, P. Zhou, Effect of molecular size and charge state of reducing sugars on nonenzymatic glycation of β-lactoglobulin, Food Research International 54(2) (2013) 1560-1568.

[44] D.L. White, B.A. Day, Z. Zeng, Z.M. Schulte, N.R. Borland, N.L. Rosi, C.E. Wilmer, A. Star, Size Discrimination of Carbohydrates via Conductive Carbon Nanotube@Metal Organic Framework Composites, J. Am. Chem. Soc. 143(21) (2021) 8022-8033.

[45] L. Zhu, M. Wu, B. Van der Bruggen, L. Lei, L. Zhu, Effect of TiO2 content on the properties of polysulfone nanofiltration membranes modified with a layer of TiO2–graphene oxide, Sep. Purif. Technol. 242 (2020).

[46] Z. Liu, Z. Ma, B. Qian, A.Y.H. Chan, X. Wang, Y. Liu, J.H. Xin, A Facile and Scalable Method of Fabrication of Large-Area Ultrathin Graphene Oxide Nanofiltration Membrane, ACS Nano 15(9) (2021) 15294-15305.

[47] K.V. Kurada, M. Mukherjee, S. De, Permeability hysteresis of polypyrrole-polysulfone blend ultrafiltration membranes: study of phase separation thermodynamics and pH responsive membrane properties, Sep. Purif. Technol. 227 (2019).

[48] M. Zhang, Y. Mao, G. Liu, G. Liu, Y. Fan, W. Jin, Molecular Bridges Stabilize Graphene Oxide Membranes in Water, Angew. Chem. Int. Ed. Engl. 59(4) (2020) 1689-1695.

[49] H. Chen, H. Wu, Q. Wang, L. Ji, T. Zhang, H. Yang, Separation Performance of Hg2+ in Desulfurization Wastewater by the Graphene Oxide Polyethersulfone Membrane, Energy & Fuels 33(9) (2019) 9241-9248.

Chapter 4

Confined and mediated intercalation of nanoparticles in graphene oxide membrane to fine-tune desalination performance

4.1. Introduction

Atomic thickness, mechanical robustness, and ease of functionalization mark two-dimensional (2D) nanosheets as promising materials for manufacturing separation membranes [1]. Graphene oxide (GO) is widely used to construct thin laminated separation membranes because of its high-aspect-ratio geometry and high processability [2]. This interlocked and layered structure of GO laminates with sub-nanometer interlayer spacings was found to be capable of blocking the diffusion of small molecules while allowing the unimpeded permeation of water [3]. Additionally, the controlled preparation of GO can be implemented by modifying the degree of oxidation, functional groups, and lateral size, providing straightforward strategies for the enhancement of membrane performance [4]. In view of the aforementioned merits, GO-based membranes with precise and fast molecular transport properties are applicable to a wide range of membrane processes, including gas separation [5] and water treatment [6-8].

The membrane pore properties are key to effective separation. The interlayer spacing between two adjacent GO nanosheets is the main transport channel and a key factor in determining the separation performance of GO membranes [9]. Although GO membranes with lamellar structures exhibit considerable performance in the water separation process, the separation efficiency is limited owing to the relatively high transport resistance rendered by the densely packed structure [10]. Therefore, the

intercalation of zero- [11], one- [12, 13], two- [14], and three-dimensional [15] nanomaterials in GO-based membranes to prepare composite membranes has been explored to expand the interlayer spacing for faster water transport. However, such expanded interlayer spacings generally result in the separation of relatively large-sized solutes (e.g., dye molecules) and are rarely capable of removing small salt solutes (such as ions) from water [16]. The main reason for the unsatisfactory ion permeability of such composite membranes is considered to be the serious swelling of GO interlayers in water, which is exacerbated by the intercalated materials. As GO contains abundant hydrophilic-oxygen-containing functional groups, water molecules can easily penetrate the interlayer space and lead to swelling [17]. In addition, the uncontrollable nature and unevenness of intercalated materials interfere with the ordered stacking of GO sheets, thereby causing an over-extended layer spacing and exacerbating swelling [18]. Consequently, endowing composite GO membranes with outstanding water stability while achieving high permeance with precise rejection is crucial.

Herein, there is propose a confined and intercalation-mediated strategy to integrate nanoparticles into laminar GO membranes for improved desalination performance. Highly confined GO interlayers are necessary to avoid the loosening of the structure of the GO framework and to limit excessive interlayer expansion by the intercalated materials. In addition, using intermediates to improve the compatibility of intercalation materials and GO nanosheets is necessary to uniformize the nanoparticle distribution and prevent nanoparticle aggregation, which results in interlayer defects. In this study, solution-processable reduced GO (rGO) nanosheets and graphene quantum dot-mediated silver nanoparticles (GQD-Ag) were employed as the main framework and intercalation material, respectively, to obtain controllable interlayers for ion rejection. The chemical reduction of GO is a typical method for alleviating the instability of the framework in water. rGO membranes exhibit a compact layer spacing owing to the enhanced π-π and hydrophobic interactions that can alleviate hydration [19] between adjacent nanosheets. Subsequently, GQD-Ag nanoparticles with an appropriate size, superior dispersion, and excellent compatibility with rGO were applied as an

intercalation material. The GQDs exhibited a minimal size and properties similar to those of GO [20], making them promising for an intermediate role in nanoparticle intercalation in GO. With such confined and mediated intercalation, the composite GO membrane should exhibit improved water permeance and salt solute rejection. Additionally, Ag nanoparticles are expected to exhibit promising antibacterial activity [21] under the synergistic antibacterial effect of GQD and rGO.

4.2 Experimental

4.2.1 Materials

The GQD suspension (1 mg mL^{-1} in H_2O), and sodium hydroxide solution (NaOH, 4 mol L^{-1}) were purchased from Sigma-Aldrich Co. LLC (St. Louis, MO, USA). GQD displayed typical disk-shaped structure with a topographic height of 1–2 nm and diameter of approximately 5 nm. Silver nitrate ($AgNO_3$, 99.8%), nitric acid (HNO_3, 8%), and 25% glutaraldehyde solution were obtained from FUJIFILM Wako Pure Chemical Industries Co. Ltd. (Osaka, Japan). *E. coli* (NBRC3301) was purchased from the Biological Resource Center at the Japanese National Institute of Technology and Evaluation (Tokyo, Japan). Tryptic soy broth (TSB) purchased from Becton, Dickinson, and Company (NJ, USA) was used to culture the bacteria. SYTO™ 9 (from Life Technologies, CA, USA) was used to stain bacteria. And other chemicals were the same as previous chapters.

4.2.2 Synthesis of rGO, GQD-Ag, and Ag nanoparticles

rGO was synthesized using glucose as a green reduction agent. Before reduction, a 10 mL aqueous suspension containing GO (0.15 mg), glucose (1.5 mg), and 28% ammonia solution (40 μL) was uniformly mixed. The precursor suspension was then placed in a water bath at 94.5 °C for 60 min for the reduction process. GQD-Ag was synthesized according to a previous report [22]. Aqueous $AgNO_3$ (30 mL, 0.25 mg mL^{-1}) was thoroughly mixed with GQD (30 mL, 0.25 mg mL^{-1}). Subsequently, NaOH solution (8 mL, 4 mol L^{-1}) was added dropwise, and stirring continued at 80 °C for 20

min. Meanwhile, Ag nanoparticles without GQD for the control experiments were similarly prepared following the above protocol, without the addition of GQD. The nanomaterials prepared for comparison were designated as Ag nanoparticles, and their chemical compositions were not determined.

4.2.3 Preparation of rGO-based membranes

Pristine rGO and rGO membranes intercalated with GQD, GQD-Ag, and Ag nanoparticles (denoted as GQD/rGO, GQD-Ag/rGO, and Ag/rGO, respectively) were prepared by vacuum filtration [23]. Before filtration, the mixture of rGO solution and different intercalation materials (the mass ratio of intercalation materials to GO was 0.8) was diluted with deionized water to 300 mL and sonicated in an ice-water bath for 5 min. The above solution was then vacuum-filtered onto a nylon substrate. The prepared membranes were then dried in a desiccator for 24 h at room temperature. GQD/rGO and GQD-Ag/rGO membranes with intercalation material mass ratios of 0.1, 0.2, 0.5, 0.8, 1, and 2 were also prepared using the same method.

4.2.4 Preparation of GO, GQD/GO, and Ag-rGO membranes

A 10 mL aqueous suspension of the GO membrane was prepared by evenly mixing GO (0.15 mg), glucose (1.5 mg), and 28% ammonia solution (40 μL). A 10 mL aqueous suspension of GQD/GO (the mass ratio of GQD to GO was 0.8) consisting of GO (0.15 mg), glucose (1.5 mg), GQD (0.12 mg), and 28% ammonia solution (40 μL) was prepared. A 10 mL aqueous suspension of Ag-rGO (the mass ratio of $AgNO_3$ to GO was 0.8) was prepared by mixing GO (0.15 mg), glucose (1.5 mg), $AgNO_3$ (0.12 mg), and 28% ammonia solution (40 μL). The mixture was then placed in a water bath at 94.5 °C for 60 min for reduction. Finally, the prepared suspensions were treated using the aforementioned method and applied to prepare GO-based membranes.

4.2.5 Characterization

The morphologies of the GQD and GQD-Ag were observed by field-emission transmission electron microscopy (FE-TEM) (JEM-2100 F, JEOL Ltd, Japan). The membrane characterization was the same as previous chapters.

4.2.6 Desalination performance

The separation performance of rGO-based membranes was explored using a cross-flow membrane cell (flow rate: 6 mL min^{-1}, effective membrane surface area 7.06 cm^2), as reported previously [24]. And the water permeance and salts rejection evaluating were stated in previous chapters.

4.2.7 Determination of molecular weight cutoff (MWCO) values

The MWCO of the GO membranes was evaluated by neutral solutes transport model, which were listed in chapter 3.

4.2.8 Assessment of antibacterial activity

The antifouling performance of the membranes was assessed using static bacterial adhesion and diffusion inhibition zone tests [25]. The first step was bacterial cultivation. *E. coli* was dispersed in TSB solution (30 g L^{-1}, 20 mL) and shaken at 37 °C, 120 rpm for 12 h. Subsequently, 0.4 mL of the *E. coli* suspension was transferred to 20 mL of sterilized TSB solution for further cultivation for 4 h. Finally, the bacterial concentration was diluted to an optical density of 0.05 by UV spectrophotometer (V650, Jasco, Japan). The second step was sample preparation. The membranes were cut into rectangles (2 cm × 1 cm) and circles (1 cm diameter) for the bacterial adhesion and diffusion inhibition zones, respectively. For bacterial adhesion in static state experiments, the samples were immersed in 2 mL of bacterial solution with an optical density of 0.05 and incubated at 37 °C and 120 rpm for 24 h. Then, the sample membranes were thoroughly washed with NaCl solution (0.85 wt%) and the adhered bacteria were stained by SYTO™ 9 (0.15 μL mL^{-1}). The stained samples were then

transferred to 2 mL of 2.5% glutaraldehyde in 0.85 wt% NaCl solution for fixation in the dark for 3 min. Finally, the experimental results were observed using confocal laser scanning microscopy (CLSM) (FV1000D; Olympus Corporation, Japan). For the diffusion inhibition zone test, 200 μL of the bacterial suspension (optical density of 0.05) was smeared evenly on agar plates. The sterilized circular samples were then placed in the middle of an agar plate and cultured at 37 °C for 24 h. Finally, the inhibition zone was observed around the membrane samples.

4.2.9 Measurement of the releasing rate of Ag ions

The release of Ag^+ from the GQD-Ag/rGO membranes was assessed using batch experiments. A membrane sample with an area of 4 cm^2 was immersed in deionized water (40 mL), sealed, and placed on an orbital shaker at 100 rpm. The same volume of deionized water was then replaced every 24 h. Finally, the Ag^+ concentration of the water sample was analyzed by inductively coupled plasma atomic emission spectroscopy (ICP, Optima 7000 DV ICP-OES, Perkin Elmer, USA) after acidification with 1% HNO_3.

4.3 Results and discussion

4.3.1 Synthesis and intercalation of mediated nanoparticles

rGO membranes with confined and tunable interlayer spacings were designed to exclude ions from water. Original GO-based membranes exhibited low rejection (32.7%) of Na_2SO_4 (**Fig. 4.1a**), resulting from excessive intercalation of water molecules, which highlights the prerequisite of interlayer confinement. Conversely, rGO-based membranes can effectively prevent swelling and enhance the steric hindrance of ions, to deliver a high Na_2SO_4 rejection of 97.0%. Hence, rGO laminates are promising for use in confined intercalation of nanoparticles. **Fig. 4.2a** illustrates rGO-based membranes intercalated with different materials. GQD and GQD-Ag were introduced into the rGO laminates to increase the interlayer spacing for lower transport resistance. From the transmission electron microscopy (TEM) image observations,

GQD exhibited typical disk-shaped structures with diameter of approximately 5 nm, while the synthesized GQD-Ag showed a composite GQD and Ag nanoparticle morphology, with a uniform size of approximately 25 nm (**Fig. 4.2b**). Considering the nanosize of GQD, Ag nanoparticle in GQD-Ag should possess a similar size of its composites with GQD. The cross-sections of the rGO, GQD/rGO, and GQD-Ag/rGO membranes consistently displayed thin-layer composite structures (**Fig. 4.1b**), while the surface morphology of the GQD-Ag/rGO membrane exhibited a clear difference from the other membranes (**Fig. 4.2c**). GQD had negligible effects on the wrinkled surface morphology of rGO laminates, as GQD can be seen as nanoscale graphene fragments [26], which are compatible with the rGO membrane. The GQD-Ag/rGO membrane contained nanoparticles of GQD-Ag covered by GO with an even distribution. In addition, the x-ray photoelectron spectroscopy (XPS) spectra of C1s and Ag3d from the different membranes further confirmed the successful synthesis and intercalation of the nanomaterials into the structure. As shown in **Fig. 4.2d**, the following C1s region of peaks was observed at 284.6 eV, 286.6 eV, 288.4 eV, and 290.3 eV, and are attributed to C–C, C–O, C=O, and O–C=O bonds, respectively [27]. The stepwise enhancement of the O–C=O peak intensity could be due to the addition of GQD with higher O/C ratio than rGO [28]. Meanwhile, the O–C=O peak density of GQD-Ag/rGO is higher than that in GQD/rGO, possibly due to the oxidation of some oxygen-containing functional groups of GQD during the synthesis of GQD-Ag (**Table 4.1**). Additionally, two peaks at 374.2 eV and 368.2 eV were observed, resulting from $Ag3d_{3/2}$ and $Ag3d_{5/2}$, respectively. The splitting in Ag3d with a difference of 6.0 eV was consistent with the theoretical value for metallic silver [29]. Specifically, the redox reactions between GQD and Ag occurred simultaneously during the nucleation process. The phenolic groups of GQD underwent ionization to form phenolate anions and then converted into semiquinone structures through oxidation reactions. Meanwhile, the electrons of the phenolate anions migrated to Ag^+, which then reduced Ag^+ to Ag^0 by getting the electrons. In addition, GQD is considered to be attached on the surface of Ag nanoparticles due to Ag^+ tends to nucleate near the functional groups of GQD and

the size of Ag (approximately 25 nm) is much larger than that of GQD (approximately 5 nm). The above results confirm the successful synthesis of GQD-Ag composite material and its distribution in the rGO membrane.

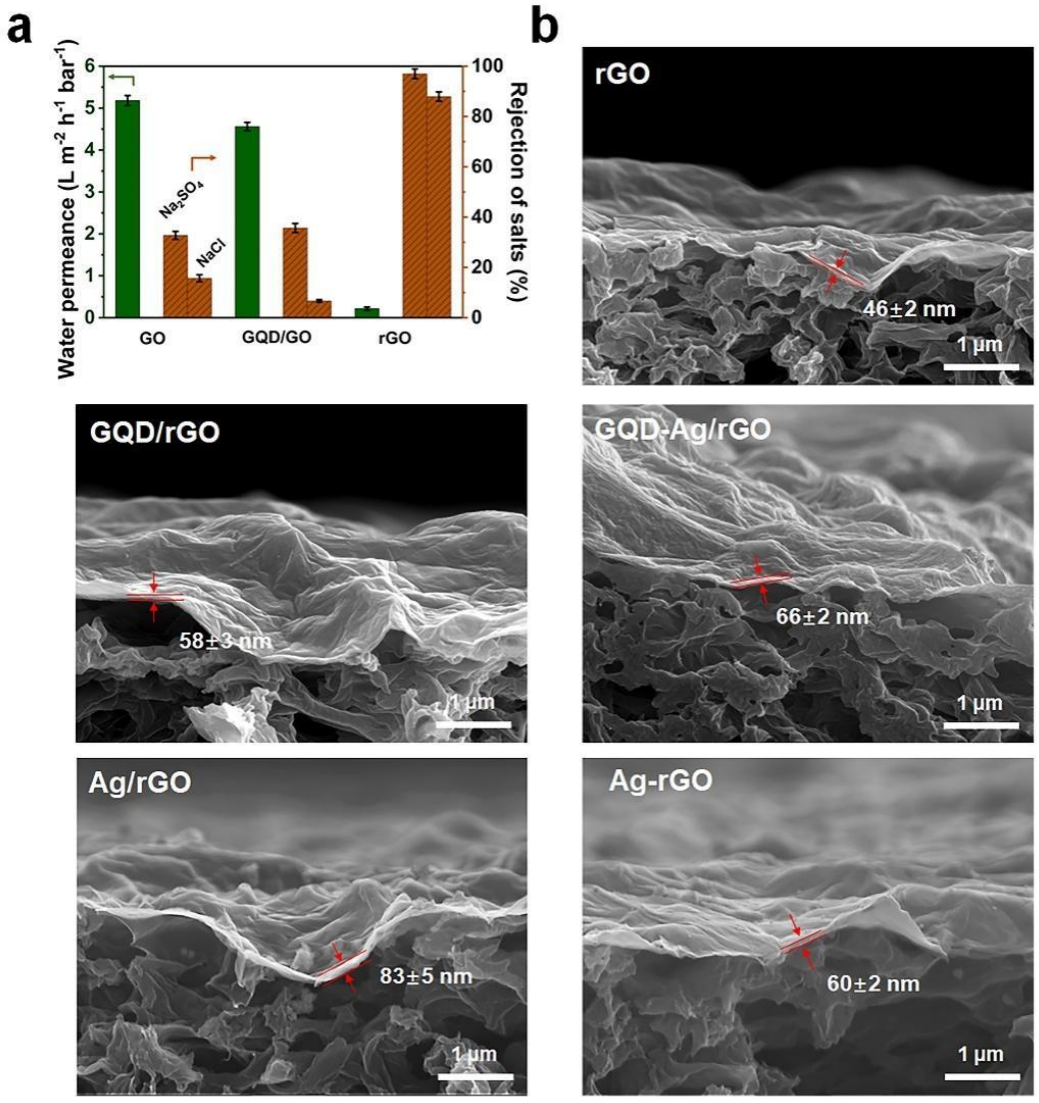

Fig. 4.1 (a) Separation performance of GO, GQD/GO (weight ratio of GQD to GO is 0.8), and rGO laminates, (b) SEM cross-sectional view of pristine rGO, GQD/rGO, GQD-Ag/rGO, Ag/rGO, and Ag-rGO (in-situ growth) membranes (the indicated thickness in the SEM images is the average value of 6 measurements from different regions for each sample).

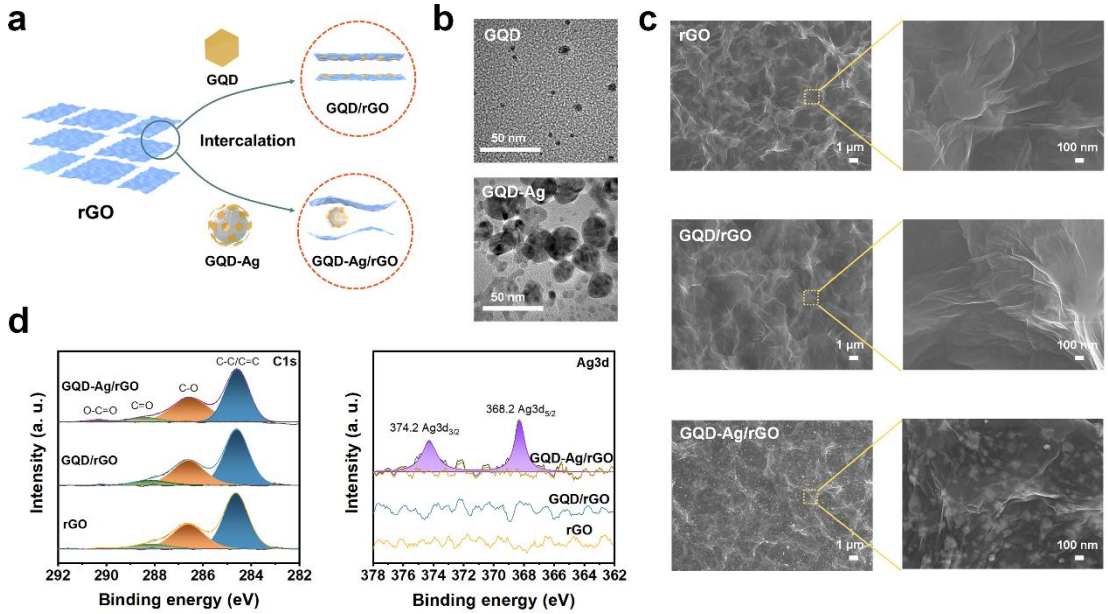

Fig. 4.2 (a) Schematic of the preparation of GQD/rGO and GQD-Ag/rGO; (b) TEM images of GQD and GQD-Ag; (c) SEM images of the surface of rGO, GQD/rGO, and GQD-Ag/rGO membranes at different magnifications; (d) C1s and Ag3d of XPS spectra of rGO, GQD/rGO, and GQD-Ag/rGO membranes.

Table 4.1 XPS compositional analysis of the C 1s spectra of the rGO, GQD/rGO and GQD-Ag/rGO.

Sample	Peak area (%)			
	C–C	C–O	C–O	O–C=O
rGO	60.90	34.08	4.27	0.75
GQD/rGO	58.32	36.00	4.83	0.85
GQD-Ag/rGO	57.79	36.64	4.67	0.90

4.3.2 Effects of different intercalation materials and methods

The incorporation of nanomaterials breaks the tightly stacked structure of the rGO membrane and increases the interlayer spacing for the transport of water molecules [30]. To further study the effects of different intercalation materials on the membrane properties, the desalination performance (including water permeance and rejection) was

measured (**Fig. 4.3a**). The pristine rGO membranes exhibited high rejection of Na_2SO_4 (97.0%) but low permeance (0.22 L m^{-2} h^{-1} bar^{-1}) as a result of the tight packing of nanosheets [31] with small interlayer spacing. With the intercalation of GQD, water permeance of the GQD/rGO membrane was increased to 0.49 L m^{-2} h^{-1} bar^{-1}, with slightly compromised salt rejection. In contrast, the GQD-Ag/rGO membrane exhibited water permeance five times 1.12 L m^{-2} h^{-1} bar^{-1} than that of pristine rGO membranes, while maintaining relatively high Na_2SO_4 rejection (94.6%). The performance of rGO membranes intercalated with only Ag nanoparticles (without GQD) were also investigated. Comparatively, while the Ag/rGO membrane synthesized via intercalation of bare Ag nanoparticles could further improve permeance to an extent (1.36 L m^{-2} h^{-1} bar^{-1}), its salt rejection was largely compromised (84.5% Na_2SO_4). From these results, it was found that: the improvement of water permeance is related to the size and distribution of nanoparticles; GQD plays a critical role in improving the compatibility between nanoparticles and GO for maintaining high salt rejection.

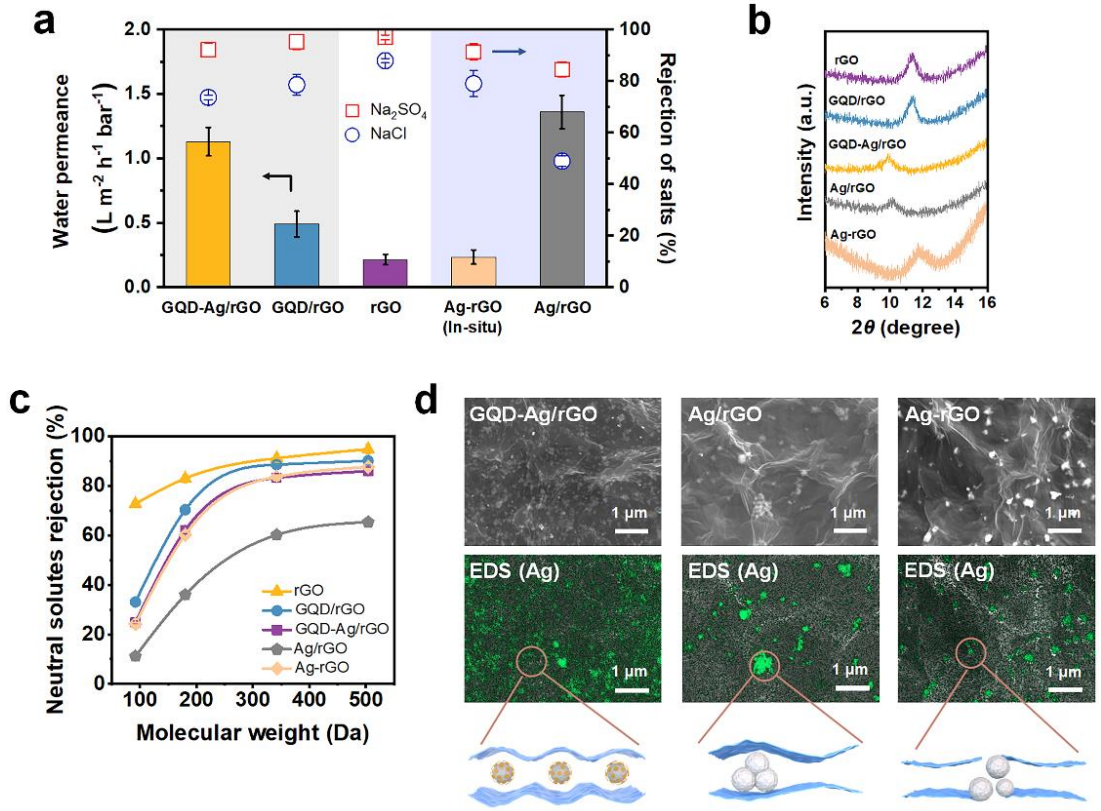

Fig. 4.3 (a) Separation performance, (b) XRD diffraction patterns, and (c) molecular weight cut-off (MWCO) of pristine rGO, GQD/rGO, GQD-Ag/rGO, Ag/rGO, and Ag-

rGO (in-situ growth); (d) SEM images, EDS-mapping, and schematic of the surface of GQD-Ag/rGO, Ag/rGO, and Ag-rGO. Feed salt concentration: 500 ppm. Applied pressure: 10 bar.

To evaluate the roles of nanoparticles and GQD, it is further characterized the interlayer properties of the prepared membranes. The interlayer spacings of the rGO membranes containing different intercalated materials were revealed by the XRD diffraction patterns (**Fig. 4.3b**). The characteristic peak position of the rGO membrane is similar to that of the rGO membrane with the embedding of GQD, indicating that the nanoscale size of GQD physically limits its capacity to extend the interlayer spacing. In contrast to the above membrane, with the intercalation of the GQD-Ag and Ag nanoparticles into the rGO laminates, the characteristic peak of rGO showed obvious shifts to smaller 2θ values, indicating an effectively enlarged interlayer spacing [32]. Additionally, molecular weight cutoff (MWCO) curves (**Fig. 4.3c**) obtained from the rejection results of neutral organic solutes with varying molecular weights were obtained for the different membranes. The results more clearly distinguish the interlayer spacing difference between the differently intercalated membranes. GQD contributed to the compatibility of Ag nanoparticles in the membrane with similar rejection curves for GQD/rGO and GQD-Ag/rGO, whereas Ag/rGO exhibited a significantly reduced rejection capability. The interlayer spacing and MWCO results corresponded well with the water permeances of the different membranes.

While the water permeance was reasonably increased by the nanomaterial interaction, a varying extent of salt rejection decline was observed. The NaCl rejection decline was more obvious than that of Na_2SO_4 (**Fig. 4.3a**) because NaCl rejection is more dependent on the interlayer spacing change. Although GQD-Ag/rGO and Ag/rGO showed similar interlayer spacings, the salt rejection decline was more serious for Ag/rGO. Scanning electron microscopy (SEM) images and energy-dispersive x-ray spectroscopy (EDS) mappings of Ag for the above membranes were then obtained to observe the distribution and aggregation conditions of the nanoparticles (**Fig. 4.3d**). Ag

nanoparticles without GQD mediation showed a lower distribution density and a higher degree of agglomeration [33], while the introduction of GQD effectively improved the dispersion of Ag nanoparticles in the membrane matrix. This satisfactory dispersion was also observed in the cross-sectional view of the GQD-Ag/rGO membrane (**Fig. 4.4**). Furthermore, the change in thickness of rGO membrane further reflects the influence of different intercalation materials on membrane structure (**Fig. 4.1b**). The thickness gradually increased with the coupling of GQD, GQD-Ag, and Ag nanoparticles. The Ag/rGO membrane with a larger thickness may be due to the agglomeration of Ag nanoparticles between rGO sheets. The in-situ growth of Ag nanoparticles on rGO nanosheets (Ag-rGO) led to relatively small changes in the thickness, suggesting that Ag growth did not appear within the interlayer spacings [34].

It was also explored the in-situ growth of Ag nanoparticles on rGO nanosheets (Ag-rGO) and employing the composite material for the construction of laminate membrane. The characteristic peak position of the Ag-rGO membrane (**Fig. 4.3b**) was also similar to that of pristine rGO membranes, implying that the Ag nanoparticles grown in-situ may be inclined toward the edges rather than the interlayers of the GO laminates [34]. Similar to the Ag growth on GQD, the abundant functional groups at the edge of the GO nanosheet acted as nucleation anchor sites to attract Ag^{+} ions and promote growth. Meanwhile, Ag-rGO via in-situ growth possesses better NaCl rejection (**Fig. 4.3a**) and MWCO curve (**Fig. 4.3c**) results than Ag/rGO did, further demonstrating that the different distributions of Ag nanoparticles are induced according to the in-situ growth and intercalation methods, respectively. From the surface morphology of in-situ grown Ag-rGO (**Fig. 4.3d**), moderate agglomeration of medium-size Ag nanoparticles in the Ag-rGO membrane appeared. Considering the similar interlayer spacing as pristine rGO from its XRD spectra, the location of Ag nanoparticles should be at the edges of the nanosheets (**Fig. 4.3d**), which limits the expanding of interlayer spacing for the in-situ growth method to introduce Ag nanoparticles.

Similar to the Ag growth on GO nanosheets, for the GQD-Ag, the presence of GQD can be regarded as the core of Ag heterogeneous nucleation [35] during GQD-Ag nanoparticle synthesis. Therefore, GQD would facilitate the nucleation of silver, leading to larger numbers of GQD-Ag composite materials with less agglomeration. In addition, some GQD can remain in the inter-particle gaps between nanoparticles, playing an indispensable role in improving the dispersibility of Ag nanoparticles and their compatibility with the rGO sheets [36, 37]. Therefore, the GQD-Ag/rGO membranes with controllable intercalation amount of GQD-Ag could possess a finely expanded interlayer spacing, owing to the synergistic effects of appropriate size and homogeneous distribution in the interlayers, thus increasing water permeance while maintaining relatively high level of salt rejection.

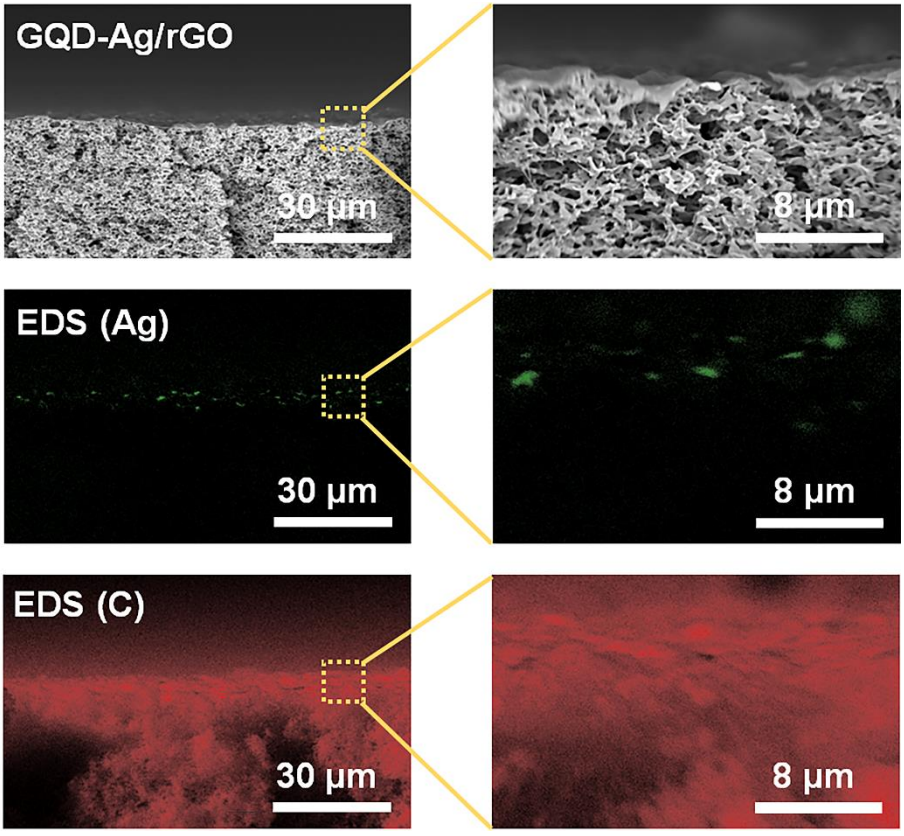

Fig. 4.4 SEM images and EDS mapping (element Ag and C) of GQD-Ag/rGO membrane with different magnifications.

4.3.3 Effect of intercalation amount on membrane performance

While GQD mediation contributed to the nanoparticle distribution in rGO

laminates, Ag nanoparticles essentially lowered the transport resistance of the interlayer channels. To highlight the role of nanoparticles and explore their capacity for permeance improvement, the effect of the intercalated ratios of GQD-Ag and GQD on the morphology and performance of rGO membranes were further explored and compared. As shown in **Fig. 4.5a** and **Fig. 4.6**, GQD did not significantly change the surface morphology of GQD/rGO, regardless of the intercalated content (mass ratios of GQD to rGO ranged from 0.1–2). By comparison, the GQD-Ag/rGO membrane surface exhibited more protrusions of nanoparticles, with an increased mass ratio of GQD-Ag to rGO (**Fig. 4.6**). Meanwhile, the distribution of the nanoparticles was homogeneous, and no notable agglomerations were observed, even when the mass ratio reached 2. The membrane performances of GQD/rGO and GQD-Ag/rGO with different intercalation ratios were also evaluated (**Fig. 4.5b**). With increased intercalation, the GQD/rGO membranes exhibited relatively stable permeance and salt rejection, whereas the GQD-Ag/rGO membranes displayed continuously enhanced water permeance but gradually compromised salt rejection. This result emphasizes the permeance-increasing effect of the Ag nanoparticles. Consistent results were also obtained from the XRD diffraction patterns (**Fig. 4.5c**) and MWCO curves (**Fig. 4.5d**), where the GQD-Ag/rGO membrane revealed a comparatively larger interlayer spacing change upon varying the intercalation. Nevertheless, when the mass ratio of intercalated GQD-Ag was higher than 0.8, the wider interlayer spacing of the rGO laminates (**Fig. 4.5c**) reduced the salt rejection at a faster rate when compared with the ratio range of 0.1-0.8. From the MWCO tests, the GQD-Ag/rGO-2 (mass ratio of GQD-Ag to GO is 2) membrane showed a relatively distant curve, away from that of the GQD/rGO membranes and less intercalated GQD-Ag/rGO membranes. Therefore, with the mediation of GQD, Ag nanoparticles could finely alter the performance of the membrane without generating fatal defects, and an appropriate amount of intercalation was beneficial for achieving a balance between water permeance and salt rejection.

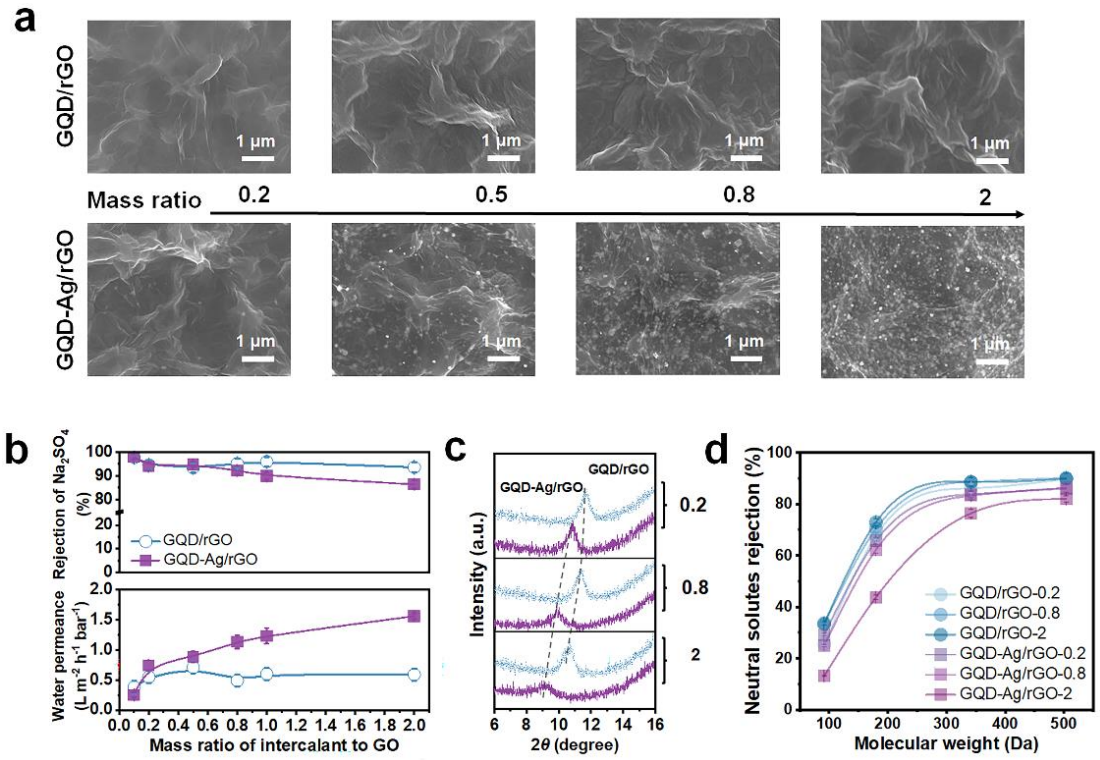

Fig. 4.5 (a) SEM images of the surface, (b) separation performance, (c) XRD diffraction patterns, and (d) molecular weight cut-off (MWCO) of GQD/rGO and GQD-Ag/rGO with different intercalated weight ratios to rGO (ranged from 0.2 to 2). Feed salt concentration: 500 ppm. Applied pressure: 10 bar.

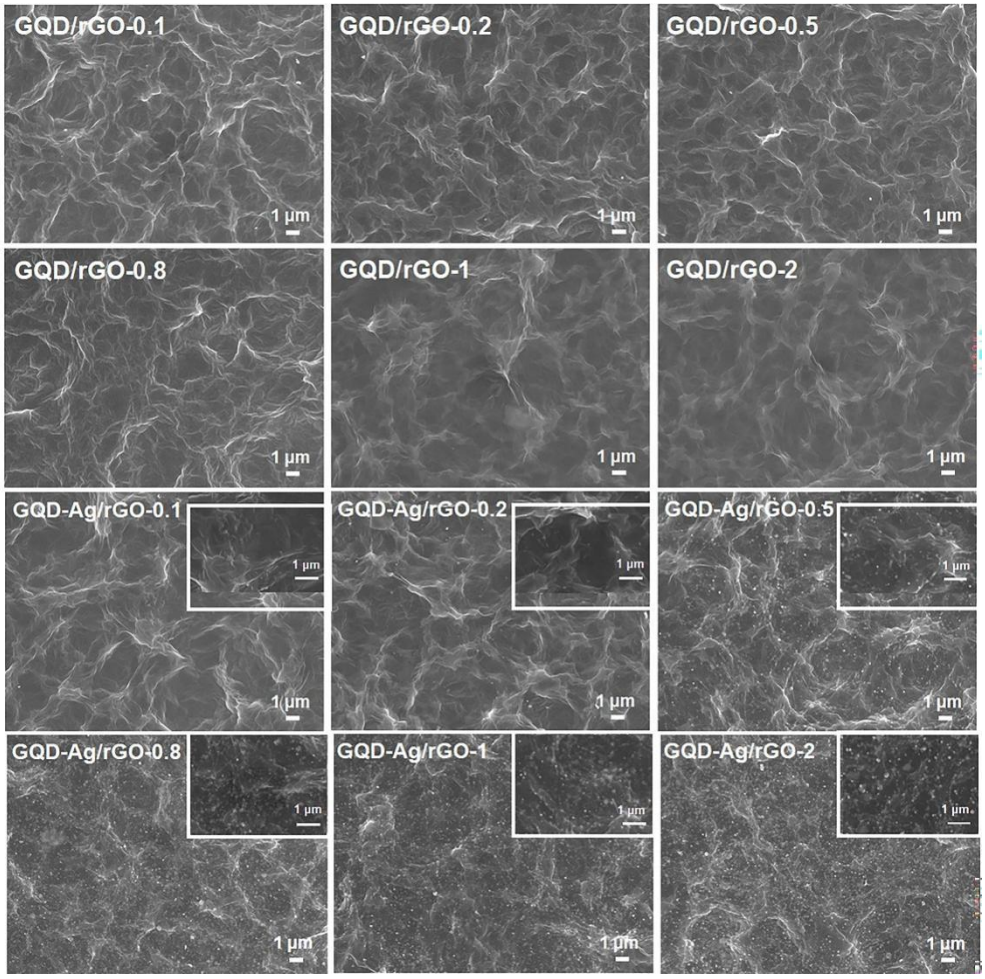

Fig. 4.6 SEM surface morphology of GQD/rGO and GQD-Ag/rGO membranes with different ratios.

4.3.4 Separation performance and membrane stability

Four common salt solutes (500 ppm Na_2SO_4, NaCl, $MgSO_4$, and $MgCl_2$) were employed to evaluate the separation mechanism of the optimal membrane (GQD-Ag/rGO-0.8). As shown in **Fig. 4.7a**, the salt rejection of the different salts by the GQD-Ag/rGO membrane exhibited a reasonable order, where $R(Na_2SO_4) > R(MgSO_4) > R(NaCl) > R(MgCl_2)$. This indicates that electrostatic repulsion induced by the Donnan effect plays an important role in the sequence of the salt rejection [7, 38]. The negatively charged GQD-Ag/rGO membrane (**Fig. 4.8a**) has strong electrostatic repulsion toward negatively charged ions but attracts positively charged ions. Meanwhile, counterions (positively charged ions) in the solution also repelled the charge balance of the

membrane. As a result, negatively charged membranes are more likely to reject salts with a smaller valence ratio (Z^+/Z^-) of cationic and anionic values because salt rejection is positively related to Z^+/Z^-. Therefore, the order of salt rejection according to Donnan exclusion theory can be estimated as: $R(Na_2SO_4) > R(MgSO_4) \approx R(NaCl) > R(MgCl_2)$, which is roughly consistent with the experimental results. It should be noted that, although the valence ratio (Z^+/Z^-) of $MgSO_4$ and NaCl is equal, the rejection of $MgSO_4$ is slightly higher than that of NaCl because the hydrated diameters of the salt ions follow the sequence: Mg^{2+}(8.6 Å) > SO_4^{2-} (7.6 Å) > Na^+ (7.2 Å) > Cl^- (6.6 Å) [7]. Overall, salt rejection is the combined result of the Donnan effect and size sieving.

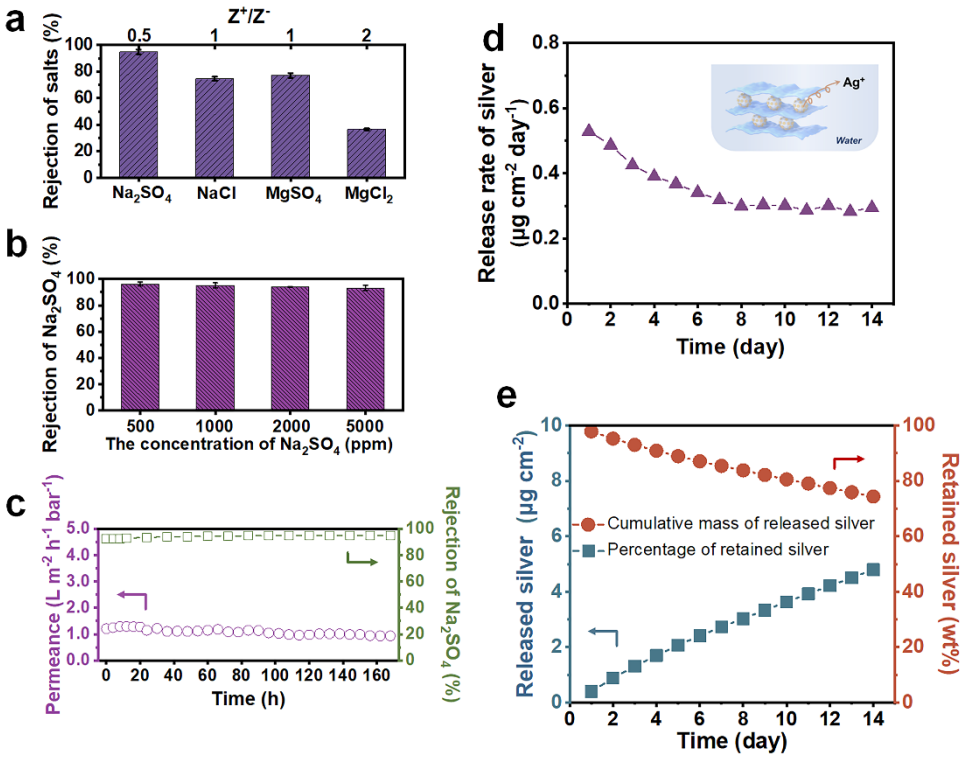

Fig. 4.7 (a) Rejection of different salts, (b) rejection of a series of Na_2SO_4 concentrations, (c) long-term stability, (d-e) Ag^+ ion release evaluation of GQD-Ag/rGO-0.8 membranes.

The effects of external conditions on membrane performance were also studied. The influence of Na_2SO_4 concentration on the salt rejection ability of the GQD-Ag/rGO-0.8 membrane is presented in **Fig. 4.7b**. As the concentration increased from 500 ppm to 5000 ppm, the rejection of the optimal membrane decreased slightly

because of the higher osmotic pressure and smaller Debye screening length (DSL) [39, 40]. In other words, the rejection of salt ions was reduced, owing to the declining permeate flux and charge neutralization [41] of the GQD-Ag/rGO membrane surface. The GQD-Ag/rGO-0.8 membrane stability was evaluated over the long-term operation (**Fig. 4.7c**). It was observed that the permeance and rejection of Na_2SO_4 were retained satisfactorily over a seven day continuous desalination process. Meanwhile, when the shearing force of feed flow continuously increased by approximately 20 times from the initial stage, the permeance and Na_2SO_4 rejection of the GQD-Ag/rGO membrane were satisfactorily maintained (**Fig. 4.8b-c**). rGO laminates with high water-stability and confinement effects can effectively inhibit excessive swelling [42] even after GQD-Ag intercalation. In addition, GQD-Ag with rigidity and homogeneous distribution can ensure the stability of the rGO laminate structure and mitigate the loss of permeance caused by the collapse of the interlayer channels. The optimized membranes also exhibited competitive rejection performance (**Table 4.2**) among literature reports. Apart from the performance issue, it is worth mentioning that some merits of GO membranes are beneficial to certain applications. GO membranes can preserve stability in both acidic as well as extremely alkaline modes [24]. With the development of high-quality commercial GO materials with uniformly large lateral size, it is expected to achieve highly competitive permeance by minimizing the layer thickness.

As Ag nanoparticles continuously release Ag^+ in an aqueous environment [43, 44], the release rate of Ag^+ from the GQD-Ag/rGO membrane may affect its structural stability and performance. The change of GQD-Ag/rGO membrane structure after long-term stability further evidences the influence of Ag^+ release (**Fig. 4.8d**). For the membrane performance, the permeance decreased slightly and rejection of Na_2SO_4 was retained satisfactorily over a seven day continuous desalination process (**Fig. 4.7c**). **Fig. 4.7d** shows the evaluation of the release rate of Ag^+, which sharply slowed during the initial seven days, followed by a steady release rate of 0.3 μg cm^{-2} d^{-1}. The sharp release of Ag^+ in the initial period could be attributed to the GQD-Ag nanoparticles that were weakly bound or located on the outermost side of the rGO laminate [45]. Subsequently,

the reasons for the gentle release rate of Ag^+ include: the enhanced interaction force between GQD-Ag and rGO owing to their favorable compatibility and increased resistance to Ag^+ from nanoparticles, due to the confined and tortuous interlayer channels in the rGO laminates. The cumulative amount of Ag^+ released over time was calculated and is shown in **Fig. 4.7e**. The percentage of released Ag^+ for the first seven days was approximately 14.58%, after which the mass loss of Ag^+ remained steady, at approximately 1.58% per day. It indicates that with the steady and relatively slow release of Ag^+, the membrane permeance will not be compromised much in a relatively long operation duration.

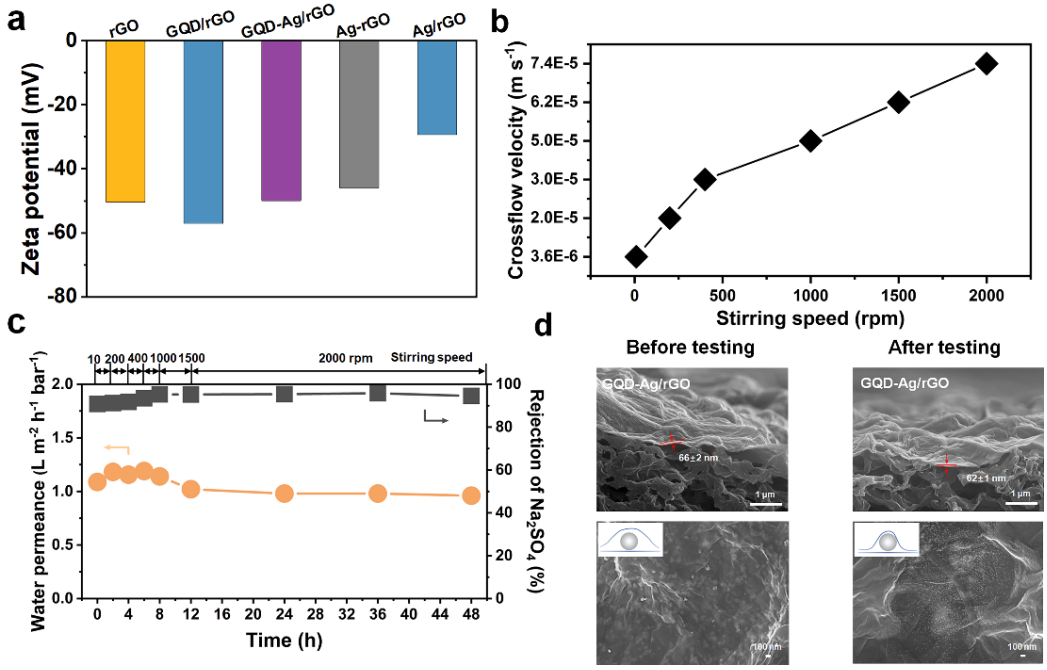

Fig. 4.8 (a) Zeta potential values for pristine rGO, GQD/rGO, GQD-Ag/rGO, Ag-rGO and Ag/rGO membranes, (b) crossflow velocity ($\mathbf{k_f}$) of GQD-Ag/rGO membrane at different stirring speed, (c) performance stability evaluation, and (d) SEM images of cross-sectional and surface morphology and schematic of GQD-Ag/rGO membranes (before and after long-term stability testing).

Table 4.2 Summary of literature reports on the desalination performance of GO-based membranes.

Membrane	Permeance [L m^{-2} h^{-1} bar^{-1}]	Feed Na_2SO_4 concentration (ppm)	Na_2SO_4 rejection ratio [%]	Reference
GO-PEI	7	2000	50	[3]
RGO-OCNT	11.1	710	78.1	[4]
G-CNTm	12.1	1420	71.2	[5]
TMPyP/GO	1.16	2000	87.7	[6]
GO@PAN	2	N/A	56.7	[7]
GO/CN/TiO_2-CNT	16	2000	67	[8]
PRGO/HNTs-PSS	8.8	1000	14.3	[9]
GO(120) NFM	11.1	2840	63.1	[10]
rPGMs	5.3	710	69	[11]
GO-TEOA	3	500	84	[12]
GO NFM	4.3	1000	90	[13]
GO-TMPyP	1.16	2000	87.7	[14]
rGO/S-GO	1.9	N/A	82.6	[15]
GO@Crown	3.04	400	88	[16]
GQD-Ag/rGO	1.12	500	94.6	This chapter

4.3.5 Antibacterial activity

As the released Ag^+ is effective for antibacterial purposes, the antibacterial performance of the pristine rGO, GQD/rGO, and GQD-Ag/rGO membranes was determined by static bacterial adhesion and disinhibition zone tests using *E.coli*. After immersing the samples into the bacterial suspension for culture, SEM images (**Fig. 4.9a**) of bacterial-adhered membranes showed that the *E.coli* colony adhered to the pristine rGO, while relatively few bacteria were observed on the GQD/rGO membranes. In comparison, the GQD-Ag/rGO membranes further minimized *E. coli* growth. As a result, the static anti-adhesion ability of the rGO-based membranes was preliminarily

determined to be: GQD-Ag/rGO > GQD/rGO > rGO. Furthermore, the specific *E. coli* states (viable or dead) and the tendency of adhesion were further monitored using confocal laser scanning microscopy (CLSM) images (**Fig. 4.9b**). The anti-adhesion trend was consistent with that of SEM characterization, in which reduced bacterial attachment was observed on the surface of the GQD/rGO membrane, and the surface of the GQD-Ag/rGO membrane had very few bacteria, either living or dead. Although the anti-adhesion capacity of the pristine rGO membrane was not satisfactory, a considerable number of bacteria on the surface of the membrane were effectively killed. The antibacterial activity exhibited by rGO and GQD/rGO was mainly attributed to their sharp edges and electrostatic repulsion [20, 46, 47]. The sharp edges may kill bacteria by directly inserting into or cutting the cell membrane, and the negative potential value of the membranes generates strong electrostatic repulsion to *E. coli,* due to most bacteria presenting an overall negative charge. The GQD-Ag/rGO membrane exhibited the highest anti-adhesion performance among the membranes, which was attributed to the combined effects of Ag^{+} released from the Ag nanoparticles. The disinhibition zone experiments also showed that the GQD-Ag/rGO membrane possessed optimal antibacterial activity, and the inhibition zone of the GQD-Ag/rGO membrane was wider and clearer than that of the pristine rGO and GQD/rGO membranes (**Fig. 4.9c**). Specifically, the antibacterial mechanism of Ag nanoparticles has two main aspects [48]: damage to biomolecules and structures caused by the attachment of bacteria to Ag nanoparticles and Ag-nanoparticle-induced generation of reactive oxidative species (ROS) that inactivate bacteria. Furthermore, Ag nanoparticles decorated with GQD displayed an increased bactericidal effect, owing to the larger active surface being exposed [49-51]. Finally, both the GQD and rGO sheets can be considered as electron transport platforms to accelerate electron transport, further enhancing the generation of ROS for sterilization.

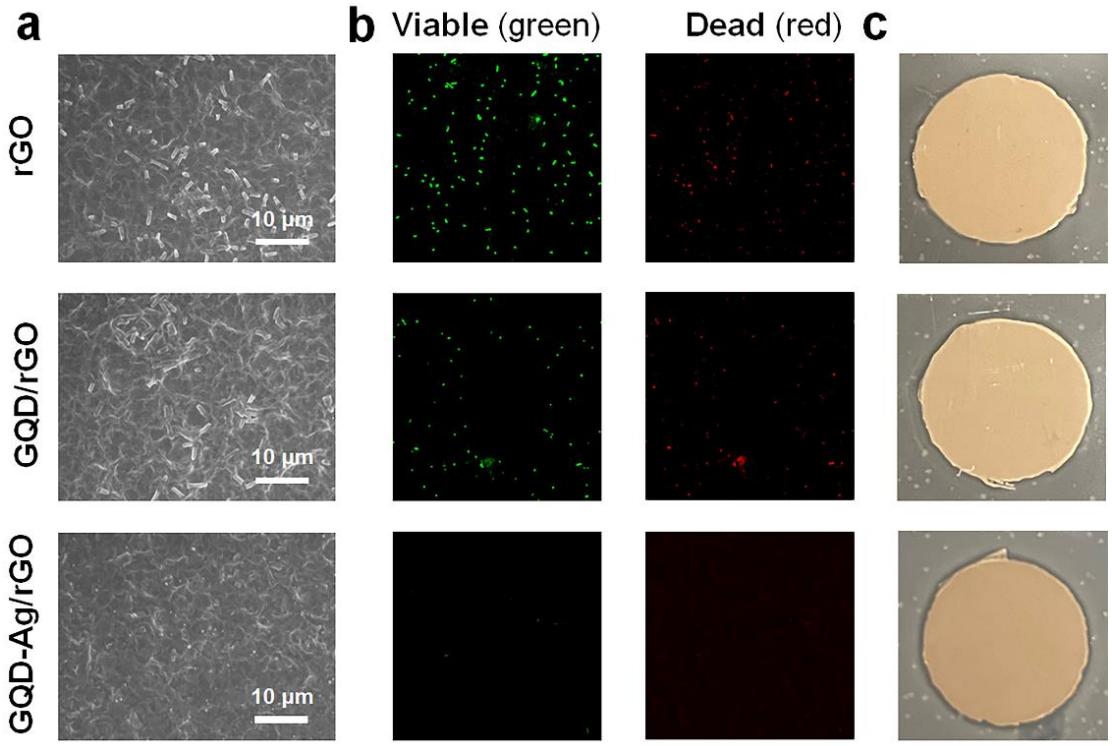

Fig. 4.9 (a) SEM characterizations, (b) CLSM images (green and red represent viable and dead bacteria, respectively), and (c) disinhibition zone tests of pristine rGO, GQD/rGO, and GQD-Ag/rGO membranes after the static bacterial adhesion tests using *E. coli* as model bacteria.

4.4 Conclusions

In summary, this chapter demonstrated a confined and mediated approach to nanoparticle intercalation within GO membranes, resulting in enhanced desalination performance. It is extensively investigated the multifunctional role of GQD-mediated Ag nanoparticles uniformly confined within rGO nanosheets. The incorporation of GQD effectively controlled the growth of Ag nanoparticles, preventing their aggregation and facilitating controlled intercalation within the GO laminates. This process appropriately enlarged the nanochannels. By precisely regulating the content of intercalated GQD-Ag, there is achieved a four-fold increase in the permeance of the optimal membrane without significantly compromising Na_2SO_4 rejection. Additionally, the GQD-Ag/rGO membrane showcased promising antifouling properties, benefitting from the synergistic effects of Ag and GQD nanomaterials. This study offers valuable

insights into fine-tuning 2D laminate structures to create fast-selective nanochannels, providing useful information for advancing desalination technologies.

References

[1] S. Kim, H. Wang, Y.M. Lee, 2D nanosheets and their composite membranes for water, gas, and ion separation, Angew. Chem. Int. Ed. 58 (2019) 17512-17527.

[2] G. Liu, W. Jin, N. Xu, Two-dimensional-material membranes: A newfamily of high-performance separation membranes, Angew. Chem. Int. Ed. 55 (2016) 13384-13397.

[3] R.R. Nair, H.A. Wu, P.N. Jayaram, I.V. Grigorieva, A.K. Geim, Unimpeded permeation of water through helium-leak–tight graphene-based membranes, Science 335 (2012) 442-444.

[4] Y. Wei, Y. Zhang, X. Gao, Z. Ma, X. Wang, C. Gao, Multilayered graphene oxide membranes for water treatment: A review, Carbon 139 (2018) 964-981.

[5] H.W. Kim, H.W. Yoon, S.M. Yoon, B.M. Yoo, B.K. Ahn, Y.H. Cho, H.J. Shin, H. Yang, U. Paik, S. Kwon, J.Y. Choi, H.B. Park, Selective gas transport through few-layered graphene and graphene oxide membranes, Science 342 (2013) 91-95.

[6] Y. Du, X. Zhang, J. Yang, Y. Lv, C. Zhang, Z.K. Xu, Ultra-thin graphene oxide films via contra-diffusion method: Fast fabrication for ion rejection, J. Membr. Sci. 595 (2020).

[7] Y. Li, W. Zhao, M. Weyland, S. Yuan, Y. Xia, H. Liu, M. Jian, J. Yang, C.D. Easton, C. Selomulya, X. Zhang, Thermally reduced nanoporous graphene oxide membrane for desalination, Environ. Sci. Technol. 53 (2019) 8314-8323.

[8] J. Li, M. Hu, H. Pei, X. Ma, F. Yan, D.S. Dlamini, Z. Cui, B. He, J. Li, H. Matsuyama, Improved water permeability and structural stability in a polysulfone-grafted graphene oxide composite membrane used for dye separation, J. Membr. Sci. 595 (2020).

[9] S. Zheng, Q. Tu, J.J. Urban, S. Li, B. Mi, Swelling of graphene oxide membranes in aqueous solution: Characterization of interlayer spacing and insight into water transport mechanisms, ACS Nano 11 (2017) 6440-6450.

[10] M. Fathizadeh, W.L. Xu, F. Zhou, Y. Yoon, M. Yu, Graphene oxide: A novel 2-dimensional material in membrane separation for water purification, Adv. Mater. Interfaces 4 (2017).

[11] Q. Chen, Z. Yu, F. Li, Y. Yang, Y. Pan, Y. Peng, X. Yang, G. Zeng, A novel

photocatalytic membrane decorated with RGO-Ag-TiO2 for dye degradation and oil–water emulsion separation, J. Chem. Technol. Biotechnol. 93 (2017) 761-775.

[12] Y. Yang, X. Yang, L. Liang, Y. Gao, H. Cheng, X. Li, M. Zou, A. Cao, R. Ma, Q. Yuan, X. Duan, Large-area graphene-nanomesh/carbon-nanotube hybrid membranes for ionic and molecular nanofiltration, Science 364 (2019) 1057-1062.

[13] W. Liu, D. Wang, R.A. Soomro, F. Fu, N. Qiao, Y. Yu, R. Wang, B. Xu, Ceramic supported attapulgite-graphene oxide composite membrane for efficient removal of heavy metal contamination, J. Membr. Sci. 591 (2019).

[14] T. Liu, X. Liu, N. Graham, W. Yu, K. Sun, Two-dimensional MXene incorporated graphene oxide composite membrane with enhanced water purification performance, J. Membr. Sci. 593 (2020).

[15] H. Zeng, Z. Yu, L. Shao, X. Li, M. Zhu, Y. Liu, X. Feng, X. Zhu, A novel strategy for enhancing the performance of membranes for dyes separation: Embedding PAA@UiO-66-NH_2 between graphene oxide sheets, Chem. Eng. J. 403 (2021).

[16] Z. Wang, F. He, J. Guo, S. Peng, X.Q. Cheng, Y. Zhang, E. Drioli, A. Figoli, Y. Li, L. Shao, The stability of a graphene oxide (GO) nanofiltration (NF) membrane in an aqueous environment: progress and challenges, Mater. Adv. 1 (2020) 554-568.

[17] A. Iakunkov, A.V. Talyzin, Swelling properties of graphite oxides and graphene oxide multilayered materials, Nanoscale 12 (2020) 21060-21093.

[18] M. Zhang, K. Guan, J. Shen, G. Liu, Y. Fan, W. Jin, Nanoparticles@rGO membrane enabling highly enhanced water permeability and structural stability with preserved selectivity, AlChE J. 63 (2017) 5054-5063.

[19] H. Liu, H. Wang, X. Zhang, Facile fabrication of freestanding ultrathin reduced graphene oxide membranes for water purification, Adv. Mater. 27 (2015) 249-254.

[20] D.L. Zhao, T.S. Chung, Applications of carbon quantum dots (CQDs) in membrane technologies: A review, Water Res. 147 (2018) 43-49.

[21] C. Shuai, W. Guo, P. Wu, W. Yang, S. Hu, Y. Xia, P. Feng, A graphene oxide-Ag co-dispersing nanosystem: Dual synergistic effects on antibacterial activities and mechanical properties of polymer scaffolds, Chem. Eng. J. 347 (2018) 322-333.

[22] L. Yu, W. Zhou, Y. Li, Q. Zhou, H. Xu, B. Gao, Z. Wang, Antibacterial thin-film nanocomposite membranes incorporated with graphene oxide quantum dot-mediated silver nanoparticles for reverse osmosis application, ACS Sustainable Chem. Eng. 7 (2019) 8724-8734.

[23] M.A. Tofighy, T. Mohammadi, Divalent heavy metal ions removal from contaminated water using positively charged membrane prepared from a new carbon nanomaterial and HPEI, Chem. Eng. J. 388 (2020).

[24] K. Guan, Y. Jia, Y. Lin, S. Wang, H. Matsuyama, Chemically converted graphene nanosheets for the construction of ion-exclusion nanochannel membranes, Nano Lett. 21 (2021) 3495-3502.

[25] T. Istirokhatun, Y. Lin, Q. Shen, K. Guan, S. Wang, H. Matsuyama, Ag-based nanocapsule-regulated interfacial polymerization Enables synchronous nanostructure towards high-performance nanofiltration membrane for sustainable water remediation, J. Membr. Sci. 645 (2022).

[26] W.W. Liu, Y.Q. Feng, X.B. Yan, J.T. Chen, Q.J. Xue, Superior micro-supercapacitors based on graphene quantum dots, Adv. Funct. Mater. 23 (2013) 4111-4122.

[27] J. Cai, W. Liu, Z. Li, One-pot self-assembly of Cu_2O/RGO composite aerogel for aqueous photocatalysis, Appl. Surf. Sci. 358 (2015) 146-151.

[28] Y. Li, Y. Hu, Y. Zhao, G. Shi, L. Deng, Y. Hou, L. Qu, An electrochemical avenue to green-luminescent graphene quantum dots as potential electron-acceptors for photovoltaics, Adv. Mater. 23 (2011) 776-780.

[29] C. Wu, Y. Yuan, Q. He, R. Song, Two-step synthesis of Ag@GQD hybrid with enhanced photothermal effect and catalytic performance, Nanotechnology 27 (2016) 48LT02.

[30] C. Chen, L. Chen, X. Zhu, B. Chen, Graphene nanofiltration membrane intercalated with AgNP@g-C_3N_4 for efficient water purification and photocatalytic self-cleaning performance, Chem. Eng. J. 441 (2022).

[31] X. Fan, C. Cai, J. Gao, X. Han, J. Li, Hydrothermal reduced graphene oxide

membranes for dyes removing, Sep. Purif. Technol. 241 (2020).
[32] Y. Mo, X. Zhao, Y. Shen, Cation-dependent structural instability of graphene oxide membranes and its effect on membrane separation performance, Desalination 399 (2016) 40-46.
[33] M. Akter, M.T. Sikder, M.M. Rahman, A. Ullah, K.F.B. Hossain, S. Banik, T. Hosokawa, T. Saito, M. Kurasaki, A systematic review on silver nanoparticles-induced cytotoxicity: Physicochemical properties and perspectives, J. Adv. Res. 9 (2018) 1-16.
[34] W.H. Zhang, M.J. Yin, Q. Zhao, C.G. Jin, N. Wang, S. Ji, C.L. Ritt, M. Elimelech, Q.F. An, Graphene oxide membranes with stable porous structure for ultrafast water transport, Nat. Nanotechnol. 16 (2021) 337-343.
[35] Y. Zhang, Z. Kang, T. Bessho, Two-component spin-coated Ag/CNT composite films based on a silver heterogeneous nucleation mechanism adhesion-enhanced by mechanical interlocking and chemical grafting, Nanotechnology 28 (2017) 105607.
[36] A.R. Sadrolhosseini, S. Abdul Rashid, S. Shafie, H. Soleimani, Laser ablation synthesis of Ag nanoparticles in graphene quantum dots aqueous solution and optical properties of nanocomposite, Appl. Phys. A 125 (2019).
[37] X. Wu, S. Liu, X. Cui, J. Lin, H. Zhang, J. Zhang, J. Wang, Manipulating microenvironments of nanochannels in lamellar membranes by quantum dots for highly enhanced nanofiltration performance, Chem. Eng. Sci. 228 (2020).
[38] S. Wang, S. Liang, L. Chen, H. Fang, Realizing ultrahigh nanofiltration performance based on small flake reduced graphene oxide membranes, Desalination 528 (2022).
[39] P. Zhang, J. Gong, G. Zeng, B. Song, S. Fang, M. Zhang, H. Liu, S. Huan, P. Peng, Q. Niu, D. Wang, J. Ye, Enhanced permeability of rGO/S-GO layered membranes with tunable inter-structure for effective rejection of salts and dyes, Sep. Purif. Technol. 220 (2019) 309-319.
[40] E.M.V. Hoek, M. Elimelech, Cake-enhanced concentration polarization: a new fouling mechanism for salt-rejecting membranes, Environ. Sci. Technol. 37 (2003) 5581-5588.

[41] J. Luo, Y. Wan, Effects of pH and salt on nanofiltration-a critical review, J. Membr. Sci. 438 (2013) 18-28.

[42] Z. Li, Y. Xing, X. Fan, L. Lin, A. Meng, Q. Li, rGO/protonated g-C3N4 hybrid membranes fabricated by photocatalytic reduction for the enhanced water desalination, Desalination 443 (2018) 130-136.

[43] J. Yin, Y. Yang, Z. Hu, B. Deng, Attachment of silver nanoparticles (AgNPs) onto thin-film composite (TFC) membranes through covalent bonding to reduce membrane biofouling, J. Membr. Sci. 441 (2013) 73-82.

[44] M.D. Firouzjaei, A.A. Shamsabadi, S.A. Aktij, S.F. Seyedpour, M. Sharifian Gh, A. Rahimpour, M.R. Esfahani, M. Ulbricht, M. Soroush, Exploiting synergetic effects of graphene oxide and a silver-based metal-organic framework to enhance antifouling and anti-biofouling properties of thin-film nanocomposite membranes, ACS Appl. Mater. Interfaces 10 (2018) 42967-42978.

[45] S. Jeon, J.H. Lee, Rationally designed in-situ fabrication of thin film nanocomposite membranes with enhanced desalination and anti-biofouling performance, J. Membr. Sci. 615 (2020).

[46] J. Liu, J. Shao, Y. Wang, J. Li, H. Liu, A. Wang, A. Hui, S. Chen, Antimicrobial activity of zinc oxide-graphene quantum dot nanocomposites: Enhanced adsorption on bacterial cells by cationic capping polymers, ACS Sustain. Chem. Eng. 7 (2019) 16264-16273.

[47] S. Liu, T.H. Zeng, M. Hofmann, E. Burcombe, J. Wei, R. Jiang, J. Kong, Y. Chen, Antibacterial activity of graphite, graphite oxide, graphene oxide, and reduced graphene oxide: membrane and oxidative stress, ACS Nano 5 (2011) 6971-6980.

[48] G. Franci, A. Falanga, S. Galdiero, L. Palomba, M. Rai, G. Morelli, M. Galdiero, Silver nanoparticles as potential antibacterial agents, Molecules 20 (2015) 8856-8874.

[49] Y. Wu, L. Zhang, Y. Zhou, L. Zhang, Y. Li, Q. Liu, J. Hu, J. Yang, Light-induced ZnO/Ag/rGO bactericidal photocatalyst with synergistic effect of sustained release of silver ions and enhanced reactive oxygen species, Chinese Journal of Catalysis 40 (2019) 691-702.

[50] A. Ghaffarkhah, E. Hosseini, M. Kamkar, A.A. Sehat, S. Dordanihaghighi, A. Allahbakhsh, C. van der Kuur, M. Arjmand, Synthesis, applications, and prospects of graphene quantum dots: A comprehensive review, Small 18 (2022) e2102683.
[51] N.A. Travlou, M. Algarra, C. Alcoholado, M. Cifuentes-Rueda, A.M. Labella, J.M. Lazaro-Martinez, E. Rodriguez-Castellon, T.J. Bandosz, Carbon quantum dot surface-chemistry-dependent Ag release governs the high antibacterial activity of Ag-metal-organic framework composites, ACS Appl. Bio. Mater. 1 (2018) 693-707.

Chapter 5

Conclusions

Recently, the accelerated processes of urbanization and industrialization have made the shortage of clean freshwater resources and pollution one of the most common global issues. Compared to traditional water treatment techniques, membrane separation technology has been proven to be the highly effective method for addressing this issue due to its advantages such as selective separation, low cost, energy efficiency, reduced chemical usage, and environmental sustainability. Meanwhile, the significant developments in the research and applications of nanomaterials have provided the potential to create advanced thin membranes with precisely designed structures and finely tunable separation performance. Among them, GO laminate membranes are expected to combine high permeance and selectivity due to their unique pore structure and mass transport properties. However, the oxygen-containing functional groups present in GO nanosheets significantly affect the stability and separation performance of nanochannels, especially in aqueous environments. Therefore, the regulation of interactions between adjacent GO nanosheets, optimization of nanochannel stability, and improvement of separation performance are comprehensively explored and discussed in this dissertation.

In Chapter 2, various confined nanochannels of GO membranes were successfully prepared to investigate the impact of nanochannel properties on separation performance. Subsequently, a series of reducing agents were introduced for further exploration of the deformation behavior and stability of nanochannels in Chapter 3. Finally, in Chapter 4, the GO membranes with excellent performance and stable nanochannels were successfully constructed by coupling appropriate intercalation materials. All the results

were described in Chapters 2-4, as follows:

5.1. Nanochannel characteristics contributing to ion/ion selectivity in two-dimensional graphene oxide membranes

This chapter demonstrated the dependence of nanochannel properties on single-salt solute selectivity. The selective transport pathway for the separation of water and ions was influenced by the constitution of different underwater nanochannels as the O/C ratio changed. The key findings are as follows: (1) Hydrated mono- and di-valent ions could not be significantly differentiated by nanochannel size of GO membrane, possibly due to the flexibility of nanochannel that cannot strictly sieve ions with specific size; (2) Difference in electrostatic interactions for mono- and di-valent ions play a more significant role and is more effective in enhancing their ion/ion selectivity within the subnanometer channel; (3) The contribution of ion competition in binary solutions to selectivity was emphasized, and binary solutions with high concentrations of high-valent ions were selectively separated more easily; (4) The water/salt selectivity increases for all types of salts as the O/C ratio decreases.

5.2. Nanochannel stability of chemically converted graphene oxide membranes

In this chapter, monosaccharide glucose (Glu), disaccharide maltose (Glu2), and trisaccharide maltotriose (Glu3) are chosen because they can function as reducing agents with the same reducing end in their molecules. They can convert GO with controlled reduction of oxygenated functional groups. Meanwhile, the saccharide molecules would be possibly attached to GO nanosheets during chemical conversion process and retained in the stacked laminate membrane as an intercalating molecule, which may also induce effects on the stability state of nanochannels. Therefore, the conversion of GO nanosheets using these different reducing agents would possibly lead to different nanochannel environment. The properties and concentration of reducing sugars were proved to be crucial factors in affecting the stability and nanochannel structure of GO membranes, thereby leading to the variation of desalination

performance. It was proved that maltose (Glu2) exhibits satisfactory ability to regulate the stability and size of nanochannels. In addition, Glu2/GO nanochannel membranes have superb stability against different extreme external environments (concentration, pressure, temperature, flow rate). These promising results presented that the chemical molecules with appropriate properties to mediate GO nanochannels have great potential and feasibility for the construction of 2D laminated membranes with stable and high separation performance.

5.3 Confined and mediated intercalation of nanoparticles in graphene oxide membrane to fine-tune desalination performance

In this chapter, there is demonstrated a confined and mediated approach to nanoparticle intercalation within GO membranes, resulting in enhanced desalination performance. It is extensively investigated the multifunctional role of GQD-mediated Ag nanoparticles uniformly confined within rGO nanosheets. The incorporation of GQD effectively controlled the growth of Ag nanoparticles, preventing their aggregation and facilitating controlled intercalation within the GO laminates. This process appropriately enlarged the nanochannels. By precisely regulating the content of intercalated GQD-Ag, there is achieved a four-fold increase in the permeance of the optimal membrane without significantly compromising Na_2SO_4 rejection. Additionally, the GQD-Ag/rGO membrane showcased promising antifouling properties, benefitting from the synergistic effects of Ag and GQD nanomaterials. This study offers valuable insights into fine-tuning 2D laminate structures to create fast-selective nanochannels, providing useful information for advancing desalination technologies.

Publication list

Chapter 2:

Zhou S, Guan K, Fang S, et al. Nanochannel characteristics contributing to ion/ion selectivity in two-dimensional graphene oxide membranes[J]. Journal of Membrane Science, 2024, 689: 122185.

Chapter 3:

Zhou S, Guan K, Li Z, et al. Nanochannel stability of chemically converted graphene oxide membranes. (Submitted)

Chapter 4:

Zhou S, Guan K, Wang Z, et al. Confined and mediated intercalation of nanoparticles in graphene oxide membrane to fine-tune desalination performance[J]. Chemical Engineering Journal, 2023, 465: 143005.

Doctoral Dissertation, Kobe University
“Nanochannel regulations of graphene oxide membranes for nanofiltration (ナノろ過用酸化グラフェン膜のナノチャネルの制御)”, 120 pages
Submitted on January 15, 2024
When published on the Kobe University institutional repository */Kernel/*, the publication date shall appear on the cover of the repository version.